AQUEOUS CORE COLLOIDOSOMES

WITH A METAL SHELL

Qian Sun
Darwin College
Department of Chemical Engineering and Biotechnology
University of Cambridge

A thesis submitted for the degree of

Doctor of Philosophy

September 2018

Aqueous core colloidosomes with a metal shell

Qian Sun

Colloidosomes are microcapsules whose shells consist of colloid particles, which are coagulated by a stabiliser or fused by sintering. In recent years, they have attracted considerable attention because of their potential applications in a range of industries, such as food, bioreactors and medicine. However, traditional particulate polymer shell colloidosomes leak low molecular weight encapsulated materials due to their intrinsic shell permeability, and this problem will limit their applications in pharmaceutical industries.

In this thesis, we report aqueous core colloidosomes coated with a silver or gold shell, which make the capsules impermeable. The shells can be ruptured using ultrasound. The silver shells are prepared by making an aqueous core capsule with a particulate polymer shell and then adding $AgNO_3$, surfactant and L-ascorbic acid to form a second shell. The gold coated colloidosomes are prepared by making an aqueous core capsule with a particulate polymer shell and then adding $HAuCl_4$, surfactant and L-ascorbic acid.

We propose to use the metal coated capsules as drug carriers to load an anticancer drug, doxorubicin. After triggering by ultrasound, encapsulated drug, broken fragments and possibly some drug attached on the surface of the capsules may all kill cancer cells. For silver coated colloidosomes, at 10 capsules/cell, they have a low cytotoxicity, showing a cell viability of more than 90% during the first 24 h and more than 60% after 72 h. Increasing the number of capsules, the cytotoxicity of the silver shells increases heavily. Compared with silver ones, the gold shells show less toxicity to cells. We also used the capsules to load an antibiotic kanamycin and triggered to release the drug and kill *E.coli*.

In addition, we set up a targeting model by modifying the colloidosomes using 4,4'-dithiodibutyric acid and attaching them with proteins - rabbit Immunoglobulin G (IgG). Label-free Surface Plasmon Resonance biosensor was used to test the specific targeting of the functional silver or gold shells with rabbit antigen. The results demonstrate that a new type of functional metal coated colloidosome with non-permeability, ultrasound sensitivity and immunoassay targeting could be applied to many medical applications.

Declaration of Originality

The author declares that this thesis and the work described in it are her original work, except for those acknowledged and referenced. The work was carried out in the Department of Chemical Engineering and Biotechnology, University of Cambridge, and the BP Institute for Multiphase Flow between October 2014 and April 2018.

This dissertation has not been previously submitted in part, or in whole, to any other universities for a degree, diploma or other qualification.

This dissertation contains a total of 35848 words, 79 figures and 5 tables.

Signed 

Date 21/09/2018

Acknowledgements

Firstly, I would like to express great appreciation to my supervisor, Prof Alex Routh. Over the past three and half years, he has helped me a great deal, and has offered me with useful advice for my PhD project. Without his help and guidance, this thesis would not have been possible.

Secondly, I wish to sincerely acknowledge all my group members, BP Institute staff, and Department of Chemical Engineering and Biotechnology staff, for their kind assistance and encouragement with my research and also my daily life in Cambridge.

Thirdly, I'd like to thank Prof Lisa Hall and her group to help me with the SPR targeting experiment and the antibiotic loading experiment.

Fourthly, I'd like to thank Prof Gleb Sukhorukov and his group from Queen Mary, University of London to help me with the anticancer drug loading experiment.

Fifthly, I am also grateful to Dr Richard Langford and Eric Tapley from the Cavendish Laboratory, Department of Physics, for their assistance with the scanning and transmission electron microscopies. Many thanks to Prof Stuart Clarke and Dr Mike Casford from Department of Chemistry, for advice about the modification reaction and assistance with the Raman microscopy.

Sixthly, thank you to Darwin College, Chemical Engineering and Biotechnology Department, and the Ottewill International Travel Scholarship committee to provide me travel bursaries, which allow me to attend international conferences to communicate and soak up the knowledge of other academics in the field.

Seventhly, I owe thanks to my husband, my parents and my lovely friends for their great support during my studies.

Finally, I am very grateful to the Chinese government and China Scholarship Council for funding my PhD study in Cambridge.

Publications

The work from this thesis has been published as follows:

Journal papers

[1] Qian Sun, Alexander F. Routh. *Aqueous Core Colloidosomes with a Metal Shell*. European Polymer Journal, 2016, 77: 155-163. Front cover page article.

[2] Qian Sun, Yao Du, Ziyan Zhao, Elizabeth A. H. Hall, Hui Gao, Gleb B. Sukhorukov, Alexander F. Routh. *Functional Silver-Coated Colloidosomes as Targeted Carriers for Small Molecules.* Langmuir, 2017, 33(15): 3755-3764.

[3] Qian Sun, Hui Gao, Gleb B. Sukhorukov, Alexander F. Routh. *Silver Coated Colloidosomes as Carriers for an Anticancer Drug*. ACS Applied Materials & Interfaces, 2017, 9(38): 32599-32606.

[4] Qian Sun, Yao Du, Elizabeth A. H. Hall, Dong Luo, Gleb B. Sukhorukov, Alexander F. Routh. *A Fabrication Method of Gold Coated Colloidosomes and Their Application as Targeted Drug Carriers*. Soft Matter, 2018, 14(14): 2594-2603. Back cover page article.

[5] Qian Sun, Ziyan Zhao, Elizabeth A. H. Hall, Alexander F. Routh. *Metal Coated Colloidosomes as Carriers for an Antibiotic.* Frontiers in Chemistry, 2018, 6: 196.

Conference presentations

[1] Poster presentation at *15th European Student Colloid Conference*. Krakow, Poland, June, 2015.

[2] Oral presentation at *ECI Conference: Design and Manufacture of Functional Microcapsules and Engineered Particles*. Sicily, Italy, April, 2016.

[3] Oral presentation at *Edwards Centre Meeting for Soft Matter*. Cambridge, UK, April, 2017.

[4] Poster presentation at *Colloid Young Researchers' Meeting 2017*. Sheffield, UK, April, 2017.

[5] Poster presentation at *7th International Colloids Conference*. Barcelona, Spain, June 2017.

[6] Oral presentation at *UK Colloids 2017: International Colloid and Surface Science Symposium*. Manchester, UK, July, 2017.

Front cover page of European Polymer Journal

Back cover page of Soft Matter

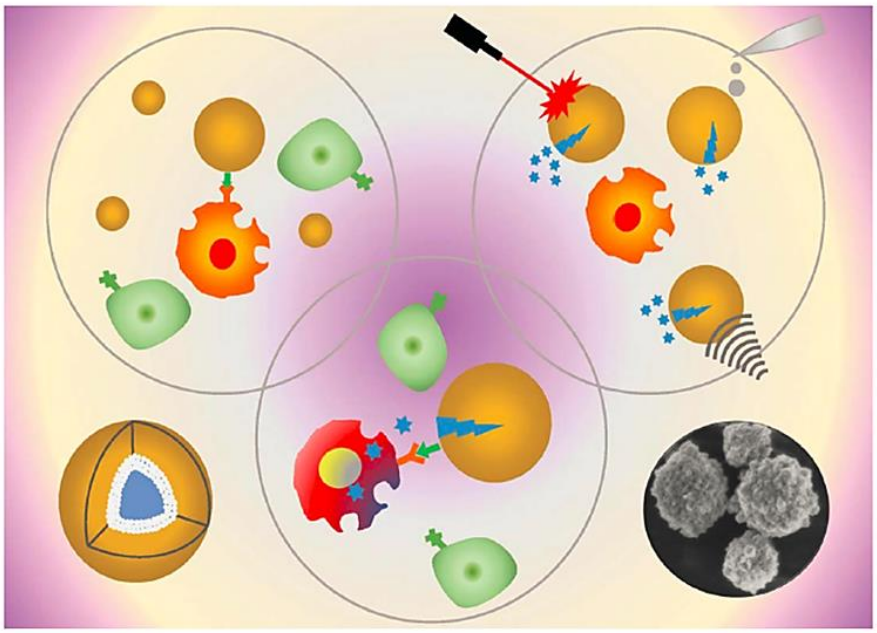

Highlighting work from the Routh and Hall research groups at the University of Cambridge and the Sukhorukov group at Queen Mary's London.

A fabrication method of gold coated colloidosomes and their application as targeted drug carriers

Aqueous core microcapsules are made with an impermeable gold shell. Attachment of proteins allows bio-specific targeting and encapsulated drugs are released using ultrasound.

As featured in:

See Alexander F. Routh *et al.*, *Soft Matter*, 2018, **14**, 2594.

ROYAL SOCIETY OF CHEMISTRY

rsc.li/soft-matter-journal

Registered charity number: 207890

Abstract

Colloidosomes are microcapsules whose shells consist of colloid particles, which are coagulated by a stabiliser or fused by sintering. In recent years, they have attracted considerable attention because of their potential applications in a range of industries, such as food, bioreactors and medicine. However, traditional particulate polymer shell colloidosomes leak low molecular weight encapsulated materials due to their intrinsic shell permeability, and this problem will limit their applications in pharmaceutical industries.

In this thesis, we report aqueous core colloidosomes coated with a silver or gold shell, which make the capsules impermeable. The shells can be ruptured using ultrasound. The silver shells are prepared by making an aqueous core capsule with a particulate polymer shell and then adding $AgNO_3$, surfactant and L-ascorbic acid to form a second shell. The gold coated colloidosomes are prepared by making an aqueous core capsule with a particulate polymer shell and then adding $HAuCl_4$, surfactant and L-ascorbic acid.

We propose to use the metal coated capsules as drug carriers to load an anticancer drug, doxorubicin. After triggering by ultrasound, encapsulated drug, broken fragments and possibly some drug attached on the surface of the capsules may all kill cancer cells. For silver coated colloidosomes, at 10 capsules/cell, they have a low cytotoxicity, showing a cell viability of more than 90% during the first 24 h and more than 60% after 72 h. Increasing the number of capsules, the cytotoxicity of the silver shells increases heavily. Compared with silver ones, the gold shells show less toxicity to cells. We also used the capsules to load an antibiotic kanamycin and triggered to release the drug and kill *E.coli*.

In addition, we set up a targeting model by modifying the colloidosomes using 4,4'-dithiodibutyric acid and attaching them with proteins - rabbit Immunoglobulin G (IgG). Label-free Surface Plasmon Resonance biosensor was used to test the specific targeting of the functional silver or gold shells with rabbit antigen. The results demonstrate that a new type of functional metal coated colloidosome with non-permeability, ultrasound sensitivity and immunoassay targeting could be applied to many medical applications.

Contents

List of Figures

List of Tables

Chapter 1.

Introduction

1.1 Encapsulation

Polymer shell microcapsules with liquid cores have attracted interest in recent years because of their capability for encapsulating and delivery of useful materials. [1, 2] They can be used in a wide variety of industries, such as food [3], medicine [4], bioreactors [5], and cosmetics [6]. Here we introduce the reasons for encapsulation, encapsulation methods, and some release mechanisms.

1.1.1 Reasons for encapsulation

Encapsulation causes interest in many industries. [1-6] The main reason is that microcapsules can isolate the core from its surroundings to protect it from harsh environments, such as pH, temperature, solvents and poisons. [7] For example, in some biological systems, the capsules can seal and protect enzymes or bacteria from denaturing by solvents, which can result in greater cell viability and bioreactor productivity. [5, 8-11]

In addition, encapsulation allows for controlled delivery of encapsulated materials to targeted areas, then release of the encapsulated ingredient. For example, in some pharmaceutical systems, sealing active drug species inside a particle or capsule, as drug delivery vehicles, with well-defined release properties is often the preferred treatment method. [12] In agricultural and environmental applications, aqueous core colloidosomes can be used to deliver potentially toxic materials, such as pesticides and herbicides to their intended environments. [13]

A further reason for encapsulation is to delay external chemical reactions until suitable conditions are achieved. This allows for an increase in lifetime of the active ingredient and,

in turn, maintains product quality. For example, in pharmaceutical applications, water core microcapsules can be used to delay the release of an active drug species. [8]

1.1.2 Encapsulation methods

Various preparation methods of encapsulation have been reported and developed, such as liposomes [14], silica shell microcapsules [15, 16], dendrimers shell microcapsules [5], and particulate polymer shell microcapsules [17, 18]. In biological applications, aqueous core microcapsules are widely used for encapsulation and show great potential. In this section, a few common aqueous core microcapsule preparation methods are introduced, including self-assembly colloidosomes, layer-by-layer polyelectrolyte deposition, polymer precipitation by phase separation, polycondensation interfacial polymerization, and polymeric vesicles. [19]

1.1.2.1 Colloidosomes

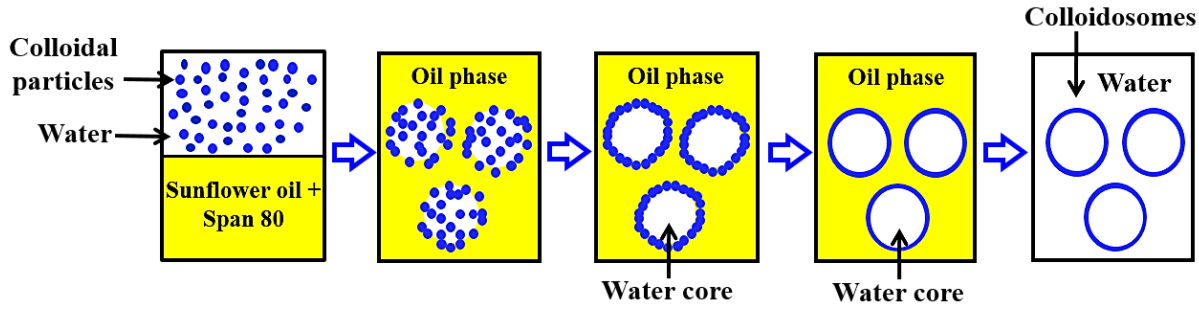

Fig. 1.1 A general overview of the fabrication method of colloidosomes.

Colloidosomes are microcapsules whose shells consist of colloid particles, which are coagulated by a stabiliser or fused by sintering. [19] Fig. 1.1 shows a general overview of the fabrication method of colloidosomes. An aqueous suspension of colloidal particles is emulsified in an oil phase. The colloidal particles, with both hydrophobic and hydrophilic groups, move to the water-oil boundary. The stability will be provided using a stabiliser to lock the particles, or heating to let the particles melt. Velev et al. [20, 21] made the first colloidosomes by emulsifying oil phase droplets in an aqueous suspension of polystyrene particles. The polymer particles coated the emulsion droplets and made the colloidosomes stable. Further research continued to fabricate colloidosomes using a direct self-assembly method [22, 23] and improved the size distribution of the fabricated colloidosomes [24, 25].

The self-assembly approach is suitable for biological encapsulation since there is no contact with harsh solvents and it is possible to control the shell permeability. The disadvantage is

that the colloidosomes prepared by this method need a further shell stabilization stage to make a robust structure. In addition, during the process of encapsulation, there may be leakages or core contamination because of incomplete shell formation.

1.1.2.2 Layer-by-layer polyelectrolyte deposition

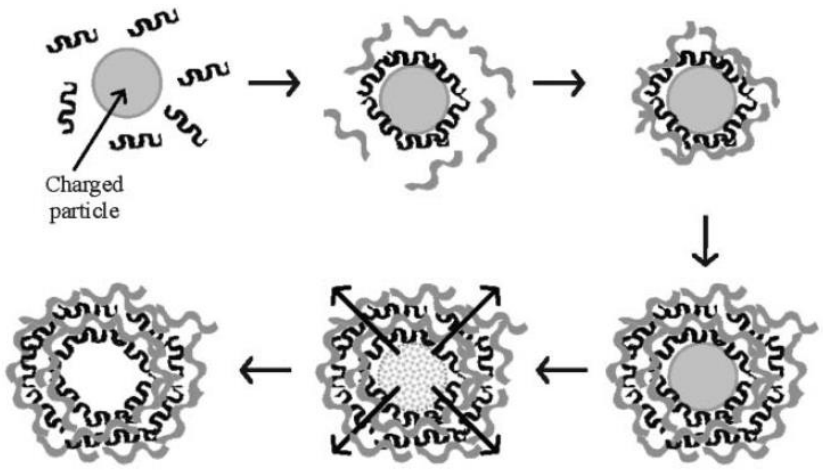

Fig. 1.2 A general overview of the fabrication of microcapsules using a layer-by-layer polyelectrolyte deposition method (image reproduced from Donath et al., 1998 [26]).

Another common encapsulation method is layer-by-layer polyelectrolyte deposition. Fig. 1.2 shows a general overview of the fabrication method. [26] This method places a charged particle in a polyelectrolyte solution of the opposite charge and the electrostatic driving force drives the polymer to form a stable film. The system is cleaned, and then, another layer is deposited. In some cases, the core is dissolved and hollow structure microcapsules obtained. [27-30]

This approach is also suitable for biological encapsulation since there is no contact with harsh solvents and it is possible to control the thickness of the capsule shells by controlling the number of polyelectrolyte layers [31, 32]. However, this method needs a relatively long time to form capsules, since it involves multiple deposition and particle cleaning steps.

1.1.2.3 Polymer precipitation by phase separation

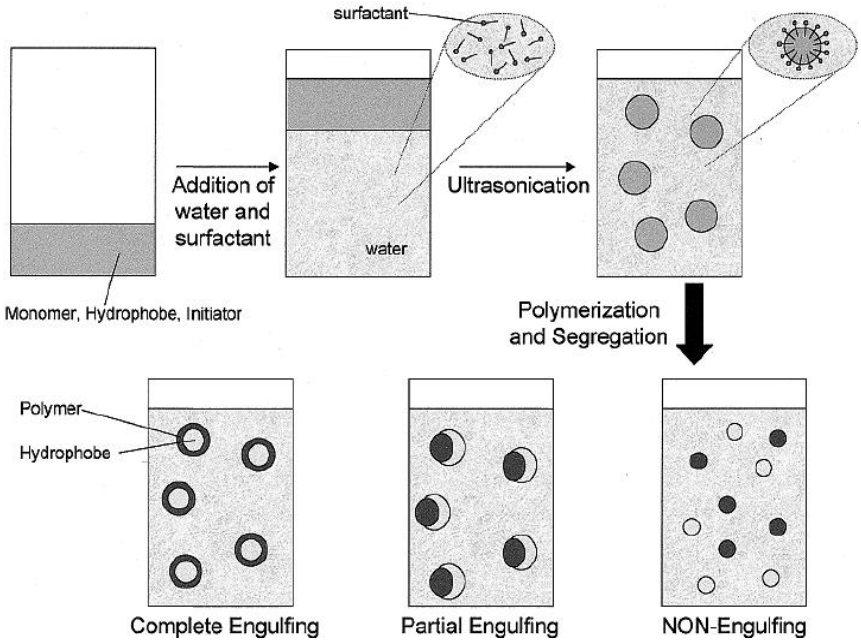

Fig. 1.3 Schematic of steps for aqueous core microcapsules using polymerization induced phase separation method (image reproduced from Tiarks et al., 2001 [33]).

Liquid core capsules can also be formed using a polymer precipitation by phase separation method. There are two approaches for this method, including polymerization induced phase separation [33-35] and solvent extraction and evaporation [36-39]. The principle of the encapsulation process using the polymerization induced phase separation method is shown in Fig. 1.3. Initially, a mixture of water with a chosen surfactant is added into a hydrophobic monomer using ultrasonication for monomer polymerization and segregation. The morphology of the demixing structure is determined by the type of surfactant and the degree of engulfing is determined by the monomers. The non-engulfing and partial engulfing cases do not form capsules; only the complete engulfing case results in a capsule. [33-35]

For solvent extraction and evaporation, the shell-forming polymer is dissolved in a solvent mixture comprising a volatile solvent and an involatile non-solvent. Then the solution is dispersed into a water/stabilizer mixture to produce an oil-in-water emulsion. The volatile solvent is then removed to form a hollow structure capsule. [36] The principle of the encapsulation process using solvent extraction and evaporation is shown in Fig. 1.4. The polymer precipitation by the phase separation method is more suitable for oil core encapsulation, and, it can produce microcapsules with relatively thick shells and narrow size

distributions. The disadvantage is that volatile organic solvents are used during the microcapsule formation, which may be harmful for the encapsulated active materials.

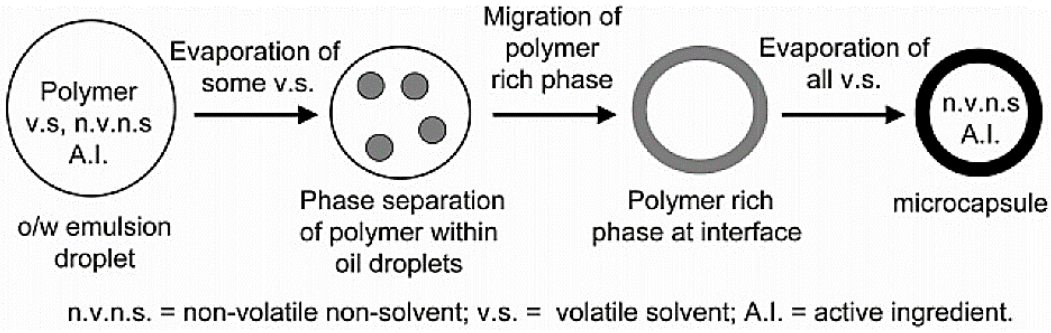

Fig. 1.4 Schematic of steps for aqueous core microcapsules using solvent extraction and evaporation (image reproduced from Dowding et al., 2005 [36]).

1.1.2.4 Polycondensation interfacial polymerization

In classical interfacial polycondensation, there are normally two steps: firstly, oil in water emulsion droplets are formed using mechanical stirring and the monomer is enclosed in the emulsion drops. Then the second complementary monomer is added to the external phase of the emulsion and a polycondensation reaction takes place at the liquid-liquid emulsion interface. [40] The first emulsification step determines the capsule size and distribution. [41-45] Fig. 1.5 shows a schematic of the polycondensation formation of shells around emulsion droplets. [19]

The advantage of this method is that it is suitable for both oil and aqueous cores, and the fabrication procedure is simple. However, the use of monomers limits the application of the capsules and it is difficult to achieve biological encapsulation using this method.

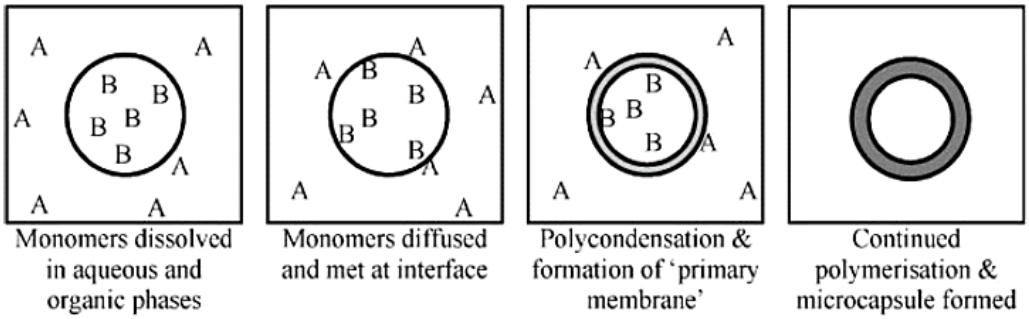

Fig. 1.5 Schematic of the polycondensation formation of shells around emulsion droplets (image reproduced from Yow & Routh, 2006 [19]).

1.1.2.5 Polymeric vesicles

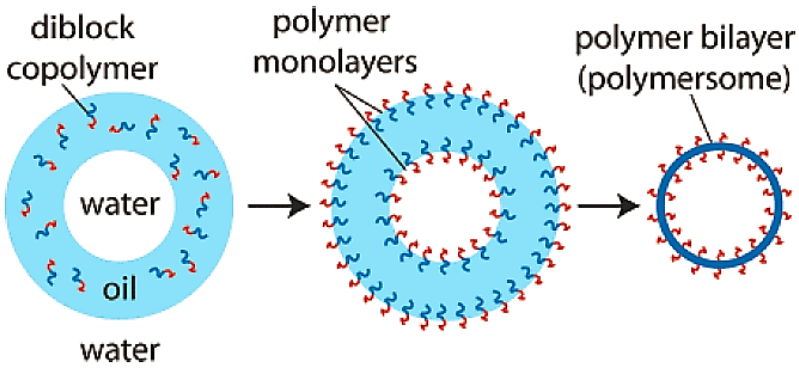

Fig. 1.6 Schematic for the formation of polymersomes from water-in-oil-in-water drops (image reproduced from Hayward et al., 2006 [46]).

Fig. 1.6 shows a schematic for the formation of polymersomes or polymeric vesicles from water-in-oil-in-water drops. [46] To form polymersomes with a diameter of 10-100 μm, one uses water-in-oil-in-water double emulsion drops of controlled architecture as templates. Then a volatile organic solvent is used as the middle phase and evaporation of the solvent leads to polymersome formation. [46]

This method offers the advantages of high encapsulation efficiencies, and controllable vesicle sizes and architectures. [47-49] In addition, polymeric vesicles improve stability and lower permeability compared to lipid vesicles and can be used for biomedical applications. [50, 51] However, the downside is the number of vesicles formed, since this is limited by droplet formation.

1.1.3 Release mechanisms and methods

After sealing the encapsulated materials, it is necessary to find a suitable method to trigger a release from the capsules. According to different mechanisms, the release methods can be divided into three ways, including physical, chemical and biological methods.

Firstly, the most common release method is physical. It uses an applied shear, pressure or other force, and results in shell rupture or mechanical deformation. For example, Gordon et al. [52] fabricated capsule adsorption to colloids and then triggered the contents by osmotic pressure from internal free polyelectrolytes. Keen et al. [10] synthesized aqueous core colloidosomes coated with calcium carbonate and used a shear force to break the capsules. Alternatively, Sun et al. [53, 54] and Gao et al. [55, 56] controlled the release of cargos in capsules

using ultrasound. Skirtach et al. [57] presented a method for remote release of an encapsulated material from polyelectrolyte capsules based on laser light illumination.

Another way to achieve release from the capsules is a chemical method. This can be carried out by melting, solvent action, hydrolysis, slow disintegration, chemical or photochemical reaction to dissolve or swell the shells. [19] For instance, Sun et al. [58] released sealed dye solution in silver shell capsules by addition of acid. Chiwele et al. [59] dissolved hydroxypropyl methylcellulose (HPMC) capsule shells rapidly in the dissolution medium with a pH below 5.8. Gun et al. [60] achieved a release of blue dye from the capsules when the pH was below 3.5, due to swelling of a particulate polymer shell. Kim et al. [61] used pH to swell polyelectrolyte multilayer microcapsules filled with dye solutions.

A third way to release from the capsules is a biological method, such as enzymatic attack. For instance, De Geest et al. [62] demonstrated the release by enzymatic reactions and monitored profiles. In addition, there are various enzymes used for release, such as dextran sulfate and poly-L-lysine. [62-64]

1.1.4 Prevention of small molecule leakage

Traditional particulate polymer shell capsules may leak low molecular weight encapsulated materials in a short time due to their intrinsic shell permeability, and this problem will limit their applications in pharmaceutical industries. In recent developments of microcapsules, the control of capsule permeability has become a rapidly growing research area, with the aim of preventing the leakage of small molecule materials.

For particulate polymer shell capsules, in order to have a long-term encapsulation and change the capsule permeability, the idea of forming a second shell to cover the original polymer was applied by many researchers. For example, Hitchcock et al. [65, 66] formed an impermeable metal film around polymer microcapsules using a three-step process. Their impermeable metal film can prevent leakage of small volatile oils in an ethanol phase for at least 21 days. However, the original polymer shell capsules lose the small volatile oils in less than 30 min under the same conditions. Keen et al. [10] used a precipitation method to synthesise a calcium carbonate shell, which was formed using an inner phase of sodium carbonate in the core of the polymer shells and an outer phase of calcium chloride. This calcium carbonate shell can seal both small molecule dye solutions and larger enzyme

molecules for a few months. Gao et al. [55] used the layer-by-layer assembly method to form polyelectrolyte microcapsules, then coated a silica shell. This polyelectrolyte/silica composite microcapsules can seal cargoes for up to 72 h.

An alternative way to prevent the leakage of small molecule materials from polymer shell capsules is to change the shell thickness or layer structure, resulting in changing the permeability. For instance, Mendelsohn et al. [67] made polyelectrolyte capsules using a layer-by-layer assembly method, and then adjusted the pH to make shells with a selective thickness. Under different pH conditions, the thickness of the shell, which adsorbed polycations or polyanions, was between 0.5 and 8 nm. Ameloot et al. [68] formed capsules using self-completing growth of MOF layers. To control the thickness of the capsule shell, they used small inter-grown crystals to seal the gaps between larger crystals, and, finally obtained a uniform capsule shell thickness between 1.5 and 2 mm. Ochs et al. [69] also formed multiple-layer film capsules using a layer-by-layer assembly method, and loaded inorganic colloidal, magnetic or plasmonic nanoparticles to control the thickness. Antipov et al. [70] made polyelectrolyte multilayer capsules, and they controlled the capsule permeability using different pH and salt concentrations.

1.2 Materials for drug delivery

Small drug molecules play an important role in medical applications and are widely used in the pharmaceutical industry. Drug delivery systems are routinely used to treat various diseases including cancer, fungal infections and muscular degeneration. [71, 72] The drug delivery vehicle should display a sufficient circulation lifetime to allow successful delivery to the targeted region. Furthermore, for toxic drugs, encapsulation in drug carriers reduces the harmful side effects. [73, 74] The trend of developing new drug delivery systems shows great commercial value and academic significance. It is reported by Research and Markets that the world drug delivery technology market will grow from $178.8bn in 2015 to $227.3bn in 2020, with an annual growth rate of 4.9%. [75, 76] Therefore, using drug carriers for drug delivery is becoming a rapidly growing research area. Below, a few common drug delivery materials are introduced, including polymers, particulate polymer shell capsules, liposomes, metal-organic frameworks, silica particles, nanoparticles, micelles, and hydrogels.

1.2.1 Polymers and particulate polymer shell capsules

Polymers have been widely used in pharmaceutical applications for encapsulation in drug delivery vehicles. [77, 78] The drug delivery system should not only have the ability to seal the drugs, but should also control the delivery and release. They can effectively deliver the drug to a target site and, thus, increase the therapeutic benefit and minimize side effects. [79] Currently, various polymers have been used in drug delivery research, such as poly (lactic acid) (PLA) [80-83], poly (glycolic acid) (PGA) [84-87], and their co-polymers poly (lactide-co-glycolide) (PLGA) [88-91]. Fig. 1.7 shows the structures of these polymers, which are well known for both biocompatibility and resorbability through natural pathways. [92] In addition, particulate polymer shell capsules and emulsions have been developed and used for delivering drugs to targeted areas. [93-98] In these cases, the polymers shells are degradable, making them suitable for biomedical applications. However, encapsulation of small molecule drugs within particulate polymer shells presents a significant challenge. Most polymer capsule shells, due to their intrinsic high permeability, tend to leak small molecules. This greatly limits their practical application.

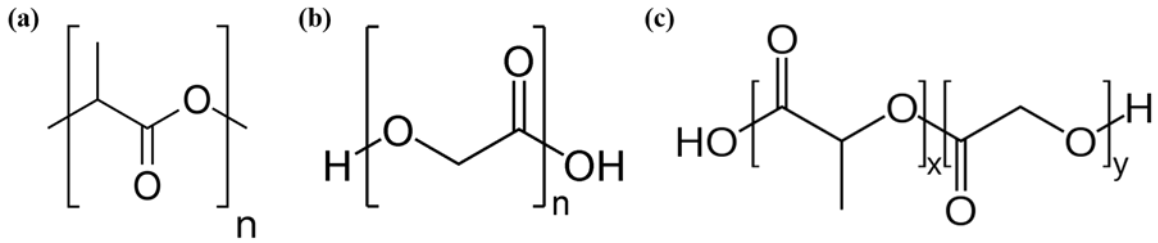

Fig. 1.7 Chemical structure of (a) PLA, (b) PGA, and (b) PLGA monomers (image reproduced from Hans & Lowman, 2002 [92]).

1.2.2 Liposomes

Liposomes are composed of phospholipids, which self-enclose to form spheres of lipid bilayers and an aqueous core within the bilayers. [99] Fig. 1.8 shows a typical liposome, and a portion of a typical lipid with multifunctional surface modifications. As drug carriers, liposomes can improve solubility of encapsulated drugs, have a good compatibility with biodegradable and nontoxic materials, and, also have a good versatility when chemically modified with attached specific surface ligands for targeting. [99-102] To use liposomes effectively, challenges, such as difficulty in targeting specific tissues and limitation of shelf-life, need to be solved.

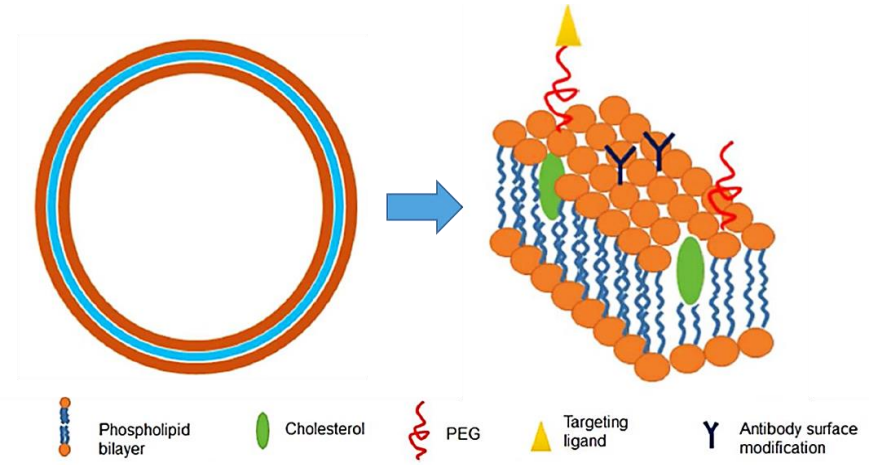

Fig. 1.8 A typical liposome, and a portion of a typical lipid with multifunctional surface modifications (image reproduced from Pattni et al., 2015 [99]).

1.2.3 Metal-organic frameworks

Metal-organic frameworks (MOFs) are a new type of porous material, which consist of metal-containing nodes and organic linkers. [103] MOFs have a high structural flexibility, which enables the adaptation of their porosity to the shape of the host molecule. [104, 105] In addition, MOFs show simultaneously hydrophilic and hydrophobic abilities. Their tuneable pore size and connectivity can be adapted to the physicochemical properties of drugs in medical applications. [106-108] Based on their special structure, MOFs can be used as drug delivery vehicles for the encapsulation and delivery of drugs. [109, 110] Fig. 1.9 shows a schematic diagram of iron carboxylate MOFs for drug delivery. [106] When using MOFs as non-toxic drug carriers, issues, such as them not being compatible for biomedical and pharmaceutical applications, need to be solved.

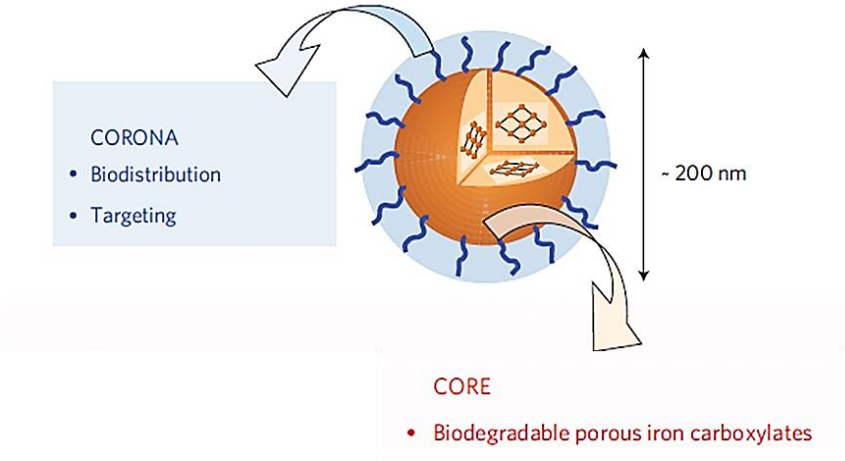

Fig. 1.9 Schematic diagram of iron carboxylate MOFs for drug delivery (image reproduced from Horcajada et al., 2010 [106]).

1.2.4 Silica particles

Silica particles have been widely developed in biological applications, since they are biocompatible and stable. [111] In addition, bioactive molecules can be easily encapsulated within silica particles by combining sol-gel polymerization with either spray-drying or emulsion chemistry. [112] The silica sol-gel fabrication process is easy and cheap. Moreover, the reaction conditions are relatively mild. Normally, silica particles can be prepared using Tetraethyl Orthosilicate (TEOS) in an ethanol/water medium [113, 114], or using silicic acid and sodium hydroxide [115].

For a drug delivery system, mesoporous silica nanoparticles are more often used, due to their high specific surface area and volume which enables them to load drugs. [116, 117] In addition, silica structures can be easily functionalized using precursors with desired functional groups. For examples, the hybrid silica monolith, which was conveniently synthesized by hydrolysis and polycondensation, can be functionalized with octyl and thiol groups. [118] The silica gel can be easily functionalized with various organic compounds with metal chelating ability as well. [119] However, the addition of such functional groups changes the final structure such as the pore size of the mesoporous silica, which will affect the loading capacity.

1.2.5 Nanoparticles

Nanoparticles are particles between 1 and 100 nanometers (nm) in size. Nanoparticles have many special properties, such as the small size, customized surface, multi-functionality and improved dispersibility. These properties highlight the potential to use nanoparticles as multifunctional drug carriers for biomedical applications. [120] For instance, some polymeric nanoparticles have a good stability and their surfaces are easily modified, so it is possible to use these polymeric nanoparticles as drug carriers to achieve both controlled drug release and disease-specific localization by adapting their surface chemistry. [121-123] Magnetic nanoparticles, such as iron oxide nanoparticles with or without a polymeric coating, are often used for current clinical diagnostic and therapeutic, magnetic resonance imaging, and also as drug carriers [124]. In addition, carbon nanomaterials, such as carbon nanotubes and graphene [125], and colloidal gold nanoparticles [126] can also be used for drug delivery.

1.2.6 Micelles

A micelle is a surfactant structure of molecules containing both a “hydrophilic head” and “hydrophobic tail”. Normally, a micelle in aqueous solution forms an aggregated hydrophilic part contacting with the solvent, and isolates a hydrophobic single-tail part in the micelle centre [127]. Among different kinds of micelles, block-copolymer micelles are often used as drug carriers. These micelles are a spherical super-molecular gathering of “amphiphilic copolymers”. [128] Amphiphilic block copolymers can contain hydrophobic drugs in the core, and their shells are hydrophilic, so they can be used as modules for the delivery of poorly soluble contents. The chemical composition, total molecular weight, and ratios of amphiphilic block copolymers can be easily adjusted, in order to control the size and morphology of the micelles. [129, 130] This feature makes micelles suitable for drug delivery applications.

1.2.7 Hydrogels

A hydrogel is a cross-linked network of water-soluble polymers, which can also be used for encapsulation and delivery of drugs. [131] Functional hydrogels, such as environmentally sensitive hydrogels, have potential in medicine and pharmaceutical applications. For example, pH-sensitive or temperature-sensitive hydrogels can be used for site-specific controlled drug delivery, by adjusting to a different pH or temperature. Specific molecule-sensitive (glucose or antigens) hydrogels can be used as biosensors or for drug delivery systems. Light-sensitive, pressure-responsive and electro-sensitive hydrogels also have the potential to be used for drug delivery and bioseparations. [132]

1.3 Targeted drug delivery

Targeted drug delivery is a method of delivering drugs to specific regions in the body. Recently, targeted drug delivery has become a rapidly growing research area, since effective delivery is an important part of drug development. [133] Targeted delivery can usually be divided into two methods - passive and active.

Passive targeting means that the drug carriers passively reach the targeted organ or tissues. In this method, the drug carriers are usually macromolecules or nanoparticles, which contain therapeutic agents. For example, one can use catheters to infuse nanoparticles drug carriers to the targeted organ or tissues. In addition, one can enhance permeability and retention effect to deliver the drug. [134, 135] Active targeting means that the drug carriers are actively targeted towards the relevant organ or tissues. After loading the therapeutic agent, the drug carriers are normally combined with a cell-specific ligand. [136] For example, the drug carriers can bind to complementary receptors on cells, so that the receptors can guide the drug carrier system to the diseased tissues. [137] Another way to achieve active targeting is to use magnetic positioning. One can combine magnetic particles with drug-containing capsules or liposomes and the magnetic force will force the drug carriers to the desired regions. [137]

1.4 Experimental methods

The main experimental methods used in this research are introduced in the following description, including scanning electron microscopy, energy-dispersive X-ray spectroscopy, transmission electron microscopy, confocal laser scanning microscopy, fluorescence microscopy, surface plasmon resonance, ultrasound, UV-Vis spectrophotometry, and Raman microscopy.

1.4.1 Scanning electron microscopy

A scanning electron microscope (SEM) is a type of microscope which produces images of samples by scanning the surface with a focused beam of electrons. SEM is often used in materials science to test the morphology and the structure of different samples. Normally, SEM samples are dried and coated with a gold or platinum film before measurement. In a typical SEM, a beam of electron is focused on a very small spot and moved over each point of the subject. [138, 139] Fig. 1.10 shows a schematic of a typical scanning electron microscope. [140]

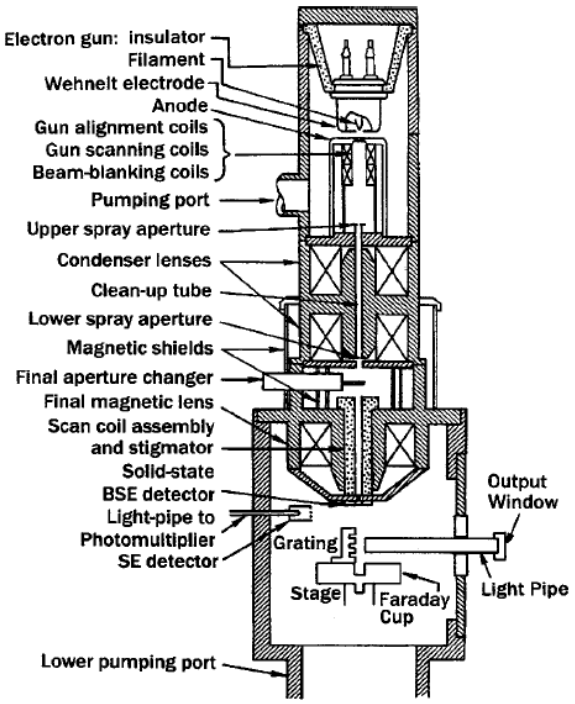

Fig. 1.10 Schematic of a typical scanning electron microscope (image reproduced from Kapp et al., 2004 [140]).

Conventional SEM is used to examine dried samples in a high vacuum. For wet conditions in a low vacuum, an environmental scanning electron microscopy (ESEM) is used. Fig. 1.11

shows a schematic representation of an environmental scanning electron microscope. [141] The main distinguishing features of ESEM compared to other electron microscope techniques is the presence of vapour (usually water) in the sample chamber and there is no need for prior sample preparation. [142]

In our research, a Zeiss X-beam FIB SEM was used at an accelerating voltage of 5.0 kV. For sample preparation, a drop of particle suspension was air-dried on a stainless steel SEM stub overnight. The particulate polymer shell colloidosome samples were gold-coated using a BioRad SEM sputter coater, in an argon environment at 1×10^{-3} mbar and 10 mA for 180 s. The gold and silver coated colloidosome samples were imaged without any treatment.

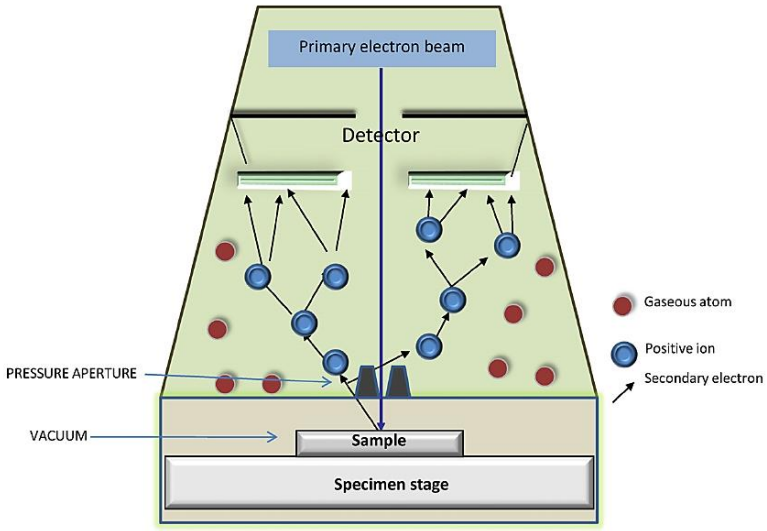

Fig. 1.11 Schematic representation of an environmental scanning electron microscope (image reproduced from Bibi et al., 2011 [141]).

1.4.2 Energy-dispersive X-ray spectroscopy

An energy-dispersive X-ray spectroscope (EDS, EDX, EDXS or XEDS) is an analytical technique for analyzing the elemental composition of samples. The EDX is used in combination with an electron microscope, normally a transmission electron or scanning electron microscope. [143, 144] It is used to find out which elements are present in the sample as well as their amounts. [145] In our research, the energy-dispersive X-ray spectroscopy we used is in combination with a Zeiss X-beam FIB scanning electron microscope. The accelerating voltage used for EDX analysis was 10.0 kV.

1.4.3 Transmission electron microscopy

A transmission electron microscopy (TEM) is a type of microscope where a beam of electrons is transmitted through a sample to form an image. TEM is also often used in materials science to test the morphology and structure of different materials. It is capable of taking images at a significantly higher resolution than SEM and normal optical microscopes, especially for high resolution observation such as for nanoparticles. [146, 147] Fig. 1.12 shows a schematic representation of a transmission electron microscope. [148]. In our research, the transmission electron microscope we used is an FEI Philips Tecnai 20 TEM at 200 kV (Tungsten, LB6) high-energy electron beam. For sample preparation, a drop of colloidosome sample was added onto a TEM grid, and then transferred to the specimen holder.

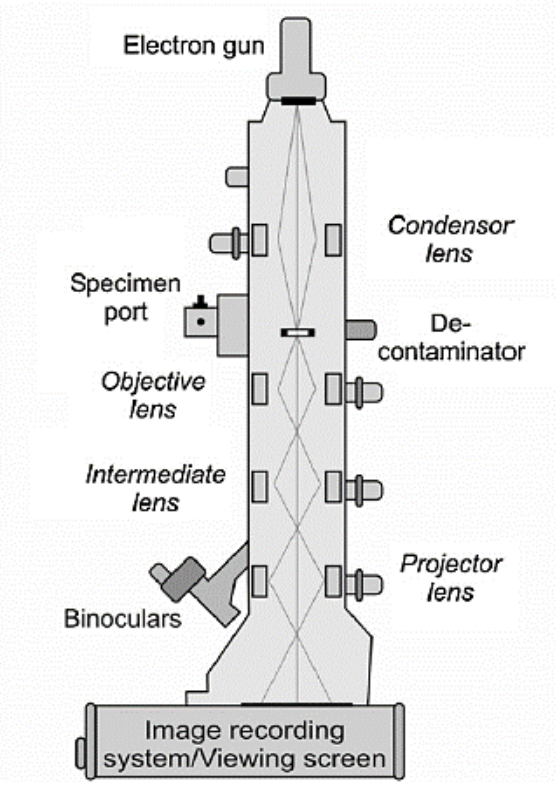

Fig. 1.12 Schematic representation of a transmission electron microscope (image reproduced from Kuntsche et al., 2011 [148]).

1.4.4 Confocal laser scanning microscopy

A confocal laser scanning microscopy (CLSM) is a kind of optical imaging microscope, which can increase optical resolution and contrast using a spatial filter to block out-of-focus light, and it also uses fluorescence to generate an image. [149, 150] In an image forming process, the sample is scanned point by point by the light beam. Only the focused point light source is collected by the detector, and the out-of-focus light is not collected. [149, 151] For every measurement, three types of images, including optical, fluorescent and merged, can be obtained. CLSM is widely used in biological applications, such as cell biology and genetics. It is also used in nano-crystal imaging and spectroscopy. [152] In our research, the confocal laser scanning microscopy we used is a Leica TS confocal scanning system (Leica, Germany) equipped with a 63×/1.4 oil immersion objective.

1.4.5 Fluorescence microscopy

A fluorescence microscope is a kind of optical microscope, which uses fluorescence or phosphorescence for reflection and absorption to study properties of samples. Actually, any microscope, which uses fluorescence to generate an image, is referred to as a fluorescence microscope, including the confocal microscope introduced above. [153, 154] Fluorescence microscopy is widely used in biological studies for observation. [155] For every measurement, the operator can get both optical and fluorescent images. In our research, the fluorescence microscope we used is a Nikon EFD-3 fluorescence microscope with a flourescein isothiocyanate filter (excitation 510-560 nm, dichroic mirror 575 nm, barrier filter 590 nm).

1.4.6 Surface plasmon resonance

Surface plasmon resonance (SPR) is a strong electromagnetic oscillation of electrons which can happen at a metal/dielectric interface. [156] The SPR wave is very sensitive to the refractive index change between the metal and the dielectric. [157] There is an incident light in a typical SPR. When the energy and momentum of the incident light matches the electromagnetic wave of SPR, then a surface plasmon resonance occurs at the interface of the two media provided their dielectric constants are of opposite signs - this occurs for a metal (typically gold or silver) and a dielectric. [158] The light energy from the incident photons links with the electrons in the metal to create a sharp resonant dip in the light intensity. In addition, the propagation of the surface plasmon waves is determined by the

refractive index of the surrounding medium. Therefore, even if there is a very small change of the refractive index near the metal layer, SPR provides a measurable shift in the resonance. [156-159] Fig. 1.13 shows a typical configuration for the exciting surface plasmon, which is the most widely used optical platform for SPR sensing. [160] In the diagram, *q* stands for the metal thickness, *x* and *y* refer to the coordinate system, ε_p, ε_m, ε_d are the permittivity of the prism, metal and dielectric respectively. [160]

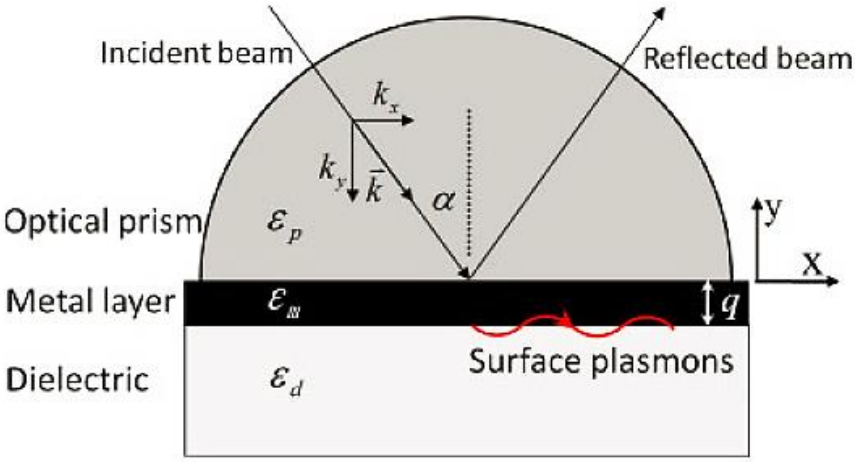

Fig. 1.13 Typical configuration for exciting surface plasmon. In the diagram, "q" is the metal thickness, "x" and "y" refer to the coordinate system, "ε_p" , "ε_m", "ε_d" are the permittivity of the prism, and metal and dielectric respectively (image reproduced from Huang et al., 2012 [160]).

As mentioned above, SPR is very sensitive to the refractive index of materials near a thin metal film, so it is used for many biosensor applications. Label-free SPR sensors have been developed and commercially used in recent years. It is possible to detect small concentrations of analytes, in a wide range of medical and scientific applications. [161-163] SPR biosensors have also been used to study the interactions of numerous biomolecules, such as deoxyribonucleic acid, proteins, enzymes, antibodies, and antigens. [164, 165] For examples, an SPR biosensor converts a biological reaction into a physiochemical signal such as a colour change or electric potential variation, by binding the surface with an analyte and a capture ligand.

In our research, we used a custom-made spectral SPR biosensor to monitor the targeting experiment. [54, 166] The biosensor setup was built and provided by Prof Lisa Hall from the Analytical Biotechnology Group at the University of Cambridge. Fig. 1.14 shows the schematic diagram of the spectral SPR sensor.

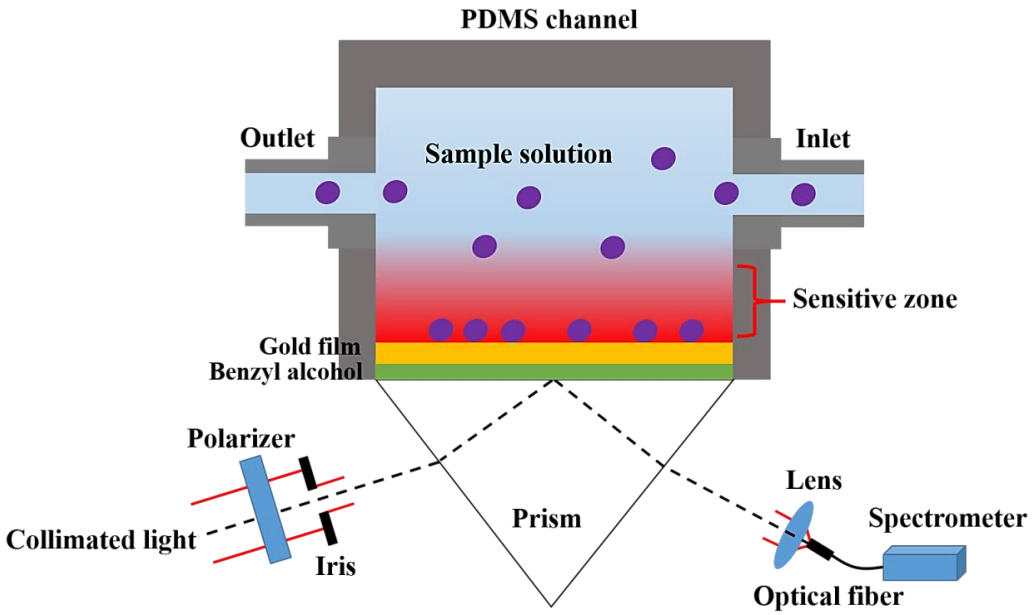

Fig. 1.14 Schematic diagram of a custom-made spectral SPR sensor (device provided by Prof Lisa Hall from the Analytical Biotechnology Group at the University of Cambridge).

1.4.7 Dynamic light scattering

Dynamic light scattering (DLS) is used to determine the size distribution of particles in suspension. This method analyses intensity fluctuations of the light scattered due to motion in bulk materials. The theory of DLS utilizes a model system of spherical particles in a sample solution. [167] DLS is used in many fields, such as chemistry, biochemistry, and physics to determine the size distribution of particles like polymers, proteins and colloids in solution or suspensions. [168, 169] In our research, the diameter of the latex particles was determined by a Brookhaven ZetaPALS dynamic light scattering.

1.4.8 Ultrasound device

Ultrasound uses sound waves with frequencies higher than the upper audible limit of human hearing. Normally, ultrasound devices provide frequencies from 20 kHz up to several gigahertz and are used in many medical applications, such as ultrasound therapy [170] and diagnosis for some disease treatment [171].In our research, the ultrasound device was provided by Prof Gleb Sukhorukov from Queen Mary, University of London. We used an ultrasonic probe operating at a frequency of 20 kHz and power output of 50 W to monitor capsule rupture. The treatment was performed using an ultrasonic processor GEX 750 (Sonics & Materials Inc., USA). In addition, we employed high intensity focused ultrasound

(HIFU) to break capsules. High intensity focused ultrasound is a non-invasive therapeutic technique, which uses high frequency sound waves to heat or destroy tissue. [172] High intensity beams can be produced using a lens to focus a suitable acoustic frequency to regions for tissue destruction. This method has been reported to reach at depths of up to at least 10 cm with exposure times of the order of 1 s. [173] Fig. 1.15 shows the home-made high intensity focused ultrasound device, which is also built and provided by Prof Gleb Sukhorukov. This set-up can produce ultrasound with a frequency of 2.65MHz and power output of 6 W, similar to some medical devices [174].

Fig. 1.15 Home-made high intensity focused ultrasound device (image provided by Prof Gleb Sukhorukov).

1.4.9 Ultraviolet-visible spectrophotometry

Ultraviolet-visible spectrophotometry (UV-Vis) is a technique for absorption or reflectance spectroscopy in the ultraviolet-visible spectral region. It uses light in both the visible and adjacent ranges. [175] For measuring, organic constituents are normally determined with UV light sources, and the visible part of the absorption spectrum is usually utilized for inorganic spectrophotometric analysis. [176] UV-Vis can be used for analytical chemistry of different analytes and the analysis is normally carried out in solution, but solids and gases may also be measured. [177] In our research, a UV-Vis spectrophotometer equipped with a tungsten lamp (Thermo Scientific, model Hελios Gamma) was used for spectrometry measurements. The dyed samples were characterized by spectrophotometry in 10 mm path length polystyrene cuvettes.

1.4.10 Raman microscopy

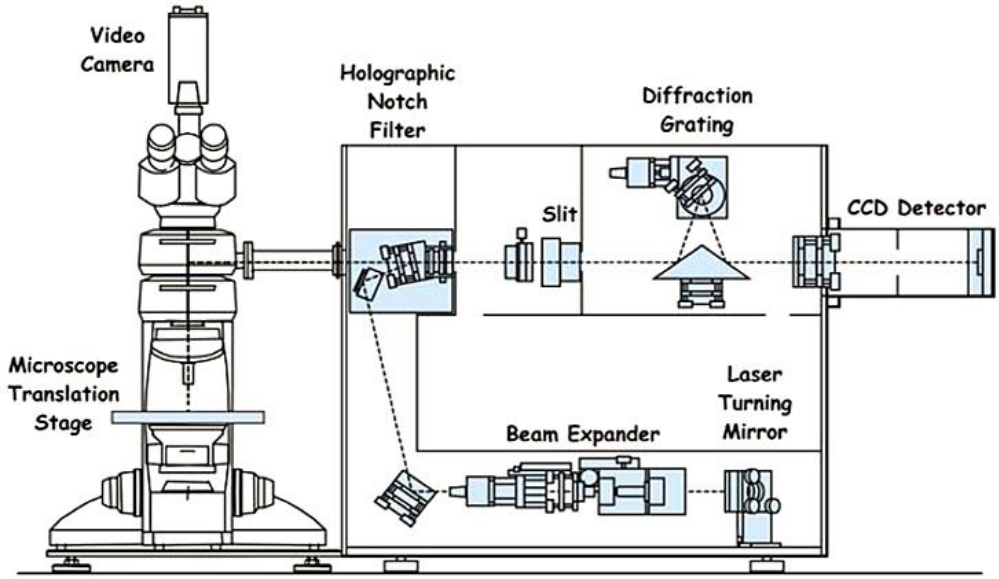

Fig. 1.16 Schematic of a research-grade Raman microscope (image reproduced from Smith & Clark, 2004 [180]).

Raman spectroscopy is a technique for molecular identification, which provides information about functional groups. It is commonly used in chemistry applications to test the composition, bonding, chemical environment, phase, and crystalline structure of sample materials. [178, 179] Fig. 1.16 shows a schematic of a research-grade Raman microscope. [180] In a typical Raman microscope, samples are examined visually at high magnification, so specific areas can be chosen and analysed. In our research, to analyse the colloidosomes before and after modification, a LabRAM HR Evolution Raman Spectroscopy (HORIBA Scientific) was used.

1.5 Aims and objectives

The purpose of this research is to prepare colloidosomes coated with a metal shell, such as silver or gold, which make the particulate polymer shell colloidosomes impermeable. Then we investigated the loading of drugs into the capsules and the use of them as drug carriers. Fig. 1.17 shows a schematic representation of microcapsule encapsulation and release of small molecules. Particulate polymer shell capsules leak small molecules, whereas metal coated capsules remain impermeable and can be ruptured with ultrasound.

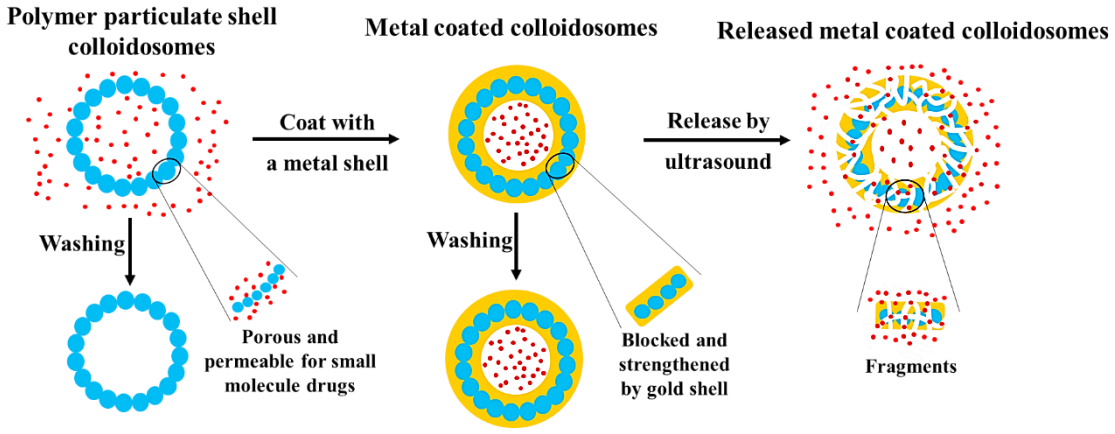

Fig. 1.17 Schematic representation of microcapsules encapsulation and release of small molecules.

The specific objectives were as follows:

1. To prepare colloidosomes coated with a metal shell, such as silver or gold, which can make the particulate polymer shell colloidosomes impermeable.

2. To load cargos in the impermeable colloidosomes and explore release mechanisms and methods.

3. To set up a targeting model using a biosensor to see if the colloidosomes are able to be used as a targeted carriers for small molecule materials.

4. To load different drugs, such as an anticancer drug or antibiotic, and together with a cell viability experiment, to see if the colloidosomes are able to be used as drug carriers.

Chapter 2.

Preparation of silver and gold coated colloidosomes

The results from this chapter have been published in European Polymer Journal, Langmuir, and Soft Matter:

Qian Sun, Alexander F. Routh. *Aqueous Core Colloidosomes with a Metal Shell*. European Polymer Journal, 2016, 77: 155-163.

Qian Sun, Yao Du, Ziyan Zhao, Elizabeth A. H. Hall, Hui Gao, Gleb B. Sukhorukov, Alexander F. Routh. *Functional Silver-Coated Colloidosomes as Targeted Carriers for Small Molecules*. Langmuir, 2017, 33(15): 3755-3764.

Qian Sun, Yao Du, Elizabeth A. H. Hall, Dong Luo, Gleb B. Sukhorukov, Alexander F. Routh. *A Fabrication Method of Gold Coated Colloidosomes and Their Application as Targeted Drug Carriers*. Soft Matter, 2018, 14(14): 2594-2603.

2.1 Introduction

This chapter describes the method for fabrication of aqueous core colloidosomes with a silver shell as well as a gold shell. This seals the core and makes the shell impermeable. The silver coated colloidosomes were prepared by making an aqueous core capsule with a particulate polymer shell and then adding $AgNO_3$, surfactant and L-ascorbic acid to form a second shell. The gold coated colloidosomes were prepared by making an aqueous core capsule with a particulate polymer shell and then adding $HAuCl_4$, surfactant and L-ascorbic acid. To break the shells, ultrasound treatment was used. Then we used the silver or gold

coated colloidosomes to encapsulate cargos, such as dye solution, to test the release mechanisms.

2.2 Experimental section

2.2.1 Materials

The water used in all experiments was deionized of resistivity 18.2 MΩ•cm produced by a Pure Lab Ultra apparatus. The vortex mixer was a TopMix FB15024 (Fisher Scientific). The dialysis tubing was Spectra/Por Dialysis membrane with a MWCO of 12000-14000 (Spectrum Laboratories). Sodium dodecyl sulfate (SDS, Fisher Scientific), Allura Red AC (Sigma-Aldrich), L-ascorbic acid (Fisher Scientific), silver nitrite (Fisher Scientific), and gold chloride (Fisher Scientific) were used as received without purification. Here, Allura Red AC was used as a dye to test the release. The reason we used Allura Red AC is that this dye does not affect the colloidosome synthesis process, it is small enough to diffuse from the porous particulate polymer shells and it is not very pH sensitive. Fig. 2.1 shows the chemical structure of Allura Red AC.

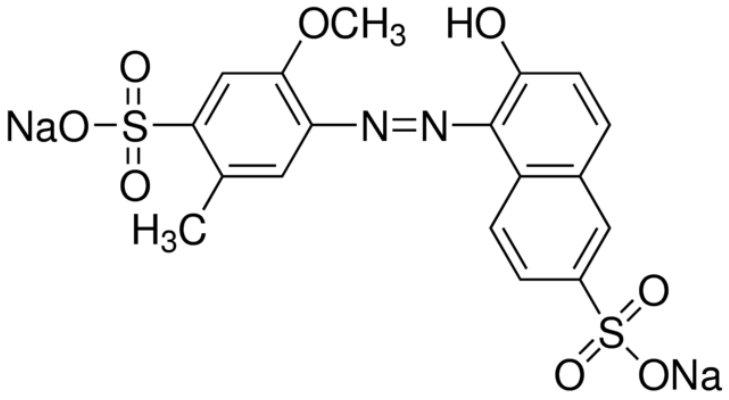

Fig. 2.1 Chemical structure of Allura Red AC.

Poly (methyl methacrylate-co-butyl acrylate) latex particles were synthesized by Polly Keen via emulsion polymerization [10]. Briefly, a pre-emulsion of seed particles (1.33 wt%) plus surfactants was made up in the reactor. Then the main process was carried out in semi-batch mode with a programmed feed to the reactor. The monomer and initiator were gradually fed into the reactor over 4 hours. The aqueous suspension of methyl methacrylate (MMA) and butyl acrylate (BA) were in the ratio of 65:35 by weight. Finally, the monomer chasers

(redox initiators) were added at the end for reaction, and thus, devolatilize, any residual monomers and/or low molecular weight oligomers from the product via further polymerisation. Fig. 2.2 shows the chemical structure of methyl methacrylate and butyl acrylate.

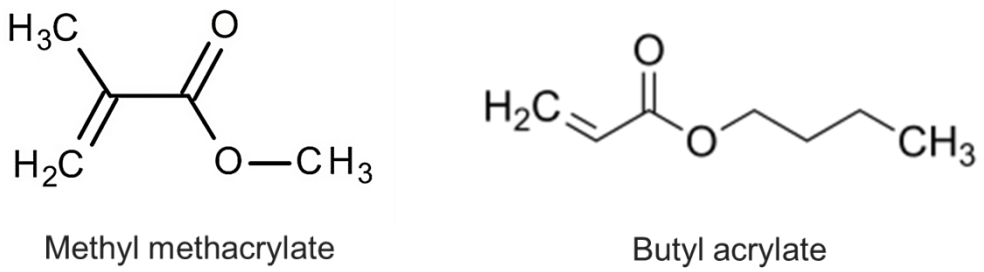

Fig. 2.2 Chemical structure of methyl methacrylate and butyl acrylate.

The diameter of the latex particles was determined by dynamic light scattering using a Brookhaven ZetaPALS. The measured diameter was 153 nm. The glass transition temperature of poly (methyl methacrylate-co-butyl acrylate) was found using differential scanning calorimetry to be 35 °C.

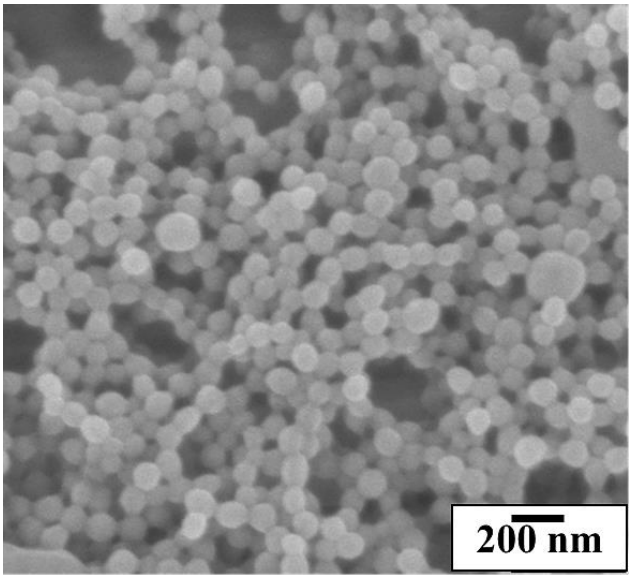

Fig. 2.3 SEM images of P(MMA-co-BA) latex particles .

To produce particulate polymer shell colloidosomes, an aqueous suspension of the particles was emulsified in sunflower oil and fused by sintering at 50 °C for 1 h. After sintering, the latex particles melt into smooth shells, and can be used as base capsules for forming a metal shell. Fig. 2.4 shows SEM images of particulate polymer shell colloidosomes. The diameter of the smooth particulate polymer shell capsules in Fig. 2.4a and b was between 0.7 μm and

2 μm and the average diameter was around 1.2 μm. The thickness of the particulate polymer shells is the diameter of a single latex particle, about 153 nm.

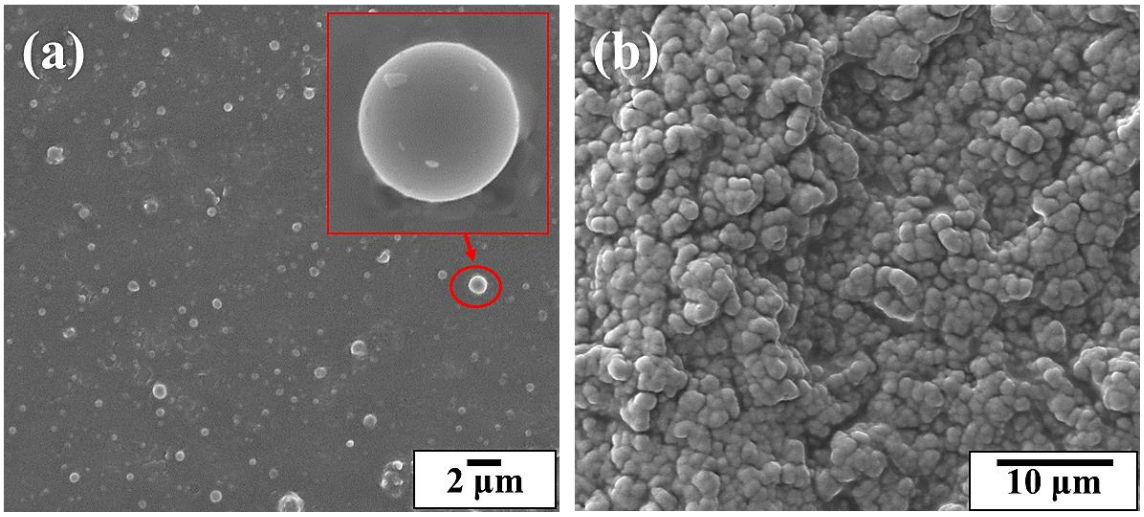

Fig. 2.4 SEM images of particulate polymer shell colloidosomes: (a) low concentration, (b) high concentration.

2.2.2 Fabrication of silver coated colloidosomes

Fig. 2.5 shows a typical method for fabrication of the silver coated colloidosomes. 4 mL Span 80 was mixed with 200 mL sunflower oil in a 400 mL beaker using a Silverson high shear mixer (model SL2). 2 mL of 5.6 wt% latex particles was then added to the sunflower oil over 30 s. Cyclic mixing was employed, whereby homogenization was carried out for 60 s, followed by 30 s rest. This was repeated five times. This process enabled emulsions droplets to be more uniform and smaller, since in every cycle the emulsions droplets will be cut into smaller ones. After emulsification, the emulsion was heated in a water bath at 50 ± 0.5°C. Once the temperature inside the emulsion tubes reached 50 ± 0.5 °C, the timer was started, and the emulsions were sintered for 1 h. The aim of this process is to melt the latex particles into smooth shells.

After sintering, 20 mL of the liquid mixture was transferred into an empty centrifuge tube and centrifuged at 2500 rpm for 10 min at 20°C. The waste oil, together with the small volume of water which had leaked out from the colloidosomes was removed via pipetting. After removing the oil phase, 24 mL of a 0.1 wt % aqueous solution of $AgNO_3$ and 2 mL of a 1 wt% aqueous solution of SDS were added, and the mixture was agitated using the vortex mixer. SDS was used to avoid colloidosome aggregation. Addition of 2 mL of a 15 wt% L-ascorbic acid aqueous solution started the silver reduction reaction, which was allowed to

proceed for 1 h. To obtain the final aqueous dispersion of silver coated microcapsules, the mixture was centrifuged, at 20°C and 1500 rpm for 2 min followed by redispersal in a 0.1 wt% SDS solution, used to avoid aggregation.

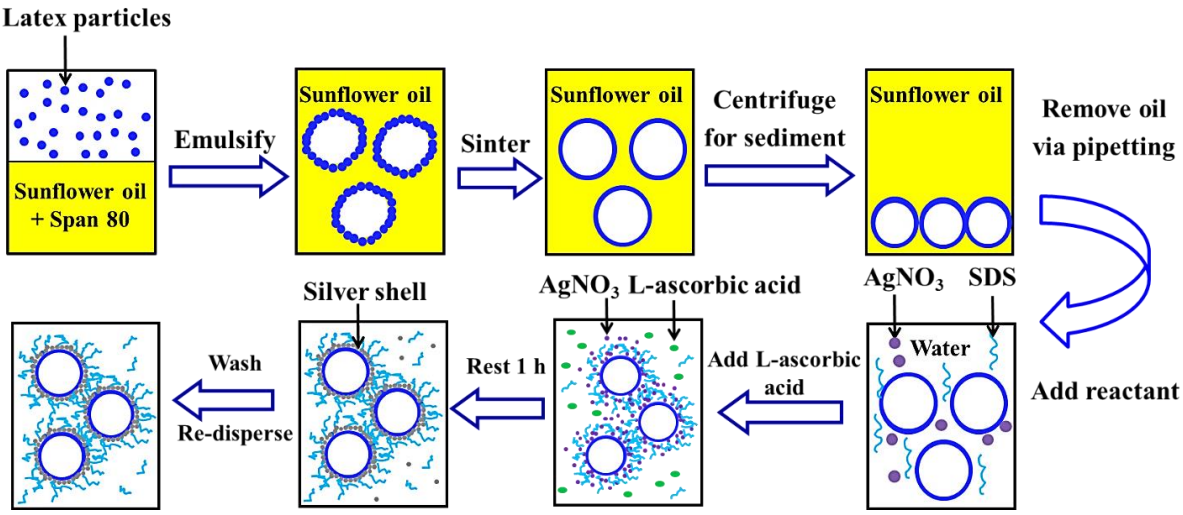

Fig. 2.5 A typical method for fabrication of the silver coated colloidosomes.

2.2.3 Fabrication of gold coated colloidosomes

Fig. 2.6 shows a typical method for fabrication of gold coated colloidosomes. The method was almost the same as producing silver coated colloidosomes. The difference is that 20 mL of a 1 wt % aqueous solution of $HAuCl_4$ and 2 mL 1 wt% aqueous solution of SDS were added to the tube to make the gold shells, and the microcapsules were redispersed in the aqueous phase using a vortex mixer. Then 2 mL of a 15 wt% L-ascorbic acid solution was added to the tube and rested for 1 h, to allow the gold reduction reaction to occur. After the gold reduction reaction, the mixture was centrifuged at 1500 rpm for 2 min at 20℃ to recover the sediment and the supernatant was removed via pipetting. The resulting gold coated microcapsules were washed and redispersed using a 0.1 wt% SDS solution, which is used to avoid aggregation of the gold coated colloidosomes.

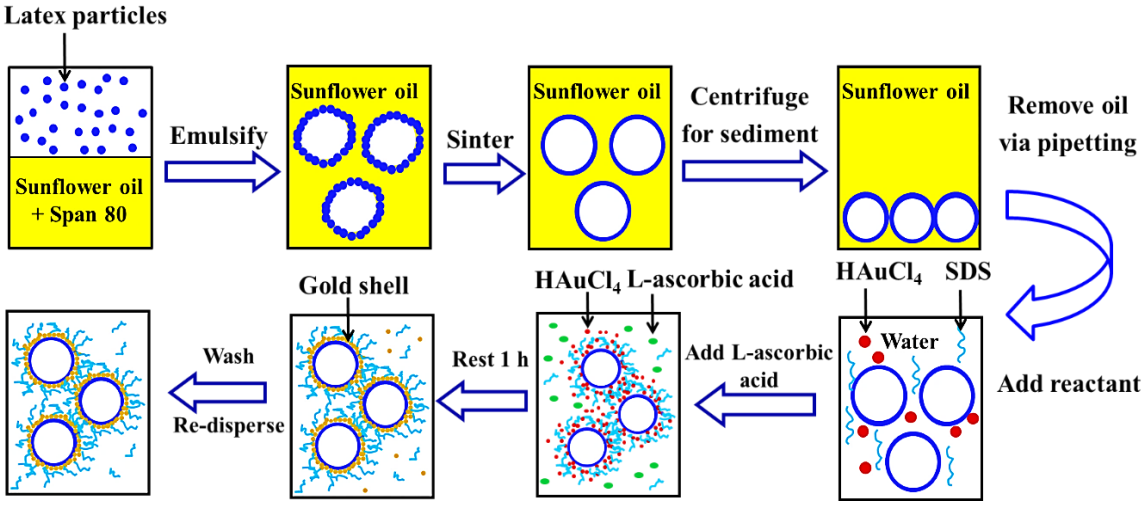

Fig. 2.6 A typical method for fabrication of the gold coated colloidosomes.

2.2.4 Release by ultrasonic treatment

An ultrasonic probe, operating at a frequency of 20 kHz and power output of 50 W, was used to release the cargo from the colloidosomes, as shown in Fig. 2.7. Different times of application were employed using an ultrasonic processor GEX 750 (Sonics & Materials Inc., USA). The temperature change was kept below 5°C by using an ice bath.

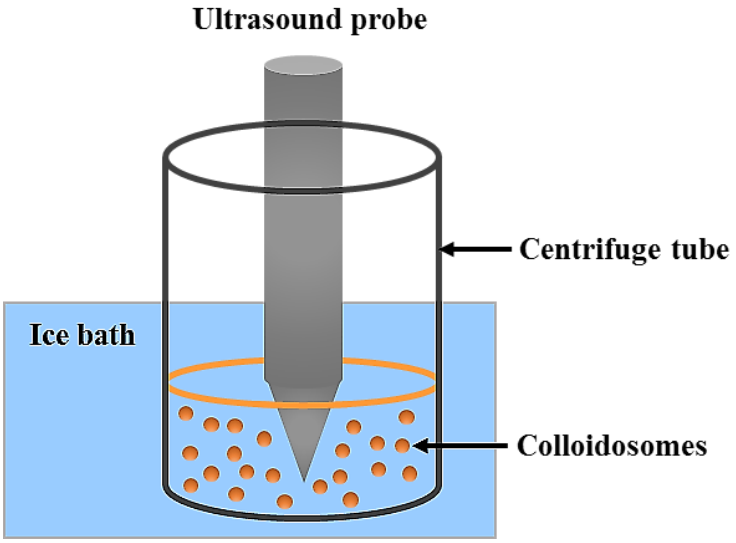

Fig. 2.7 Schematic of ultrasound set up for releasing the metal shell colloidosomes.

2.2.5 Dye encapsulation and dye release

To encapsulate dye in the silver shell colloidosomes, a mixture of 5.6 wt% latex particles and 2 wt% Allura Red AC dye solution was prepared. Then 2 mL of this mixture was added

into a mixture of 4 mL Span 80 and 200 mL sunflower oil for emulsification and sintering. The waste oil phase was removed and the colloidosomes containing Allura Red AC dye were redispersed in $AgNO_3$ solution, with subsequent addition of the L-ascorbic acid and SDS solutions, to form the silver shell, sealing the capsules.

To measure the dye release, 20 mL samples were introduced into a dialysis tubing which was then kept into a larger container with 450 mL of water. A magnetic stirrer was employed and 3 mL samples from the container were taken for spectroscopic characterization at regular intervals. After measurement, the samples were transferred back to keep the same volume of the water for dye release.

The steps followed to encapsulate the dye solution in the gold shell colloidosomes were the same as above. The only difference was that the waste oil phase was removed and the colloidosomes containing Allura Red AC dye were redispersed in $HAuCl_4$ solution, with subsequent addition of the L-ascorbic acid solution and SDS solution, to form the gold shell. All the other capsule preparation steps are the same as reported above.

2.2.6 Sample characterization

The colloidosomes were imaged by scanning electron microscopy (SEM). A Zeiss X-beam FIB SEM was used at an accelerating voltage of 5.0 kV. The same instrument was used for energy-dispersive X-ray spectroscopy (EDX), to determine the elemental composition of the colloidosomes. In this case an accelerating voltage of 10.0 kV was used. A drop of particle suspension was air-dried on a stainless steel SEM stub overnight. The particulate polymer shell colloidosomes samples were then gold-coated using a BioRad SEM coating system sputter coater, in an argon environment at 1×10^{-3} mbar and 10 mA for 180 s. The silver and gold coated colloidosome samples were imaged without any treatment.

The colloidosomes were also imaged by transmission electron microscopy (TEM). An FEI Philips Tecnai 20 TEM was used at 200 kV (Tungsten, LB6) high-energy electron beam. A drop of colloidosome sample was added onto a TEM grid and then transferred to the specimen holder.

A UV-Vis spectrophotometer equipped with a tungsten lamp (Thermo Scientific, model Heλios Gamma) was used for spectrometry measurements. The dyed samples were

characterized by spectrophotometry in 10 mm path length polystyrene cuvettes. The absorbance value at 500 nm was recorded using ultra-pure water as the reference.

Confocal laser scanning microscopy (CLSM) images were captured with a Leica TS confocal scanning system (Leica, Germany) equipped with a 63×/1.4 oil immersion objective at an excitation wavelength of 480 nm and emission wavelength of 500-650 nm. Fluorescent images were also captured with a Nikon EFD-3 fluorescence microscope by a flourescein isothiocyanate filter.

2.3 Results and discussion

2.3.1 Silver coated colloidosome optimization

In this section, we present how we found the optimized reaction conditions of silver coated colloidosomes. To make silver shells, a common and easy method is to prepare silver particles using chemical reduction, since the experimental conditions of this method are simple and the reaction time of $AgNO_3$ is relatively short. Various experimental parameters were explored and optimized in this part. Table 2.1 shows different reaction conditions of silver shell for optimization.

Table 2.1 Different reaction conditions of silver shell for optimization.

Optimization conditions	**Reaction conditions**
Reducing agent	Na_3Citrate, L-ascorbic acid
Concentration of $AgNO_3$ solution	0.1 wt%, 0.25 wt %, 0.5 wt%, 1.0 wt%
Concentration of L-ascorbic acid solution	5 wt%, 10 wt%, 15 wt %
Placement of reactants	Make L-ascorbic acid-core colloidosome first, then add $AgNO_3$ to form silver shells Make water-core colloidosome first, then add $AgNO_3$ and L-ascorbic acid to form silver shells

Reducing agent. We chose Na_3Citrate and L-ascorbic acid as reducing agents. These are commonly used for reducing metals, such as silver and gold. Initially, we used one reducing agent in the core of colloidosome, then added $AgNO_3$ solution. The aim of

this design is to force the reaction to happen on the surface of the polymer shells, since the inner phase reducing agent will diffuse from the polymer shells and reach the outer phase $AgNO_3$ solution (1.0 wt%). To make a reducing agent core for the particulate polymer shell colloidosomes, the latex particle suspension (11.2 wt%) was mixed with a reducing agent to get a mixture, which contained 5.6 wt% latex particles and a certain concentration of reducing agent. All the other capsule preparation steps are the same as reported in section 2.2.2.

When using Na_3Citrate (20 wt%) as a reducing agent at 60 °C, there was no obvious silver forming reaction, as shown in Fig. 2.8a. A high temperature is required when using Na_3Citrate to form silver particles. Alternatively, we used $AgNO_3$ solution in the core and Na_3Citrate in the wash solution to form silver shells, using the same experimental conditions, but there was still no obvious silver forming reaction. When using L-ascorbic acid (15 wt%) as a reducing agent, there were some silver particles forming either in the solution or on the polymer shells, as shown in Fig. 2.8b. We also used $AgNO_3$ solution in the core and L-ascorbic acid in the wash solution to form silver shells, using the same experimental conditions, but there were very few silver particles forming even after 1 h, as shown in Fig. 2.8c.

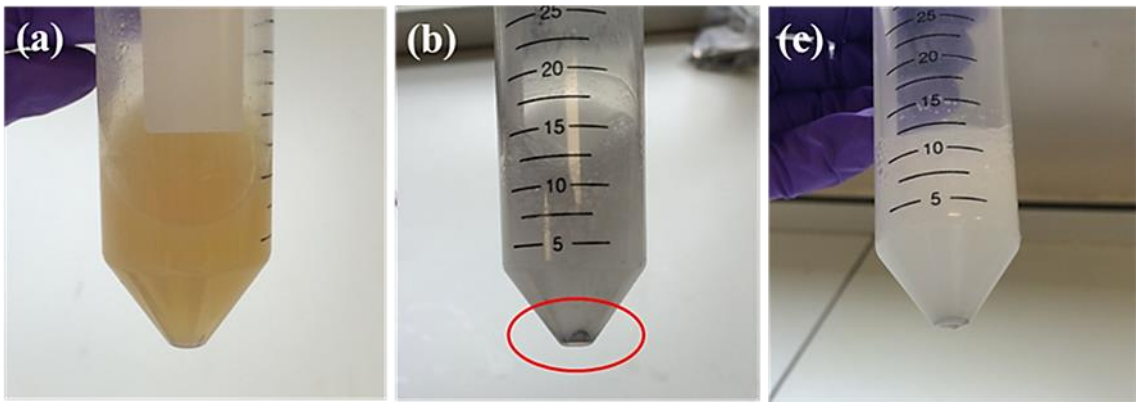

Fig. 2.8 Experimental phenomenon when using (a) Na_3Citrate, and (b) L-ascorbic acid as reduction agents in the core of particulate polymer shell to form silver shells, and (c) when using $AgNO_3$ solution in the core of particulate polymer shell to form silver shells.

Fig. 2.9 shows the SEM and EDX images of the silver shell colloidosome sample, which was made with L-ascorbic acid as the reducing agent in the core of the polymer shells. As can be seen, part of the particulate polymer shells was covered by silver particles, while there were also some broken polymer shells. As shown in Fig. 2.9b, the large silver peaks suggest silver particles are surrounding the colloidosome surface. The carbon peak arises from the particulate polymer shell, and the aluminium peak arises from the SEM stub. Based on this result, we chose L-ascorbic acid as the reducing agent for further optimization.

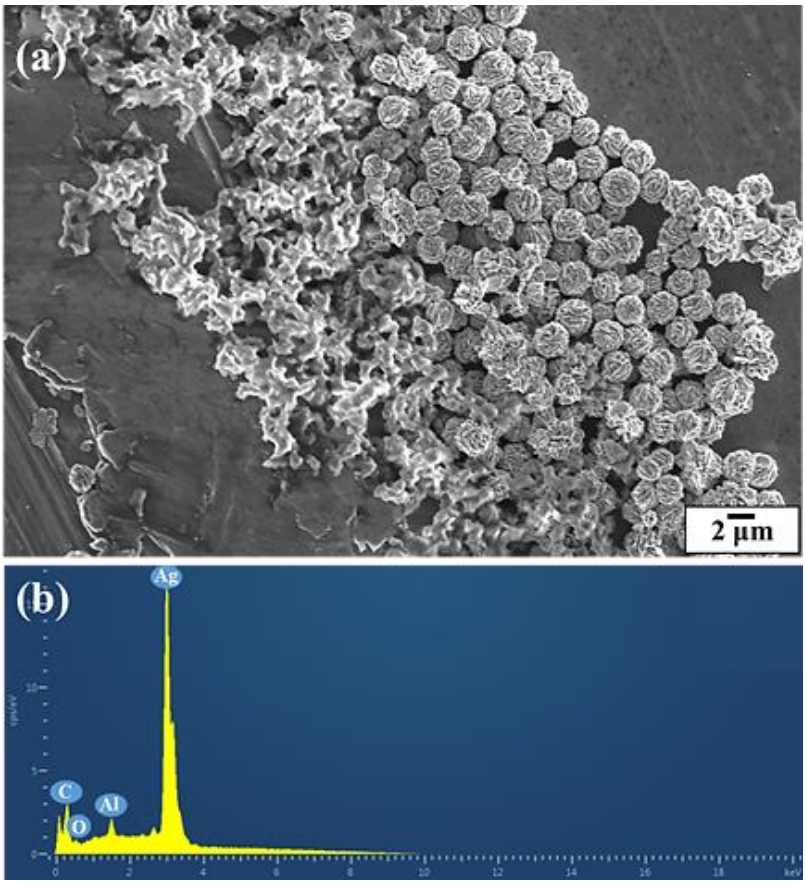

Fig. 2.9 (a) SEM and (b) EDX images of the silver shell colloidosomes sample, which was made by L-ascorbic acid as reduction agents in the core of polymer shells.

Concentration of $AgNO_3$ solution. In this section, the concentration of $AgNO_3$ solution was varied: 0.1 wt%, 0.25 wt %, 0.5 wt%, and 1.0 wt%. We did not use too low concentration of the $AgNO_3$ solution, only to 0.1 wt%, considering the silver shell formation. All particulate polymer shell colloidosomes were made with a 10.0 wt% L-ascorbic acid-core, and the reaction kept at room temperature for 1 h. Fig. 2.10 shows the SEM images of the silver shell colloidosomes using different concentrations of $AgNO_3$ solution. It can be seen in Fig. 2.10a that silver coated colloidosomes were found. The silver particles grow on the surface of the polymer shells to form silver shells, and they were

homogenous at a concentration of 0.1 wt%. As the concentration of $AgNO_3$ solution progressed to 0.25 wt%, the silver shells were still to be found, but some line-like silver particles grew as well. Once the concentration of $AgNO_3$ solution reached 0.5 wt% and 1.0 wt%, as shown in Fig. 2.10c and d respectively, the sizes of the silver coated colloidosomes were uneven, and there were some line-like silver particles and broken polymer shells forming. So, based on this result, we chose 0.1 wt% $AgNO_3$ solution for further optimization.

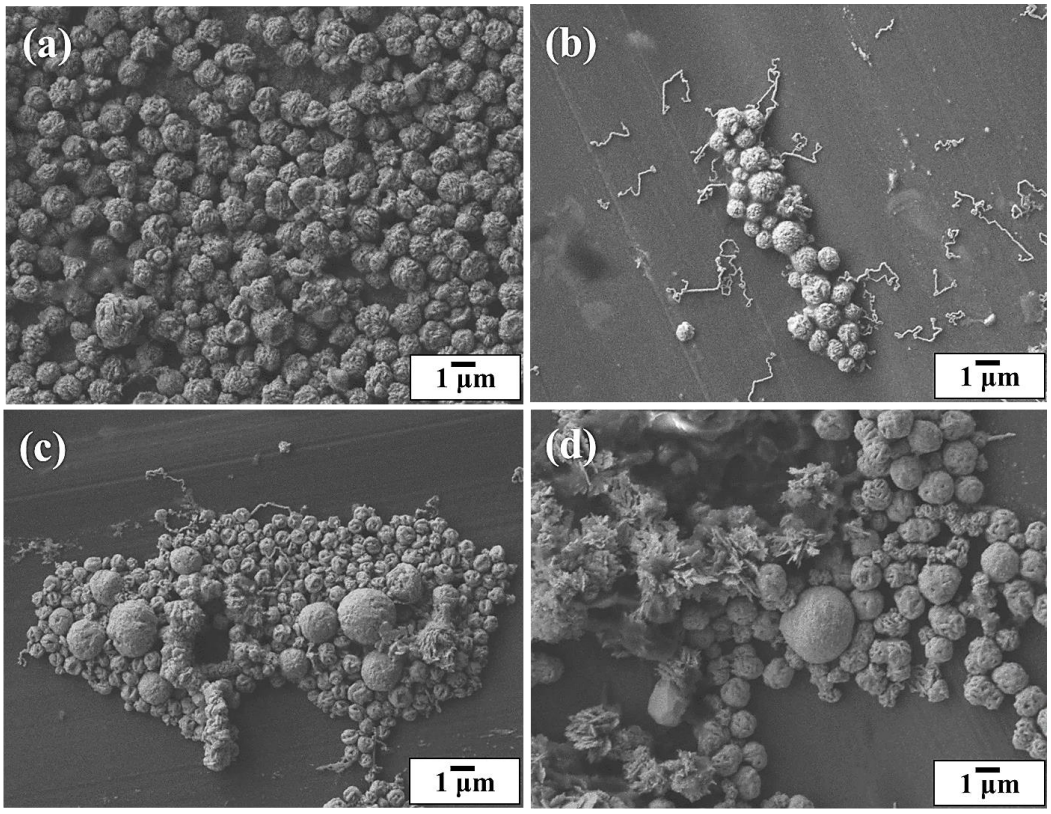

Fig. 2.10 SEM images of the silver shell colloidosomes using different concentrations of $AgNO_3$ solution: (a) 0.1 wt%, (b) 0.25 wt %, (c) 0.5 wt%, and (d) 1.0 wt%

Concentration of L-ascorbic acid solution. In this section, we made different concentrations of L-ascorbic acid-core particulate polymer shell colloidosomes: 5 wt%, 10 wt %, and 15 wt%. Considering the solubility of L-ascorbic acid in water, we did not try a higher concentration. The concentration of $AgNO_3$ solution was 0.1 wt%, and the reaction was kept at room temperature for 1 h. Fig. 2.11 shows the SEM images of the silver shell colloidosomes using different concentrations of L-ascorbic acid. When the concentration of L-ascorbic acid was 5 wt%, the silver coated colloidosomes were found and their morphology was spherical and homogenous. As the concentration of the L-ascorbic acid progressed to 10 wt% and 15 wt%, silver coated colloidosomes were still found with a larger size. In order to decide on a suitable concentration, we loaded the

Allura Red AC dye solution into the colloidosomes to see the permeability. The dye encapsulation steps are the same as reported in section 2.2.5. After loading dye solution and washing three times, we found the silver shell colloidosomes, which were produced using 5 wt% and 10 wt% of L-ascorbic acid, leaked dye solution and 15 wt% ones did not. In addition, samples using 15 wt% L-ascorbic acid have a higher dye encapsulation efficiency. So, based on this result, we chose 15 wt% L-ascorbic acid solution for further optimization. The details about dye encapsulation and dye release are discussed in section 2.3.4.

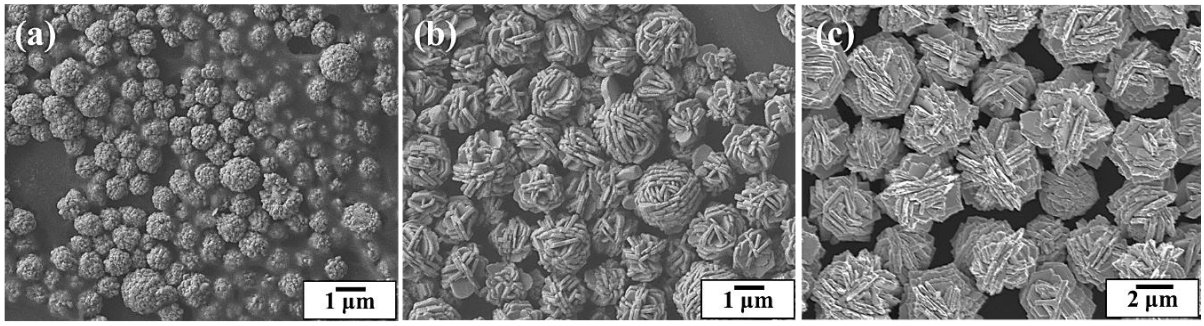

Fig. 2.11 SEM images of the silver shell colloidosomes using different concentrations of L-ascorbic acid: (a) 5 wt%, (b) 10 wt %, and (c) 15 wt%.

Placement of reactants. In this section, we made silver coated colloidosomes using different placement of reactants to see if we can improve the shell permeability and encapsulation efficiency of the colloidosomes. Initially, we made L-ascorbic acid-core colloidosomes, then added $AgNO_3$ to form silver shells. Alternatively, we made water-core colloidosomes, then added L-ascorbic acid and $AgNO_3$ to form the silver shell. In this experiment, the concentration of L-ascorbic acid was 15 wt%, and the concentration of $AgNO_3$ solution was 0.1 wt%. Fig. 2.12 shows the SEM images of the silver shell colloidosomes made using these two methods. The morphology of the colloidosomes are similar. The particulate polymer shells are fully covered by silver particles with a sheet shape. The silver particles made from water-core colloidosome are thinner than the ones made from L-ascorbic acid-core colloidosome. Then we encapsulated the Allura Red AC dye solution in the colloidosomes to see the permeability of the two type of silver shells. The details about dye encapsulation and dye release will be discussed in section 2.3.4. After loading dye solution and releasing them by the addition of acid, we found that although both types of colloidosomes are impermeable, the silver shell colloidosomes which were produced using a water-core colloidosome first, have a higher encapsulation efficiency nearly twice that of

the ones produced using L-ascorbic acid. So, based on this result, we chose to make water-core colloidosome first, then add $AgNO_3$ and L-ascorbic acid to form the silver shell.

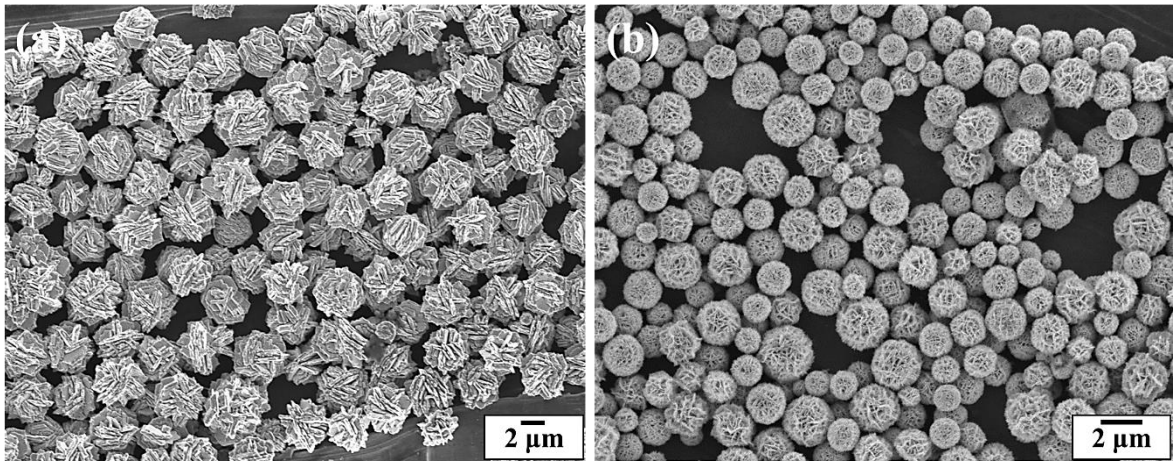

Fig. 2.12 SEM images of the silver shell colloidosomes reacting for different placement of reactants: (a) make L-ascorbic acid-core colloidosome first, then add $AgNO_3$ to form silver shells, and (b) make water-core colloidosome first, then add $AgNO_3$ and L-ascorbic acid to form silver shell.

Optimized reaction conditions. After optimization, we chose the following experimental conditions to make silver coated colloidosomes. Water-core particulate polymer shell colloidosomes were made first. 20 mL of the liquid colloidosome mixture was centrifuged, and the waste oil phase was removed via pipetting to get the particulate polymer shell colloidosome sediment. Then 24 mL of a 0.1 wt % aqueous solution of $AgNO_3$ and 2 mL of a 1 wt% aqueous solution of SDS were added. Addition of 2 mL of a 15 wt% L-ascorbic acid aqueous solution started the silver reduction reaction, which was allowed to proceed for 1 h. SDS was used to avoid the aggregation of silver coated colloidosomes.

Fig. 2.13a to d show the SEM, TEM, and EDX images of the silver coated colloidosomes produced with optimized conditions. As can be seen in Fig. 2.13a and b, the particulate polymer shells are fully covered by sheet-like silver particles, which form a film to improve the strength and impermeability of the colloidosomes. The silver coated colloidosome diameter is between 0.9 µm and 3.2 µm. The colloidosome sizes were measured using the software "Image J" based on the SEM images. For the TEM image, shown in Fig. 2.13c, the electrons cannot pass through the water core, and the edge of the silver particles sees a little melting, when using a high voltage of electrons. Fig. 2.13d shows the EDX image of the colloidosomes. The large silver peaks suggest that the silver particles are surrounding the colloidosome surface. The

strong carbon peak arises from the particulate polymer shell. The SEM stub is responsible for the aluminium peak and the other weak peaks arise from the surfactant. In addition, we used Allura Red AC-containing silver coated colloidosomes as a model. It can be seen from the fluorescent image in Fig. 2.13e that the dye solution can be successfully loaded on the surface of the colloidosomes or inside the colloidosomes. To test if the colloidosomes are impermeable or not, a dye release experiment was performed and discussed in section 2.3.4.

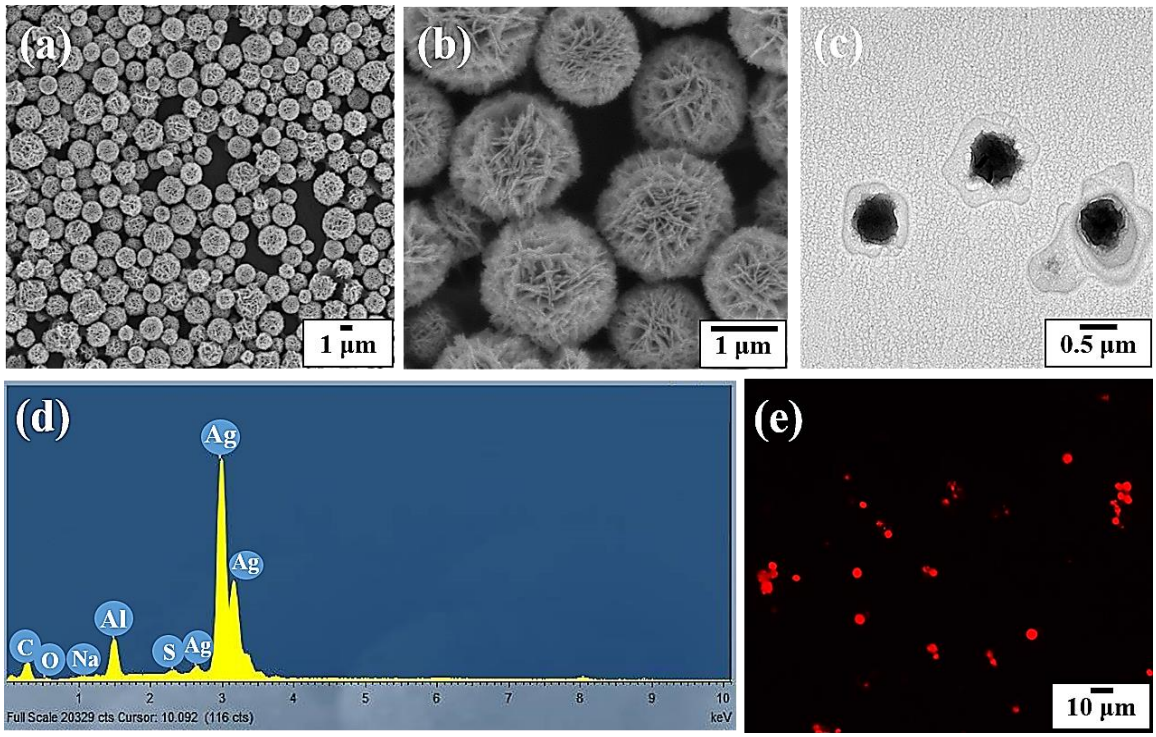

Fig. 2.13 SEM, TEM, EDX and fluorescence microscope images of the silver coated colloidosomes produced with optimized conditions: (a) low magnification SEM image of silver coated colloidosomes, and (b) high magnification SEM image of a few gold coated colloidosome, (d) EDX image of silver coated colloidosomes, and (e) fluorescence microscope image of dye-containing silver coated colloidosomes.

2.3.2 Gold coated colloidosomes optimization

In this section, we used the reduction method to prepare gold coated colloidosomes, which is similar to the silver shell system. Gold shells can be achieved by reducing $HAuCl_4$ solution with a reducing agent. Based on the previous silver coated colloidosomes synthesis process, various experimental parameters for gold shells,

including reducing agent and concentration of $HAuCl_4$ solution, were explored and optimized.

Reducing agent. Similar to the silver shell synthesis, we used Na_3Citrate and L-ascorbic acid as reducing agents. We chose Na_3Citrate as our first choice, since this reducing method is commonly used for producing gold particles. Firstly, we made water-core colloidosomes, then added Na_3Citrate and $HAuCl_4$ at 60 °C to form the gold shell. A high temperature is required when using Na_3Citrate to form gold particles. However, there were no gold shells forming, just some free gold particles in solution. Subsequently, we used 20 wt% Na_3Citrate in the core of the particulate polymer shell colloidosomes, then added 0.5 wt% $HAuCl_4$ solution at 60 ℃ to force the reaction to happen on the surface of the polymer shells. All the other colloidosome preparation steps are the same as reported in section 2.2.3.

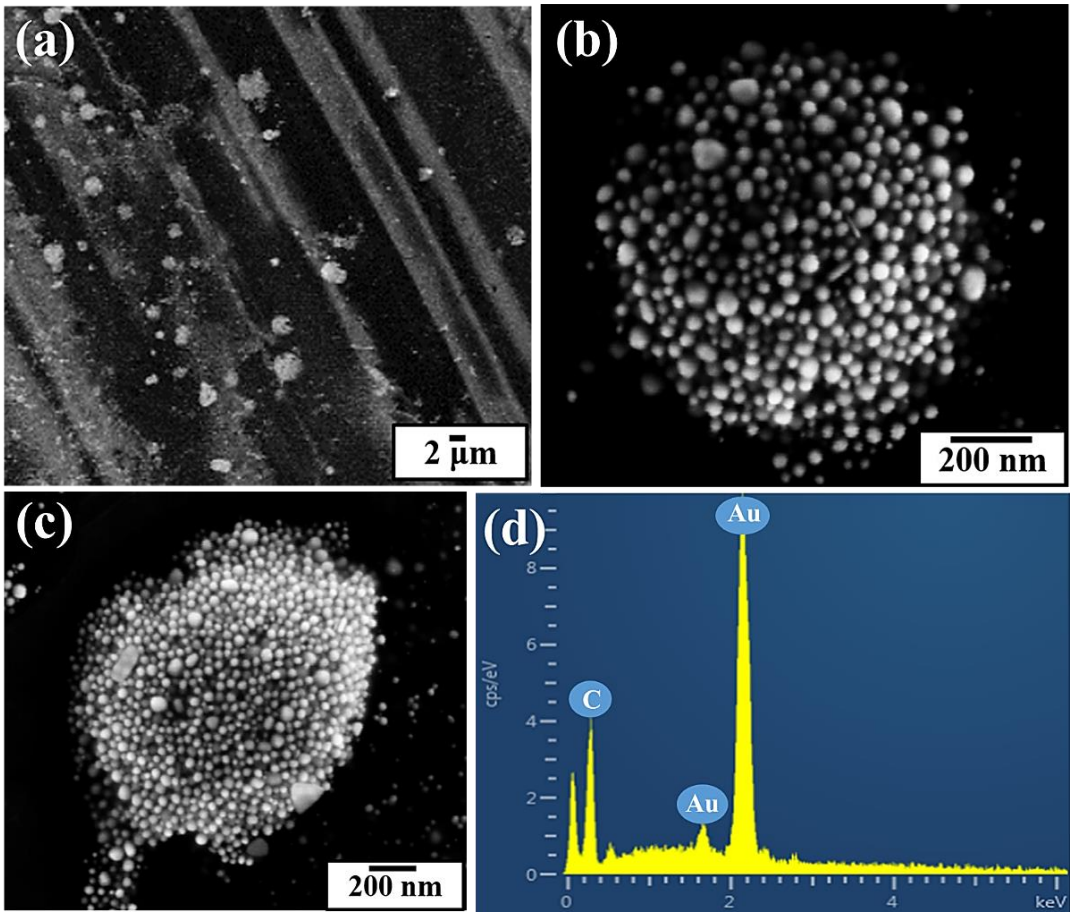

Fig. 2.14 SEM and EDX images of the gold coated colloidosomes, which were made using Na_3Citrate in the core of the particulate polymer shells to form gold shells: (a) low magnification SEM image of a few gold coated colloidosomes, and (b)(c) high magnification SEM images of single gold coated colloidosome, and (d) EDX images of a single gold coated colloidosome.

Fig. 2.14 shows the SEM and EDX images of the gold coated colloidosomes, which were made using Na_3Citrate in the core. It can be seen that the particulate polymer shell was covered with spherical gold nanoparticles. However, the gold particles just grew near the particulate polymer shells and did not form a film. The size of gold coated colloidosomes in Fig. 2.14b and c are about 1 μm and 1.3 μm. The size of the gold nanoparticles, which cover the polymer shells, is estimated at between 10 and 70 nm. The particle sizes are measured by the software "Image J". Fig. 2.14d shows the EDX image of the gold coated colloidosomes. The EDX result shows obvious gold peaks, which suggests that the nanoparticles surrounding the surface of the colloidosomes are gold. There is also a strong peak of carbon, which indicates that the polymer shell is under the gold.

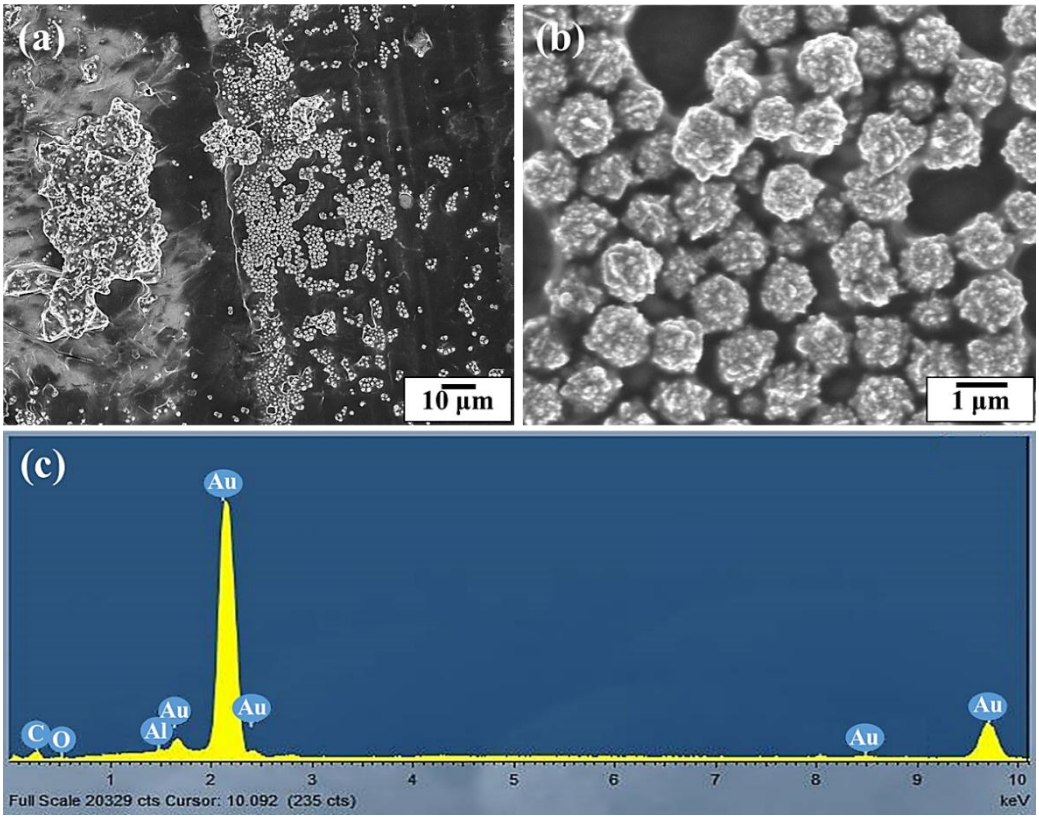

Fig. 2.15 SEM and EDX images of the gold coated colloidosomes, which were made using L-ascorbic acid in outer phase of particulate polymer shells to form gold shells: (a) low magnification, (b) high magnification, (c) EDX image of the gold coated colloidosomes.

Alternatively, we used L-ascorbic acid as the reducing agent. We made water-core colloidosome first, then added L-ascorbic acid and $HAuCl_4$ at room temperature to form a gold shell. In this experiment, the concentration of L-ascorbic acid was 15 wt%, and the concentration of $HAuCl_4$ solution was 0.5 wt%. All the other

colloidosome preparation steps are the same as reported in section 2.2.3. Fig. 2.15 shows the SEM images of the gold coated colloidosomes. As can be seen, most of the particulate polymer shells were fully covered by gold particles, while there were also heavily aggregated gold shells forming as shown in Fig. 2.15a. The EDX image in Fig. 2.15c shows obvious gold peaks, which suggests that the nanoparticles covering the surface of the polymer shells are gold. There is also a carbon peak and a weak oxygen peak, which arise from the polymer shells, and the SEM stub is responsible for the aluminium peak. Based on this result, we chose L-ascorbic acid as the reducing agent in the outer phase of particulate polymer shells to form gold shells for further optimization.

Concentration of $HAuCl_4$. In this section, different concentrations of $HAuCl_4$ solution were used: 0.1 wt%, 0.5 wt%, and 1.0 wt%. Based on the silver shell synthesis, water-core particulate polymer shell colloidosomes were made first, and a certain concentration of $HAuCl_4$ and 15.0 wt% L-ascorbic acid solution were added. The reaction was kept at room temperature for 1 h.

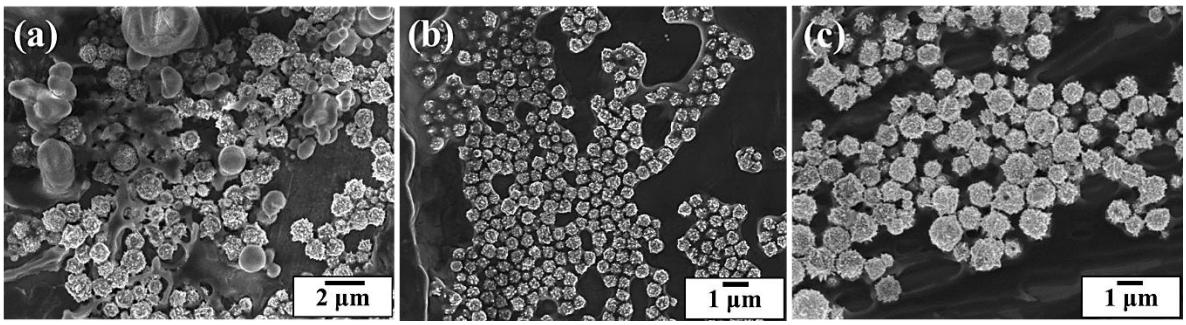

Fig. 2.16 SEM images of the gold coated colloidosomes, which were made using different concentration of $HAuCl_4$ to form gold shells: (a) 0.1 wt%, (b) 0.5 wt%, and (c) 1.0 wt%.

Fig. 2.16 shows the SEM images of the gold coated colloidosomes, which were made using different concentrations of $HAuCl_4$ to form gold shells. It can be seen in Fig. 2.16a that some gold coated colloidosomes were found, and there were still some uncoated polymer shells. This result suggests that the concentration is not high enough to form efficient gold shells. As the concentration of $HAuCl_4$ solution increased to 0.5 wt%, more gold shells were found, but there were some aggregated gold shells forming as well. Once the concentration of $HAuCl_4$ solution reached 1.0 wt%, the gold particles could homogenously grow on the surface of the polymer shells to form a gold shell without any aggregation, which is shown in Fig. 2.16c. Based on this result, we chose 0.1 wt% $HAuCl_4$ solution for producing gold coated colloidosomes and a dye release experiment was carried out to measure the permeability of the gold shell, as reported in section 2.3.4.2.

Optimized reaction conditions. After optimization, we chose the following experimental details to make gold coated colloidosomes. Water-core particulate polymer shell colloidosomes were made first. 20 mL of the liquid colloidosomes mixture was centrifuged and the waste oil phase was removed via pipetting to get the particulate polymer shell colloidosomes sediment. Then 20 mL of a 1.0 wt % aqueous solution of $HAuCl_4$ and 2 mL of a 1 wt% aqueous solution of SDS were added. Addition of 2 mL of a 15 wt% L-ascorbic acid aqueous solution started the gold reduction reaction which lasted for 1 h. SDS was used to avoid the gold coated colloidosome aggregation.

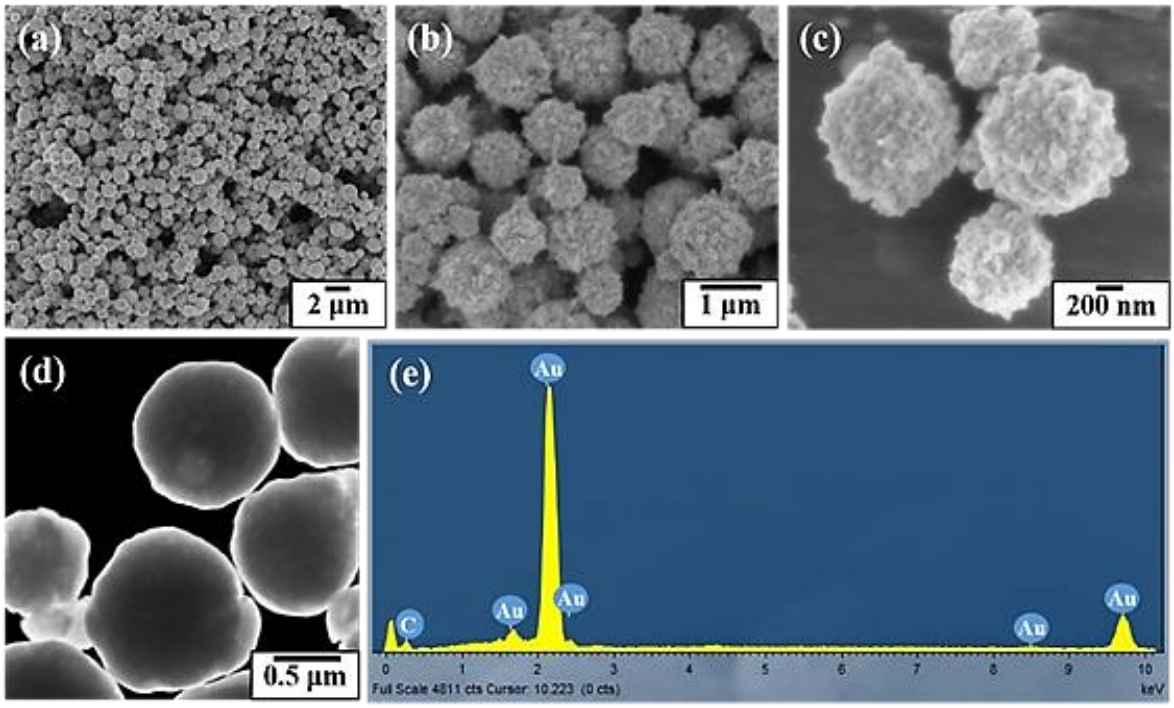

Fig. 2.17 SEM, TEM, and EDX images of the water core gold coated colloidosomes produced with optimized conditions: (a) (b) (c) different magnification SEM images of gold coated colloidosomes, (d) TEM image of a few gold coated colloidosomes, and (e) EDX image of gold coated colloidosomes.

Fig. 2.17 shows the SEM, TEM and EDX images of the gold coated colloidosomes produced with optimized conditions. As can be seen in Fig. 2.17a to c, the particulate polymer shells are fully covered by gold particles to form gold shells, which can improve the strength and impermeability of the colloidosomes. The diameter of the gold coated colloidosomes is from about 0.8 µm to 2.1 µm. We planned to measure the thickness of the gold shells using TEM, but the electrons cannot pass through the colloidosomes as shown in Fig. 2.17d. The thickness of the gold shell of the colloidosomes is estimated to be around 50 nm. The thickness of the gold shell is calculated from the diameter of the polymer shell colloidosomes

(0.7 μm to 2 μm) and the gold shell colloidosomes (0.8 μm to 2.1 μm). Fig. 2.17e shows the corresponding EDX image which has high gold peaks. This suggests that the particles surrounding the surface of the colloidosomes are gold. There is also a peak of carbon, arising from the particulate polymer shell.

2.3.3 Release by ultrasonic treatment

In order to release the metal capsules, we used an ultrasonic probe, which was operated at a frequency of 20 kHz and power output of 50 W to break the metal shell colloidosomes. For both silver and gold colloidosomes, we tried various sonication times.

2.3.3.1 Silver coated colloidosomes

A suspension of microcapsules was subjected to ultrasound sonication for different durations. Fig. 2.18 shows SEM images of silver shell colloidosomes after various sonication times. It can be seen that some of the capsules were broken into fragments after 120 s of treatment and most of the capsules were destroyed after 240 s.

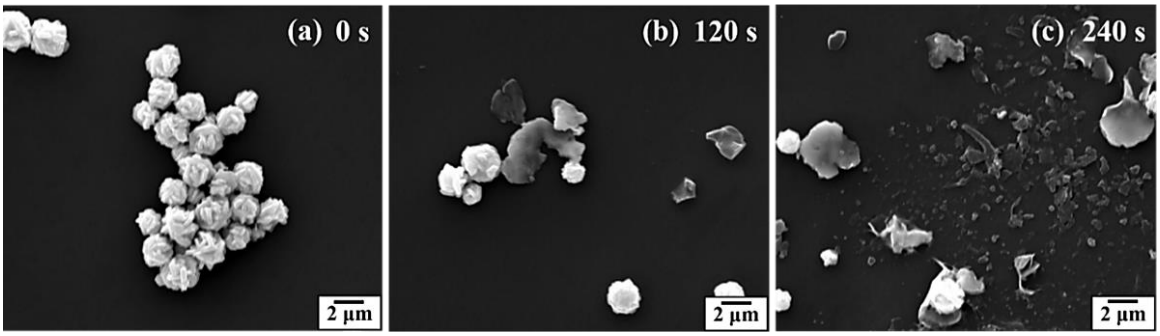

Fig. 2.18 SEM images of silver shell colloidosomes after various sonication times operating at a frequency of 20 kHz and power output of 50 W: (a) untreated, (b) 120 s and (c) 240 s.

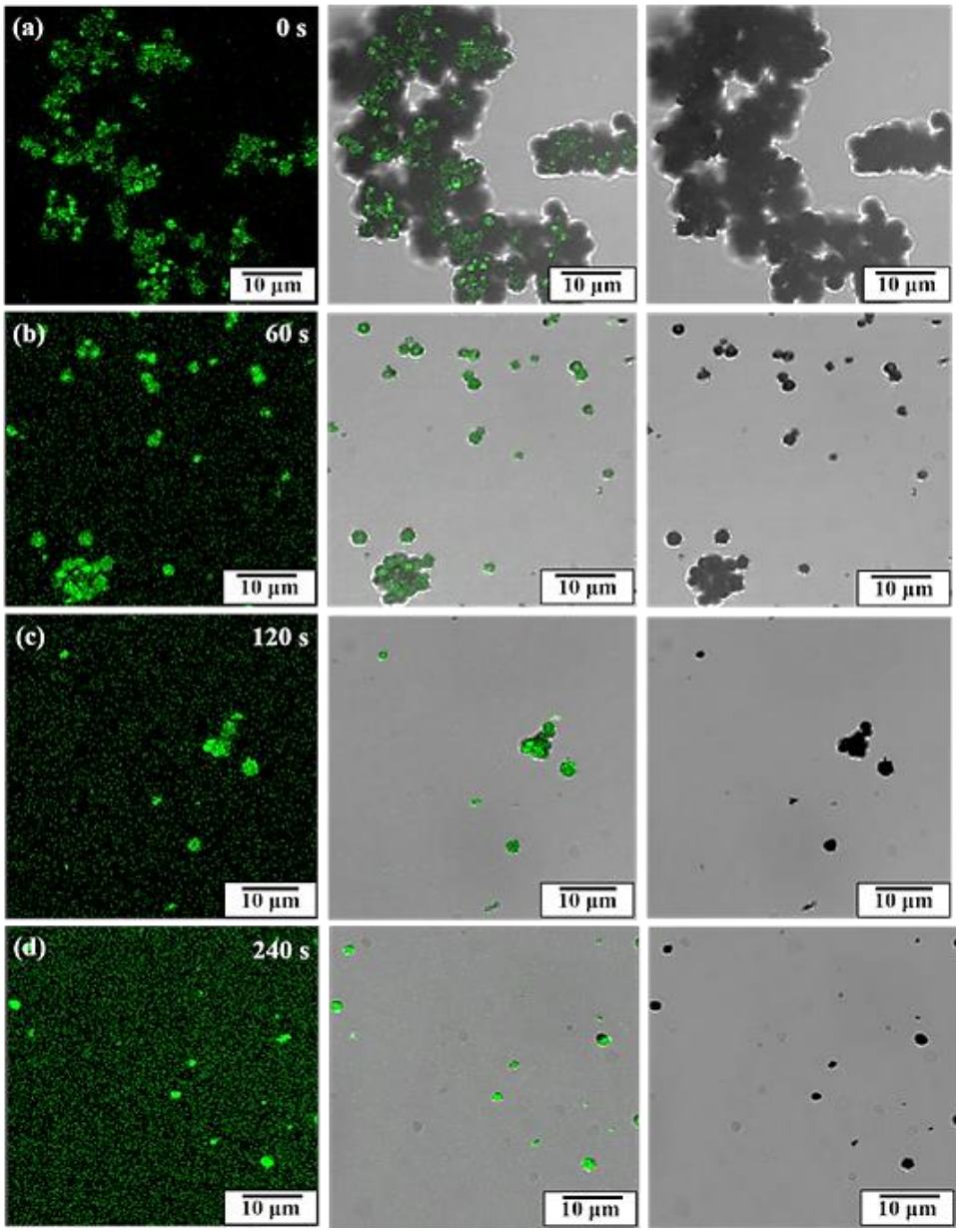

Fig. 2.19 CLSM images of dye-containing silver shell colloidosomes after various sonication times with λex =480 nm, fluorescent dye (left), bright field (right), and merged (middle) images. The ultrasound was operated at a frequency of 20 kHz and power output of 50 W after various sonication times: (a) untreated, (b) 60 s, (c) 120 s and (d) 240 s.

Fig. 2.19 shows CLSM images of dye-containing silver shell colloidosomes after various sonication times. The colloidosomes were dyed using Allura Red AC. It was seen that intact dye-containing silver shell colloidosomes were found without sonication. After 60 s and 120 s of ultrasound treatment, there were some fluorescent dots appearing in the images. These may be either the dye solution attached on the surface of small broken silver shells or some released dye. After 120 s of ultrasound treatment, a significant number of the capsules were broken into fragments. For longer sonication times, more capsules were broken. After 240 s

sonication, only a few colloidosomes survived and there were a large portion of small dots appearing in the CLSM images. These are likely to be small pieces of broken shell with dye attached on the surface or some released dye.

2.3.3.2 Gold coated colloidosomes

Fig. 2.20 shows SEM images of gold shell colloidosomes after various ultrasound sonication times also operating at a frequency of 20 kHz and power output of 50 W. As can be seen, some of the gold coated colloidosomes were broken into fragments after 240 s of treatment and most of the capsules were destroyed after 480 s. For longer sonication times, more capsules were broken. After 960 s sonication, only very few colloidosomes survived and there were a large number of small pieces of broken shell. Compared with the previous silver shells, the gold shells need longer ultrasound times for breaking. This may be the result of the different morphology and structure of the shells.

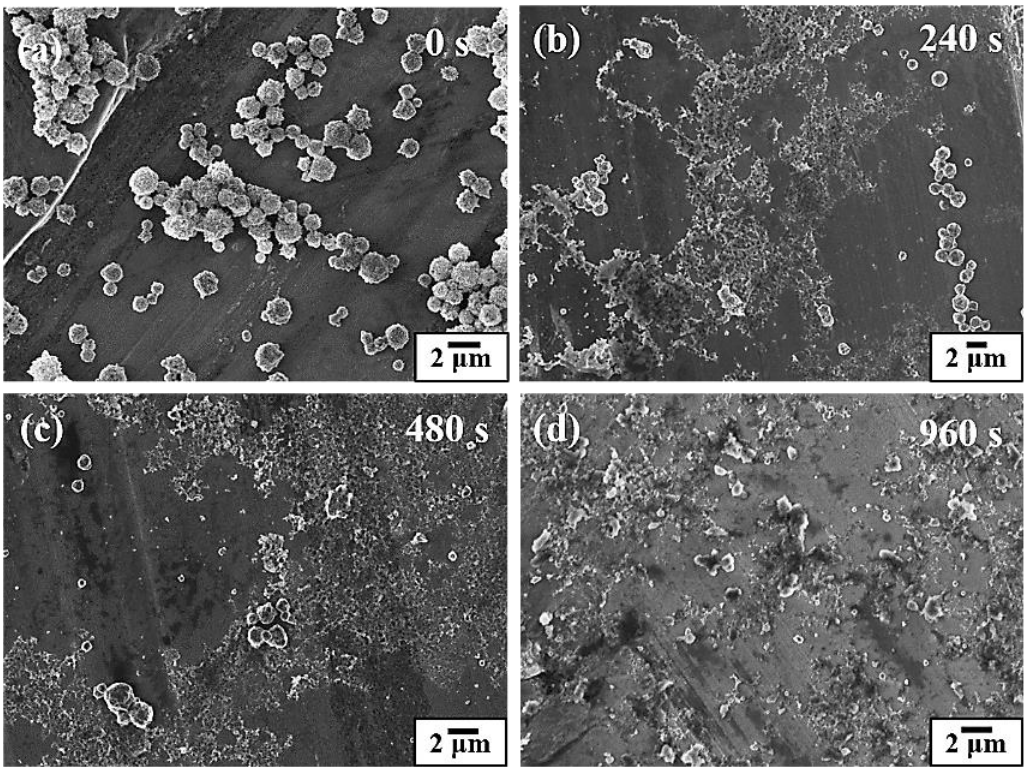

Fig. 2.20 SEM images of gold shell colloidosomes after various ultrasound sonication times operating at a frequency of 20 kHz and power output of 50 W: (a) 0 s, (b) 240 s, (c) 480 s and (d) 960 s.

2.3.4 Dye encapsulation and dye release

In order to test the permeability of the silver and gold coated colloidosomes, a hydrophilic dye Allura Red AC was encapsulated within the microcapsules to test the dye release, and the dyed water was characterized by spectrophotometry. This was carried out in a UV-Vis spectrophotometer, and the absorbance value at 500 nm was recorded.

2.3.4.1 Silver coated colloidosomes

Table 2.2 shows the calculation of the dye loss data and encapsulation efficiency of silver shells. As shown in the table, during manufacture, 17.5 % of the total dye was lost in the waste oil phase, which may contain the lost dye in sunflower oil and also a very small amount of dye leaking from the polymer shells after centrifugation. 59.8 % was lost in the washing solution during the silver forming reaction process. So the remaining dye encapsulated in the silver coated colloidosomes was about 22.7 %.

Table 2.2 Calculation of the dye loss data and encapsulation efficiency of silver shells. All the dye data was measured three times to get an average result, and the standard error of the measurements were typically ±~3%, which are not shown for clarity. All the dye absorbance data was measure in the sensitive zone of the UV-Vis spectrophotometer.

Dye data	Mass	Total / lost dye	Encapsulation efficiency	Released dye
Dye added in the experiment	40.0 mg	100 %	----	----
Dye measured in waste oil phase	7.0 mg	17.5 %	----	----
Dye measured in the washing solution	23.9 mg	59.8 %	----	----
Dye remaining in the silver coated colloidosomes	9.1 mg	----	22.7 %	----
Dye released by the addition of acid	4.28 mg	----	----	47.0 %
Dye released by ultrasound	0.77 mg	----	----	8.5 %

This encapsulation efficiency was compared with other drug delivery materials or capsules. For examples, Vallet-Regí et al. [181] made mesoporous PLGA-SiO_2 materials to load drugs in water, with a loading efficiency between 22.4% and 45.6%. Hitchcock et al. [65, 66] made an impermeable metal film around polymer microcapsules, which prevents loss of small volatile oils and has an encapsulation efficiency higher than 49 %. Keen et al. [10] made calcium carbonate coated colloidosomes encapsulating small molecules for several months

with an encapsulation efficiency of around 23%. For our samples, although the silver shell can change the permeability of the particulate polymer shells, we also decreased the encapsulation efficiency to a certain extent, which is lower than some drug delivery materials and capsules. It is also clear that further optimisation possibilities exist.

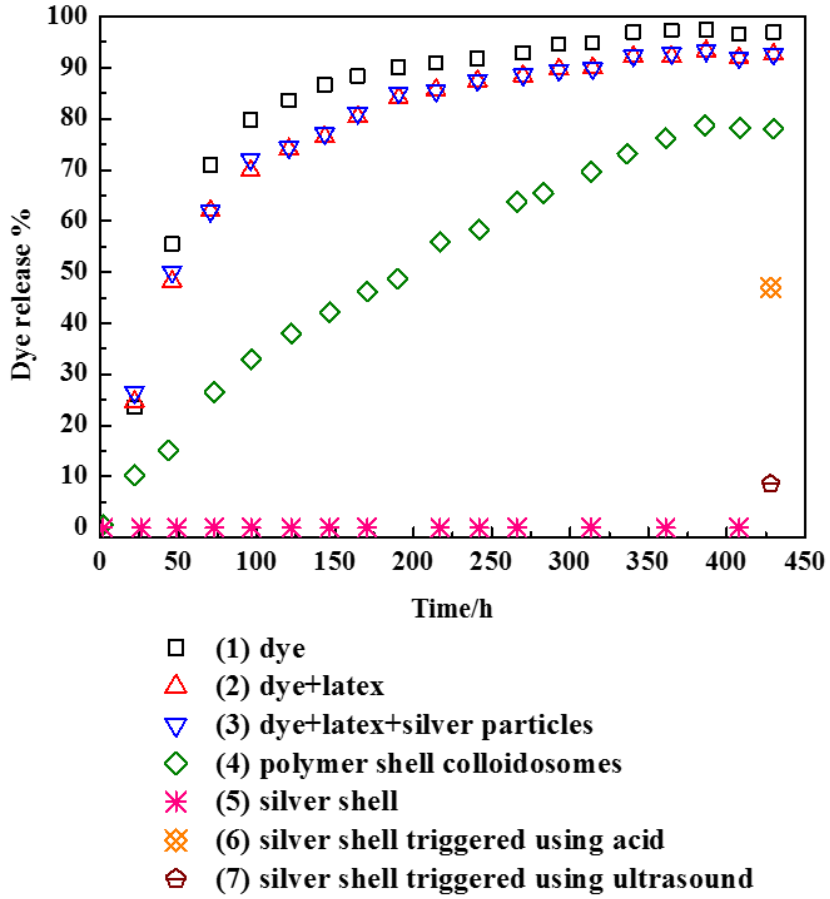

Fig. 2.21 Release of Allura Red AC dye from blank dye, dye with free-moving latex particles, dye with free free-moving latex particles and silver particles, and dye encapsulated in polymer or silver shell colloidosomes. All the dye data was measured three times to get an average result, and the standard error of the measurements were typically ±~3%, which are not shown for clarity. All the dye absorbance data was measure in the sensitive zone of the UV-Vis spectrophotometer.

Fig. 2.21 shows the release of Allura Red dye from colloidosomes. The samples were sealed with either a silver shell or a particulate polymer shell. Before measuring the dye release of silver coated colloidosomes, some blank tests were carried out to investigate if any chemical reactions exist between Allura Red dye, free-moving latex particles and silver particles. Three blank tests were: (1) Allura Red dye (28 mg) in ultra-pure water (20 mL); (2) Allura Red dye (28 mg) in ultra-pure water (18.6 mL) and latex particles (1.4 mL, 5.6 wt % particle suspension in ultra-pure water), which was stirred for 1 min; (3) Allura Red dye (28 mg) in

ultra-pure water (18.6 mL), latex particles (1.4 mL, 5.6 wt % particle suspension in ultra-pure water) and free silver particles, which were produced by mixing L-Ascorbic acid and $AgNO_3$ directly. The amount of silver in the control is the same as in the colloidosome synthesis procedure. The release data was normalized by the amount of encapsulated dye. This is the amount of dye added to the experiment minus the amount measured in the waste oil and washing solution. All mixtures were transferred into 10 cm of dialysis tubing and immersed in gently stirred ultra-pure water (450 mL). Fig. 2.21 illustrates the dye release profiles for the blank tests. It can be observed that all three control samples (samples 1, 2 and 3) leaked dye solution without any trigger and have similar trends. The final release percentage of samples 2 and 3 was approximately 92%. For sample 1, the final release percentage was a little higher, around 96.5%. It should be noted that the free-moving latex or the dialysis tube may absorb a small amount of dye. Fig. 2.21 also illustrates the dye release profile for particulate polymer shell colloidosomes (sample 4). The release rate from particulate polymer shell colloidosomes was slower than unencapsulated material in dialysis tubing and the time to reach 50 % release was approximately 210 h. The final release percentage of sample 4 was approximately 78%. This is lower than the control samples and indicates that some dye may be absorbed onto the particulate polymer shells, either on the surface or remaining inside the polymer shells.

The silver shell colloidosomes for this experiment were prepared by making the particulate polymer shell capsules first, then redispersing them in $AgNO_3$ solution, and adding L-Ascorbic acid. The calculation of the encapsulation efficiency and dye loss data are shown in Table 2.2. It can be seen that there was negligible dye outside the silver shell colloidosomes (sample 5). When 5 mL 1 wt% nitric acid was added, dissolving the shell (sample 6), the measured release yield was 47 %. It should be noted that the high temperature (65 °C) and nitric acid can destroy some of the dye, resulting in the lowering measured efficiency. We did a control experiment: 5mL 1 wt% nitric acid was added to the same amount and concentration of dye solution and heated at 65 °C for different durations. Then we tested the absorbance of the dye solutions using UV-Vis spectroscopy. After 10 min, there was about 20-30% loss. After 20 min, there was about half dye loss. With prolonged time, more dye was destroyed. After 30 min, there was nearly no dye remaining.

When ultrasound treatment was used to break the silver shell colloidosomes (sample 7), a release yield of around 8.5% was measured. We wish to demonstrate the release of

colloidosomes by ultrasound. For the particular situation in this study, the capsules were used at a rather high concentration so that the triggered dye solution reaches the sensitive zone of the UV-Vis. Therefore, the distance between the capsules and ultrasonicator probe has an effect on the resulting released amount. For future biological experiments (in vitro or for envisaged in vivo study), a low concentration of colloidosomes will be used in order to minimize their toxicity to normal cells or tissues. The release results demonstrate the complete sealing of the capsules and the dye release can be achieved using nitric acid or ultrasound.

2.3.4.2 Gold coated colloidosomes

Table 2.3 Calculation of the dye loss data and encapsulation efficiency of gold shells. All the dye data was measured three times to get an average result, and the standard error of the measurements were typically ±~3%, which are not shown for clarity. All the dye absorbance data was measure in the sensitive zone of the UV-Vis spectrophotometer.

Dye data	Mass	Total / lost dye	Encapsulation efficiency	Released dye
Dye added in the experiment	40.0 mg	100 %	----	----
Dye measured in waste oil phase	7.0 mg	17.5 %	----	----
Dye measured in the washing solution	26.7 mg	66.7 %	----	----
Dye remaining in the gold coated colloidosomes	6.3 mg	----	15.8 %	----
Dye released by ultrasound	0.53 mg	----	----	8.4 %

Table 2.3 shows the calculation of the dye loss data and encapsulation efficiency of gold shells. It can be seen form the table, during manufacture, 17.5 % of the total dye was lost in the waste oil phase, which may contain the lost dye in sunflower oil and also a very small amount of dye leaking from the polymer shells after centrifugation. 66.7 % was lost in the washing solution during the gold forming reaction process. So the encapsulation efficiency of the gold coated colloidosomes was about 15.8 %, which is lower than the silver coated colloidosomes. As discussed above in section 2.3.4.1, similar to the silver shells, although the gold shells can change the permeability of the particulate polymer shells, the encapsulation efficiency is lower than some drug delivery materials and capsules.

Fig. 2.22 shows the release profile of Allura Red AC dye from blank dye, dye with free-moving latex particles, dye with free-moving latex particles and gold particles, and dye encapsulated in polymer or gold shell colloidosomes. Similar to the release from silver shell capsules, some blank tests were carried out to investigate if any reactions exist between Allura Red dye, free-moving latex particles and gold particles. The release data was normalized by the amount of encapsulated dye in the capsules. It can be observed in Fig. 2.22 that all three control samples (samples 1, 2 and 3) leaked dye without any trigger and have similar trends. The final release percentage of samples 2 and 3 were approximately 95.4% and 94.3%, respectively. For sample 1, the final release percentage was a little higher, around 97.8%. It should be noted that the free-moving latex and the dialysis tube may absorb a small amount of dye.

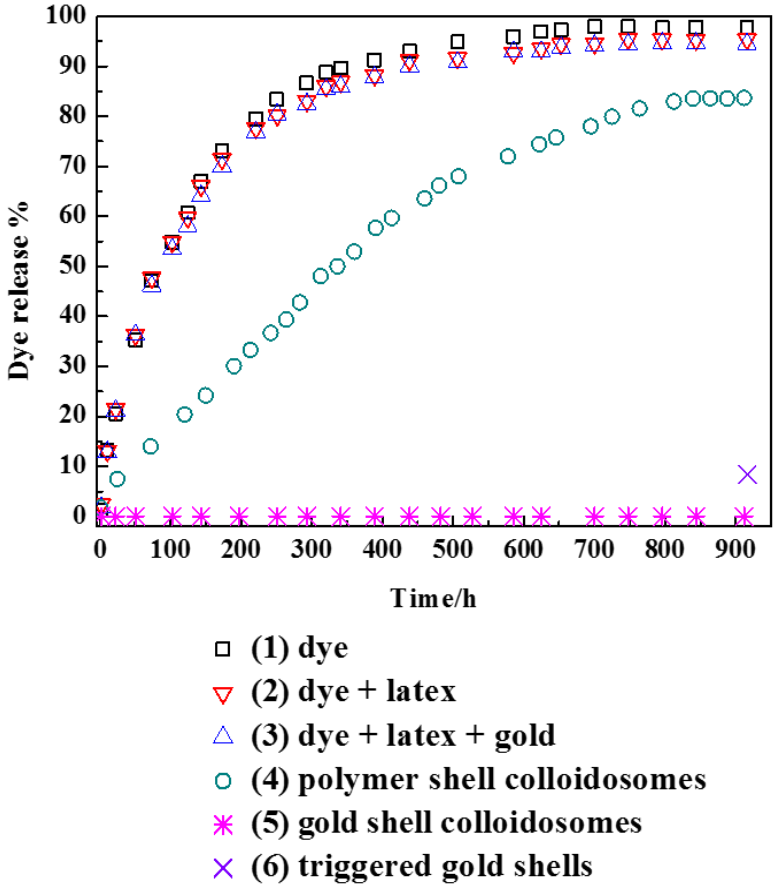

Fig. 2.22 Release of Allura Red AC dye from blank dye, dye with free-moving latex particles, dye with free-moving latex particles and gold particles, and dye encapsulated in polymer or gold shell colloidosomes. All the dye data was measured three times to get an average result, and the standard error of the measurements were typically ±~3%, which are not shown for clarity. All the dye absorbance data was measure in the sensitive zone of the UV-Vis spectrophotometer.

Fig. 2.22 also illustrates that the release rate from particulate polymer shell colloidosomes was slower than unencapsulated material in dialysis tubing, but the dye still leaked over about 500 h. The final release percentage of sample 4 was approximately 83.7%. This is lower than the blank control samples and indicates that some dye was possibly absorbed onto the particulate polymer shells, either on the surface or remaining inside the polymer shells. It can be seen that there was negligible dye released from the gold coated colloidosomes (sample 5) even after 900 h. When ultrasound treatment was used to break the capsules, the release occurred up to a maximum release yield of around 8.4%. Similar to the silver coated colloidosomes dye release, for this study, the gold shell capsules were also used at a rather high concentration. This means that the distance between the capsules and ultrasonicator probe has an effect on the amount of release. When the colloidosomes are too crowded, only the capsules near the ultrasonicator probe can be triggered. This is likely to be the reason for the relatively low apparent efficiency. These results indicate that the gold shell totally seals the encapsulated materials and the release of the dye in the gold shell can be triggered using ultrasound. It is also clear that further optimisation possibilities exist.

2.4 Conclusions

In this chapter, we present novel silver and gold coated colloidosomes, which are capable of small molecule encapsulation. The silver coated colloidosomes were prepared by making the particulate polymer shell first, then reacting L-Ascorbic acid with silver nitrate in the wash solution. The gold coated colloidosomes were prepared reacting L-Ascorbic acid with $HAuCl_4$. The two types of colloidosome were successfully demonstrated to encapsulate small molecule Allura Red AC and the shells of these structures was ruptured using ultrasound treatment.

Chapter 3.

Targeting model - Immunoassay targeting

The results from this chapter have been published in Langmuir and Soft Matter:

Qian Sun, Yao Du, Ziyan Zhao, Elizabeth A. H. Hall, Hui Gao, Gleb B. Sukhorukov, Alexander F. Routh. *Functional Silver-Coated Colloidosomes as Targeted Carriers for Small Molecules*. Langmuir, 2017, 33(15): 3755-3764.

Qian Sun, Yao Du, Elizabeth A. H. Hall, Dong Luo, Gleb B. Sukhorukov, Alexander F. Routh. *A Fabrication Method of Gold Coated Colloidosomes and Their Application as Targeted Drug Carriers*. Soft Matter, 2018, 14(14): 2594-2603.

3.1 Introduction

We plan to use the metal coated colloidosomes as targeted carriers for small molecular drugs. In general, targeting can be achieved by binding label specific cells or proteins with the capsules to find the targeted areas, or alternatively, using iron particles for magnetic positioning. Normally, fluorescent agents are used to follow the targeted tracking process. However, silver and gold particles quench fluorescent signals, especially gold particles. [182, 183] So in this chapter, a label-free Surface Plasmon Resonance (SPR) biosensor was used to test the specific targeting.

SPR biosensors are optical sensors exploiting electromagnetic waves to detect interactions between an analyte in solution and a biomolecular recognition element immobilized on the SPR sensor surface. [184] There are various measurement methods to monitor the binding event and then providing a measurable sensor response. For example, in a direct detection SPR immunoassay sensor, analyte in a sample can interact with a biomolecular recognition element immobilized on the surface of the SPR sensor. Usually the biomolecular recognition

elements are antibodies. [184] Fig. 3.1 shows a schematic of a direct detection SPR immunoassay sensor, which shows a model of the interaction between antibody and analyte. [184] Since antibodies are the most frequently used biomolecular recognition element for SPR biosensors and it is quite simple to achieve, we chose to use antibodies and direct detection for our SPR design.

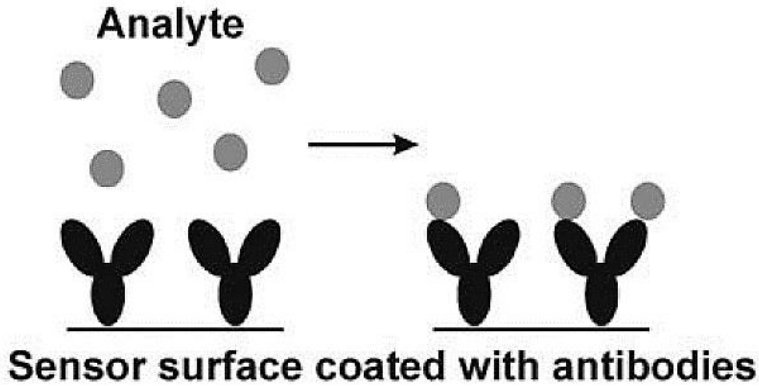

Fig. 3.1 Schematic of a direct detection SPR immunoassay biosensor. (image reproduced from Homola et al., 2003 [184])

In order to carry out the immunoassay reaction, we combined the specific antigens to the surface of our metal coated colloidosomes. Generally, to attach proteins on solid surfaces, there are two major methods: physical adsorption and chemical reaction linking. For physical adsorption, both the charge and surface area of the particles can affect the attachment of the proteins. [185] For chemical reaction linking, the small peptide region or the amino acid of proteins may bind with the surface of solids, usually with an irreversible structure change. When chemical linking happens, there will be some physical adsorption as well. [185, 186] For our experiment, in order to form a stable linking between metal shell capsules and the antigens, we chose to use a thiol chemical 4,4'-dithiodibutyric acid (including –SH and –COOH groups) to modify the surface of silver or gold shell, since it is easy to form an Ag-S or Au-S bond. [187, 188] Then the silver or gold shell colloidosome protein attachment is achieved through peptide coupling, which involves the activated carboxylic acid of 4,4'-dithiodibutyric acid and the N-terminal of the antigen.

In this chapter, a specific targeting model - immunoassay targeting of the functional silver shell and gold shell colloidosomes with rabbit antigen is described. The metal coated colloidosomes attached with the rabbit Immunoglobulin G (Rabbit-IgG / rabbit antigen) can be captured by the anti-rabbit Immunoglobulin G (Anti-rabbit IgG / rabbit antibody) on the gold film of the SPR surface. We modified the capsule surface using 4,4'-dithiodibutyric

acid and attached with rabbit antigen (Rabbit-IgG). A label-free Surface Plasmon Resonance biosensor was used to test the specific targeting of the functional capsules with rabbit antigen. Then a custom-made flow cell channel built in the Analytical Biotechnology Group at Cambridge was used to perform targeted carrier experiments, and ultrasound treatment was used to break the shells attached onto the channels, as sketched in Fig. 3.6.

3.2 Experimental section

3.2.1 Materials

The silver and gold coated colloidosomes were synthesized following sections 2.2.2 and 2.2.3. Allura Red AC dye (Sigma-Aldrich), 4,4'-dithiodibutyric acid (DDA, 95%, Sigma-Aldrich), N-hydroxysulfosuccinimide sodium salt (Sulfo-NHS, ≥ 98%, Sigma-Aldrich), N-(3-dimethylaminopropyl)-N'-ethylcarbodiimide hydrochloride (EDC, ≥ 98%, Sigma-Aldrich) and phosphate buffered saline (PBS, Sigma-Aldrich) were used as received without purification. The vortex mixer was a TopMix FB15024 (Fisher Scientific). The water used in all experiments was deionized of resistivity 18.2 MΩ•cm produced by a Pure Lab Ultra apparatus. The StabilCoat® Immunoassay Stabilizer, rabbit Immunoglobulin G (Rabbit-IgG), mouse Immunoglobulin G (Mouse-IgG) and anti-rabbit IgG produced in rabbits were purchased from Sigma-Aldrich.

Fig. 3.2 shows the crystal structure of rabbit IgG [189], and the schematic of the specific rabbit antigen-antibody interaction. The schematic shows how the rabbit antigen induces the immune system response by interacting with the rabbit antibody which matches the antigens molecular structure.

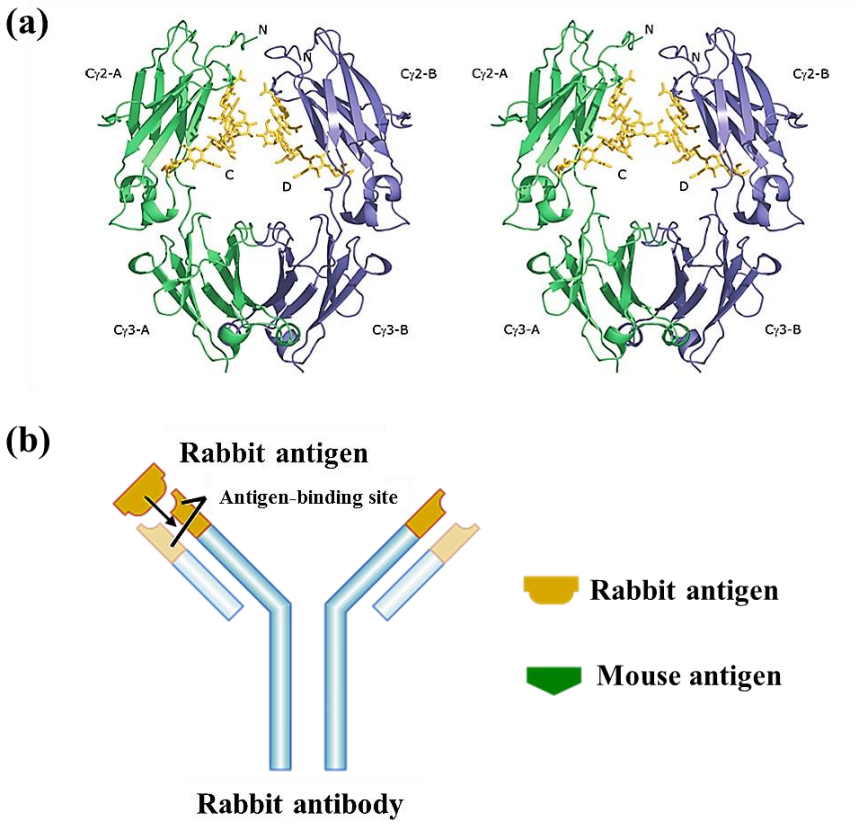

Fig. 3.2 (a) The crystal structure of rabbit IgG. In this stereo representation of the structure, the two polypeptide chains are shown in green and blue, with their oligosaccharide chains (indicated as C and D) in yellow. The position of the N-termini on both chains is indicated by the letter N. The N-terminal lower hinge region in each chain points directly towards the reader. (image reproduced from Girardi et al., 2009 [189]). (b) the schematic of the specific rabbit antigen-antibody interaction.

3.2.2 Attachment of Rabbit-IgG to silver and gold coated colloidosomes

The reaction steps to attach Rabbit-IgG on silver coated colloidosomes is shown in Fig. 3.3. A known mass of silver or gold coated colloidosomes were dispersed in 0.5 wt% 4,4'-dithiodibutyric acid (DDA) in ethanol solution using the vortex. The mixture was then gently mixed by a magnetic stirrer for 48 hours at room temperature [190]. After the reaction, the whole mixture was centrifuged at 1500 rpm for 2 min. The supernatant was removed using a pipette. The modified capsules were washed and redispersed three times using ultra-pure water.

1 mL of modified silver or gold coated colloidosomes was transferred to an eppendorf tube. 10 µL of N-hydroxysulfosuccinimide sodium salt (sulfo-NHS, 50 mg/mL) and 10 µL of N-(3-dimethylaminopropyl)-N'-ethylcarbodiimide hydrochloride (EDC, 50 mg/mL) were added to the eppendorf tube on the modified metal shell surface. The usage of sulfo-NHS

and EDC is to activate the carboxylic acid group of DDA. [190] Then the eppendorf tube was put on a rotator for 20 min. After rotating, the suspension was centrifuged at 2000 rpm for 2 min at 25°C. The supernatant was removed via pipetting and the sediment was redispersed in PBS buffer solution using a vortex mixer. This washing process was repeated three times. After washing, 16.2 µL of Rabbit-IgG (12.35 mg/ml, rabbit antigen) was added into the colloidosome suspension such that the concentration of Rabbit-IgG in the suspension was 200 µg/mL. The whole mixture was incubated with rotational mixing at 4ºC for 1 h and washed three times using PBS buffer solution. The silver or gold shell colloidosome protein attachment is achieved through peptide coupling which involves the activated carboxylic acid and the N-terminal of the protein. The modified colloidosomes were then stored at room temperature.

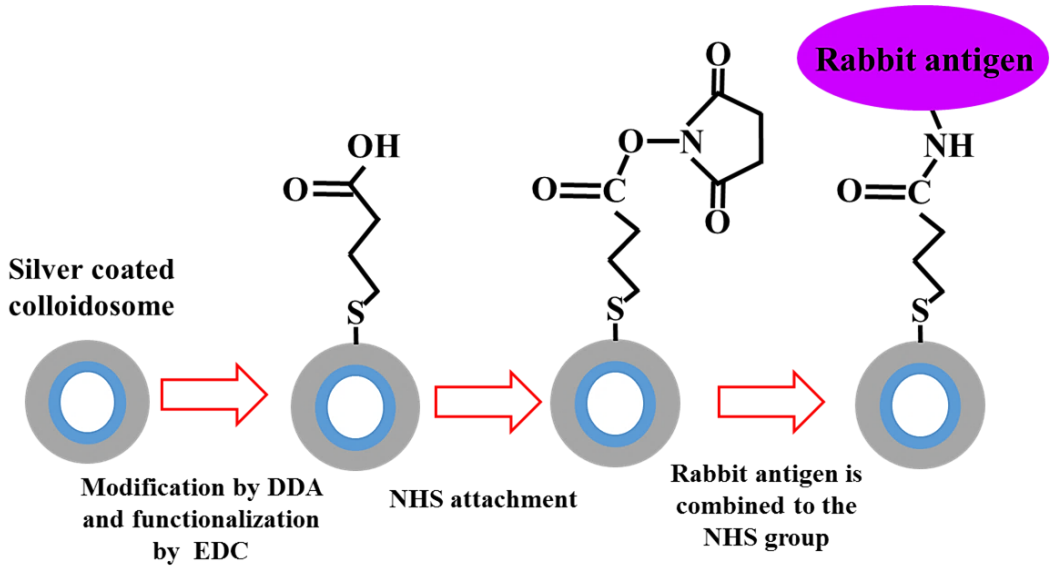

Fig. 3.3 Reaction steps to attach rabbit antigen (Rabbit-IgG) on silver coated colloidosomes surface. The whole surface of silver coated colloidosomes were attached with rabbit antigens, for clarity, only one rabbit antigen is shown in the diagram.

3.2.3 SPR gold film crosslinking

Fig. 3.4 shows the SPR gold film after combining with the rabbit antibody. A glass slide coated with a gold film of 50 nm thickness was washed with 70% ethanol and dried with nitrogen gas. 500 µL of DDA in pure water was introduced to the central part of the gold film and rested for 1 h. 10 µL of sulfo-NHS (50 mg/ml) and 10 µL of EDC (50 mg/ml) were added to the DDA solution in the central part of the gold film and left for 30 min. After resting, the gold film was washed with ultra-pure water and dried with nitrogen gas. This

washing was repeated three times. Then 500 µL anti-rabbit IgG (200 µg/ml) was placed and confined to the central area of the gold film and left for 1 h at 4˚C. After resting, the gold film was washed with ultra-pure water and dried with nitrogen gas three times and stored in PBS solution at 4˚C.

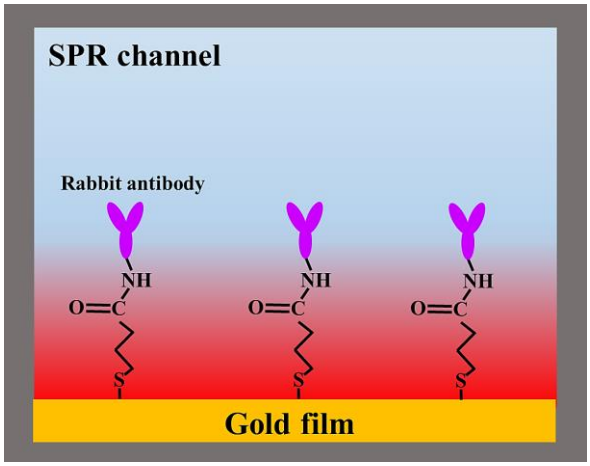

Fig. 3.4 SPR gold film after combined with rabbit antibody (Anti-rabbit IgG).

3.2.4 SPR experiment

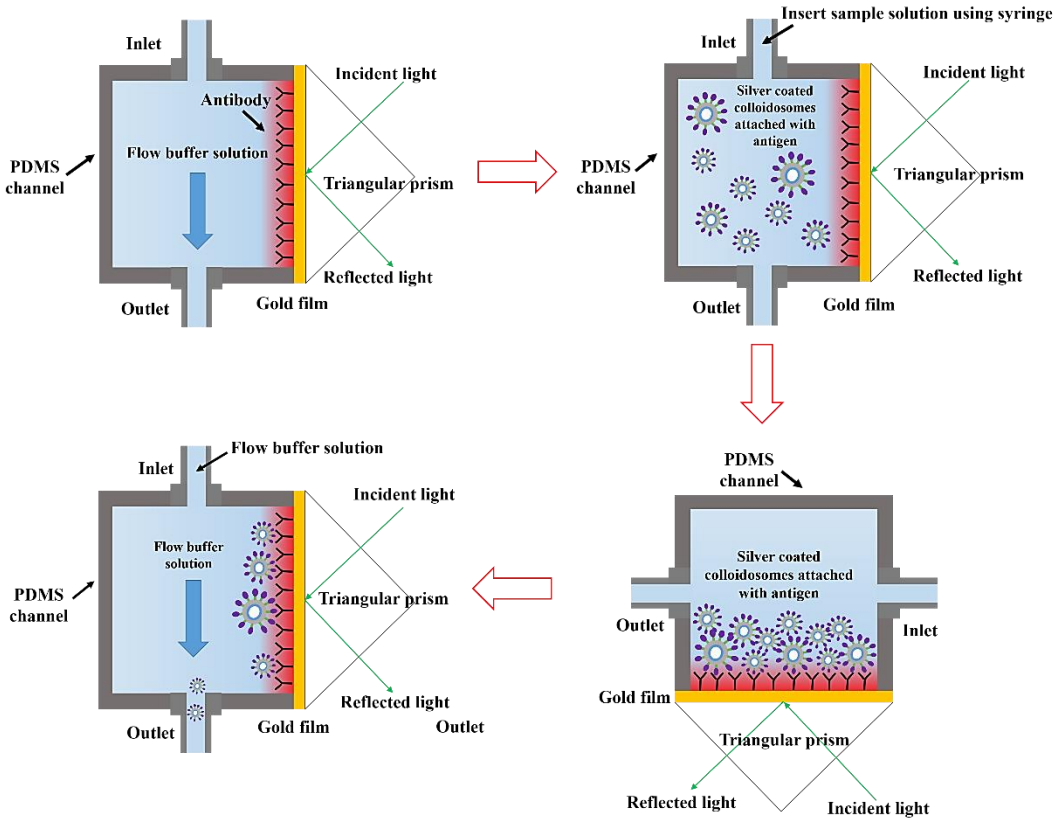

Fig. 3.5 SPR experimental flow chart using silver coated colloidosomes.

A custom-made spectral Surface Plasmon Resonance biosensor setup in the Analytical Biotechnology Group was used to perform the immunoassay experiments. Before the measurements, the silver or gold shell colloidosomes were coated with rabbit antigens. In addition, the SPR gold film was immobilized with rabbit antibody. Fig. 3.5 shows the SPR experimental flow chart using silver coated colloidosomes as an example. Firstly, a known volume of the PBS solution was flowed into the cell for 10 min. After washing, the first data was recorded. Then a suspension of modified silver coated colloidosomes with rabbit antigen in PBS solution was injected using a syringe. After the SPR channel was filled with solution, the second data was recorded. Then the cell was rotated by 90° and kept in this horizontal position for 10 min to allow the silver shell capsules to settle onto the gold film. This also allows sufficient time for the binding between the antigen crosslinked with the silver shell and the antibody crosslinked with the gold film of SPR. After resting for 10 min, the third data was recorded and the cell was then rotated back to the vertical configuration. Finally, PBS solution was flowed into the cell for 10 min to wash away any unbound analyte. After washing, the fourth data was recorded. The reflectance spectrum is analyzed and the peak wavelength is recorded.

3.2.5 Channel experiment

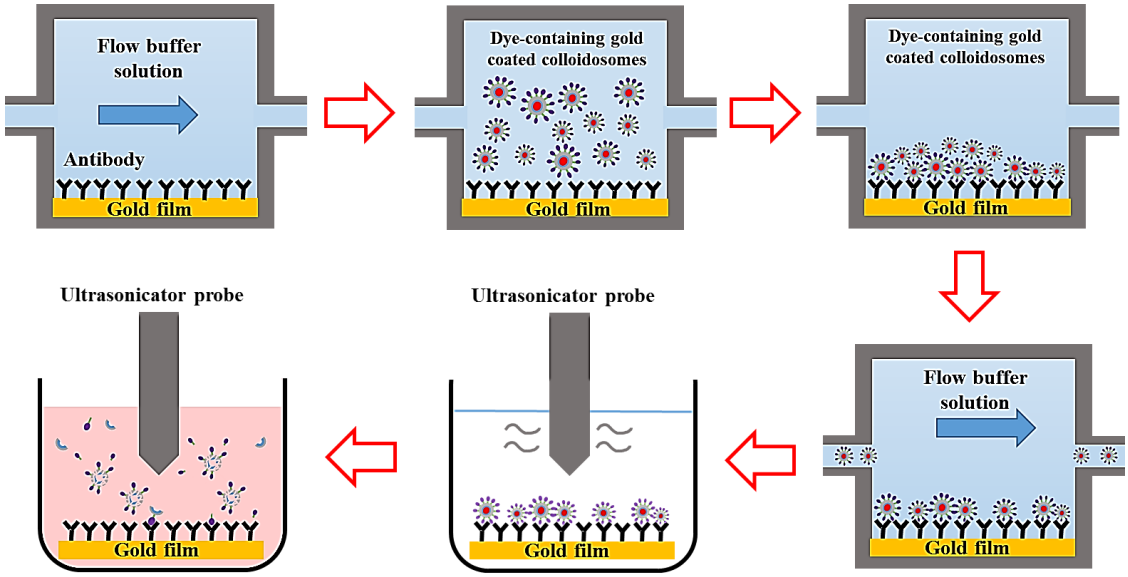

Fig. 3.6 Custom-made flow cell channel experimental flow chart using dye-containing silver coated colloidosomes.

Based on the SPR experiment results, a custom-made flow cell channel was built and the dye-containing silver or gold coated colloidosomes were used to perform targeted carrier

experiments. Fig. 3.6 shows the experimental flow chart using dye-containing silver coated colloidosomes. A gold film, which was immobilized with rabbit antibody, was set up at the bottom of the channel. Firstly, a known volume of PBS solution was flowed into the cell channel. After washing, a suspension of dye-containing modified silver or gold coated colloidosomes crosslinked with rabbit antigen in PBS solution, was injected. After the channel was filled with the suspension, it was kept in this position for 10 min to allow the capsules to settle onto the gold film. After resting for 10 min, PBS solution was flowed into the channel to wash away any unbound analyte. Finally, the gold film crosslinked with dye-containing colloidosomes was subjected to ultrasound to break the shells and release the dye.

3.2.6 Sample characterization

The silver and gold coated colloidosomes were imaged by SEM. The equipment was the same as described in section 2.2.6. An ultrasonic processor GEX 750 from Sonics & Materials Inc., USA was used to release the colloidosomes, operating at a frequency of 20 kHz and power output of 50 W. The device is the same as reported in section 2.2.4.

To analyse the colloidosomes before and after modification, a LabRAM HR Evolution Raman Spectroscopy (HORIBA Scientific) was applied.

The Thermo Scientific NanoDrop ND-1000 spectrophotometer was used to measure the concentration of protein samples without dilution. The module displays the UV spectrum, measured the protein's absorbance at 280 nm and calculated the concentration (mg/mL).

3.3 Results and discussion

3.3.1 Modification of silver and gold coated colloidosomes

After making the silver coated colloidosomes, we used DDA to modify the surface of colloidosomes and redispersed the colloidosome samples in pure water. Fig. 3.7 shows the Raman spectrum for non-modified and DDA modified silver coated colloidosomes. It can be seen that the modified silver coated colloidosomes have an additional peak at 223 cm^{-1} Raman shift. This is likely to correspond to an Ag-S bond [146], and it indicates the successful modification reaction between the silver shell colloidosomes and 4, 4'-dithiodibutyric acid as shown schematically in Fig. 3.8. In the modification reaction, the S-S structure of 4, 4'-dithiodibutyric acid was broken, and the -SH group was combined with the surface of the silver coated colloidosomes. The Raman results suggest successful modification of the colloidosome surface.

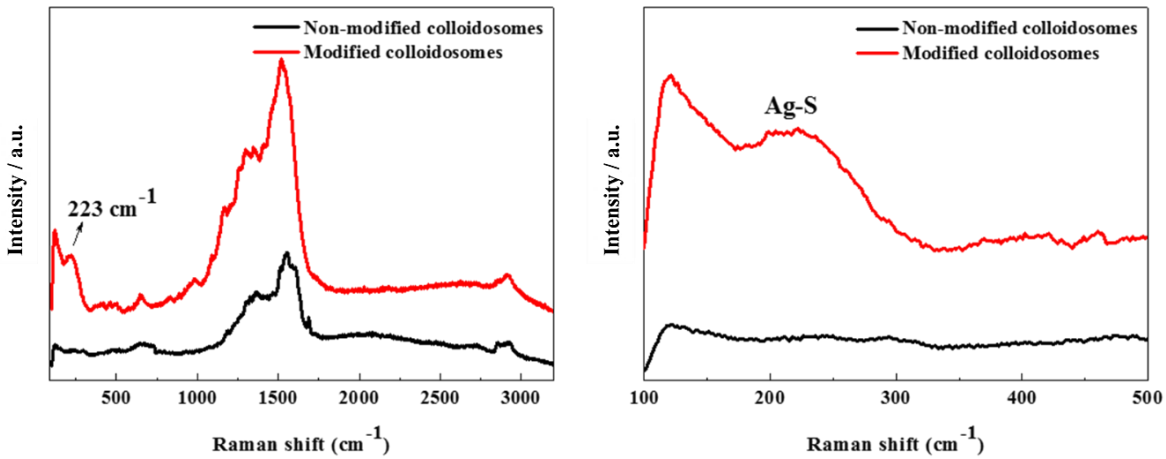

Fig. 3.7 Raman spectrum for non-modified and DDA modified silver coated colloidosomes.

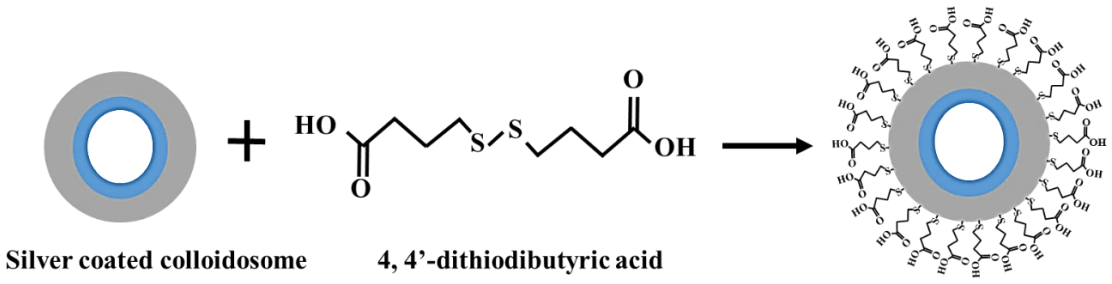

Fig. 3.8 Possible reaction between the silver shell surface and 4, 4'-dithiodibutyric acid.

Similar to silver shells, we also used DDA to modify the gold coated colloidosomes and redispersed the gold shell colloidosome samples in pure water. The Raman spectrum showing the attachment of the gold shell to the sulfur of the DDA is shown by peaks at 370 cm^{-1} in Fig. 3.9. [147]

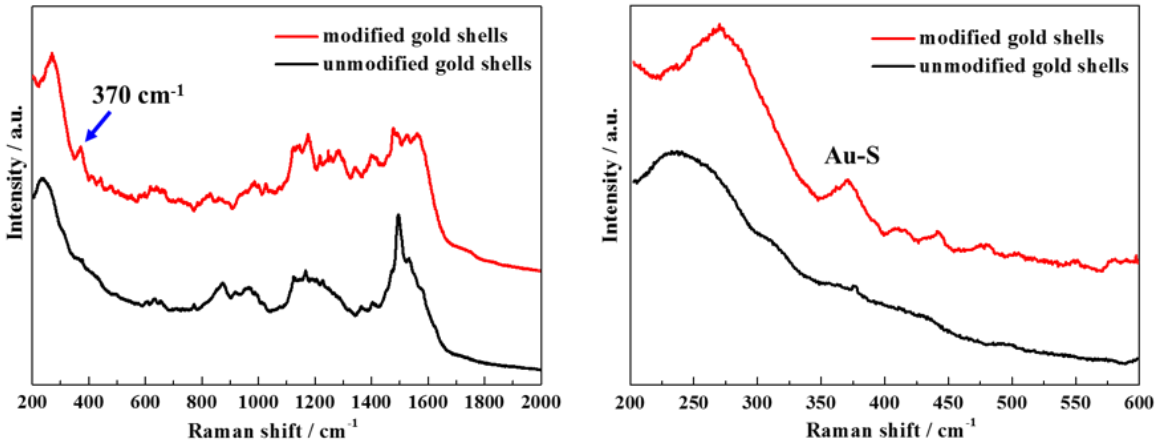

Fig. 3.9 Raman spectrum for non-modified and modified gold coated colloidosomes.

Both silver and gold shell colloidosomes for this experiment were modified by DDA solution and then combined with rabbit antigen. We used non-modified colloidosomes as a control experiment to see the loading efficiency. The concentration of the antigen solution was measured using a Nanodrop ND-1000 Spectrometer. After the antigen combination reaction, the average supernatant concentration for non-modified and modified samples were tested to calculate the loading efficiency. The loading efficiency of non-modified silver shell colloidosomes is about 5.5 μg/mg, and 7.4 μg/mg for DDA modified silver shell colloidosomes. The loading efficiency of non-modified gold shell colloidosomes is about 4.2 μg/mg, and 6.6 μg/mg for DDA modified gold shell colloidosomes. One reasonable explanation is that the silver or gold shell can adsorb some antigens by physical adsorption [191, 192]. For modified samples, there existed both physical adsorption and chemical reactions. The chemical reaction can be demonstrated by the immunoassay SPR results. These two factors caused the lower antigen concentration of the supernatant.

3.3.2 SPR targeting experiment

3.3.2.1 Using silver coated colloidosomes

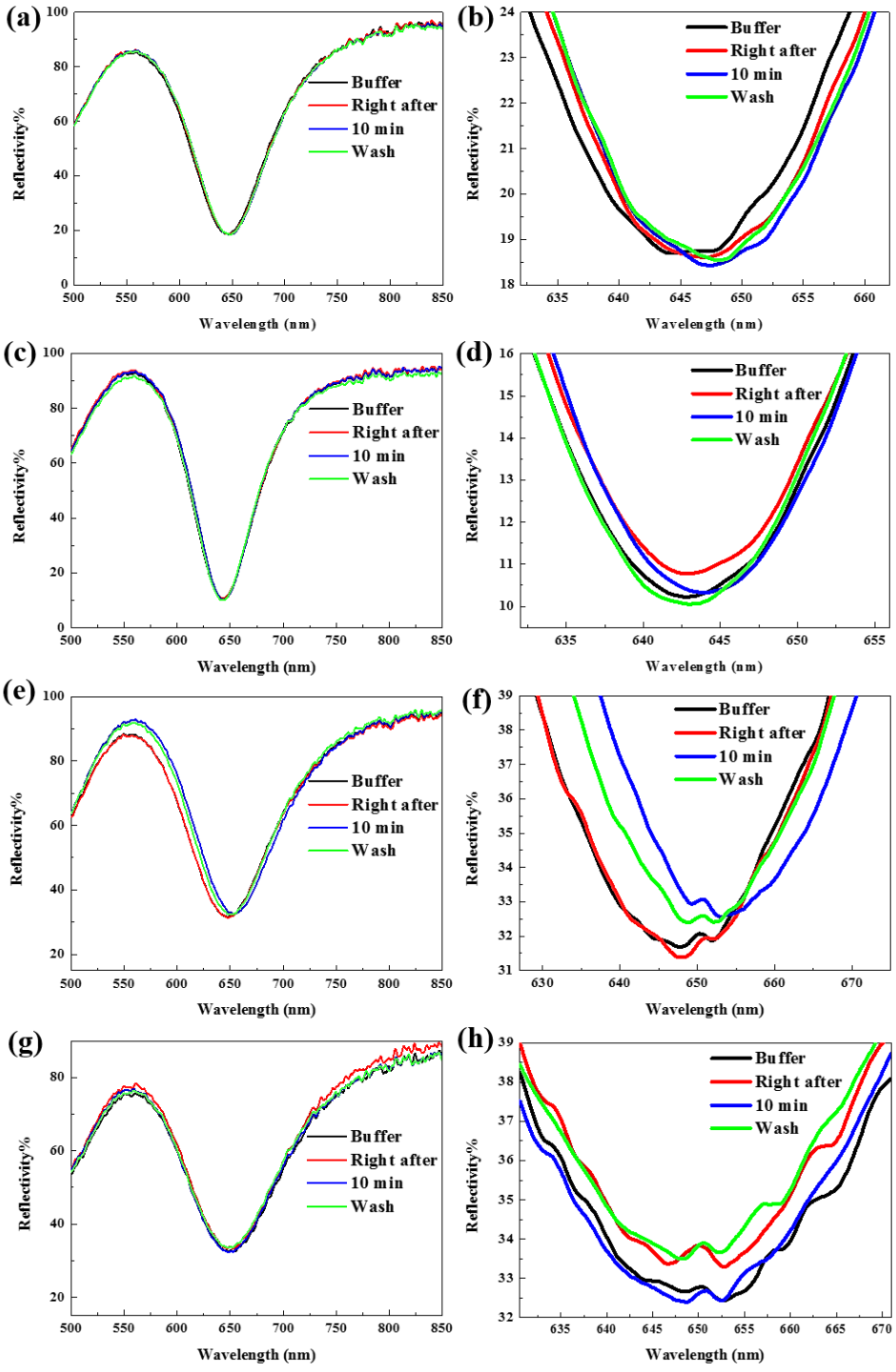

Fig. 3.10 SPR reflectivity graphs of (a) (b) the rabbit antigen solution, (c) (d) non-modified silver shell colloidosomes, (e) (f) modified silver shell colloidosomes attached with rabbit antigen, and (g) (h) modified silver shell colloidosomes attached with mouse antigen.

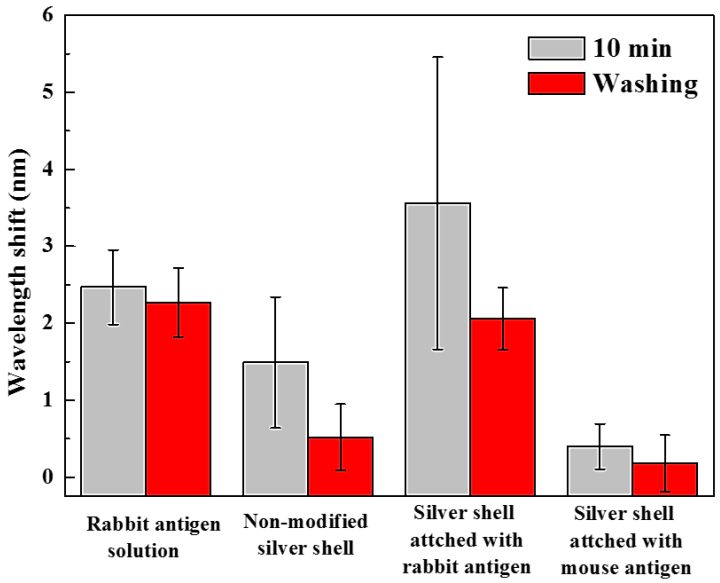

Fig. 3.11 Bar chart of the SPR wavelength shift after 10 min settling and after washing.

Fig. 3.10 shows SPR reflectivity graphs of the rabbit antigen solution, non-modified silver shell colloidosomes, modified silver shell colloidosomes attached with rabbit antigen, and modified silver shell colloidosomes attached with mouse antigen. Fig. 3.11 shows a bar chart of the SPR wavelength shift after 10 min settling and after washing. The resonance wavelength exhibits as a shift in the distribution demonstrating sensitivity to antigen and silver shell colloidosome deposition. Before measuring the reflectivity of modified samples, three blank tests were carried out to measure the quantitative red shift of the blank immunoassay reaction, and to investigate if any physical adsorption exists between the silver coated colloidosomes and the gold surface of SPR. The blank tests were: (i) rabbit antigen solution and (ii) non-modified silver shell colloidosomes, and (iii) modified silver shell colloidosomes attached with a mouse antigen. Fig. 3.10a and 3.10b illustrate that when injecting rabbit antigen solution, there was a 2.3 nm red shift even after washing. This was caused by the attachment of antigens, which were paired with the antibodies on the gold surface of SPR. Fig. 3.10c and 3.10d suggest that when injecting the non-modified silver shell colloidosomes, there was a 1.5 nm red shift at the '10 min' position. However, after washing, the reflectivity graph came back to the original position and there was almost no red shift. It can be seen from Fig. 3.10 and 3.11 that the wavelength shift of non-modified samples was negligible. This indicates that there is no obvious physical adsorption between the silver coated colloidosomes and the gold surface. The red shift after 10 min of deposition can be simply explained by the settling of the colloidosomes onto the gold surface and they

are easily washed away by the buffer solution.

Fig 3.10e and 3.10f show SPR reflectivity graphs of modified silver shell colloidosomes attached with rabbit antigen. It is seen that there was a 2.1 nm red shift after washing. The capsules were attached on the gold film because of the specific binding between the antigen and antibody pair - the binding between the antigen combined with the silver shell and the antibody combined with the gold film of SPR. Fig. 3.10g and 3.10h show SPR reflectivity graphs of modified silver shell colloidosomes attached with a mouse antigen. There was no obvious red shift after washing, which suggests there is no specific binding between mouse antigen on the capsules and the rabbit antibody on the gold film.

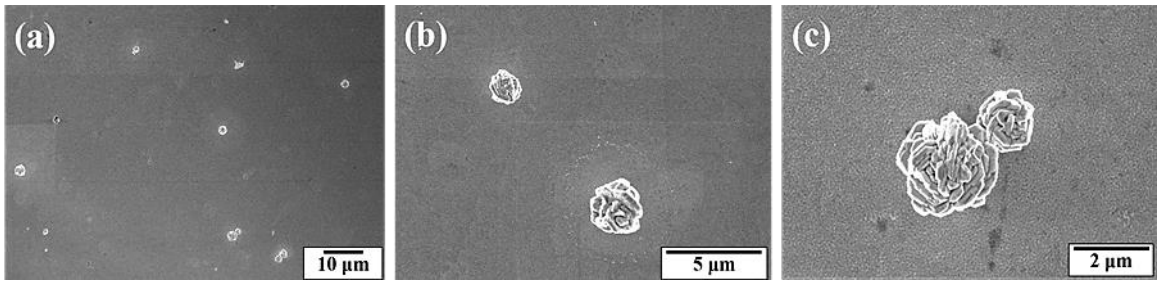

Fig. 3.12 SEM images of rabbit antigen modified silver shell colloidosomes which were combined with SPR gold film after washing.

After the immunoassay experiments for the modified silver shell colloidosomes, we removed the SPR gold film and washed it a further three times. There were still many rabbit antigen modified silver shell colloidosomes on the gold film as shown in Fig. 3.12. Fig. 3.12a is a low magnification of the gold film. Fig. 3.12b and 3.12c are different areas and different magnifications of the gold film. For the gold substrates, which were reacted to unmodified silver shell colloidosomes, and mouse antigen modified silver shell colloidosomes, there were only a few impurities and dust on the gold film surfaces with no silver shells.

3.3.2.2 Using gold coated colloidosomes

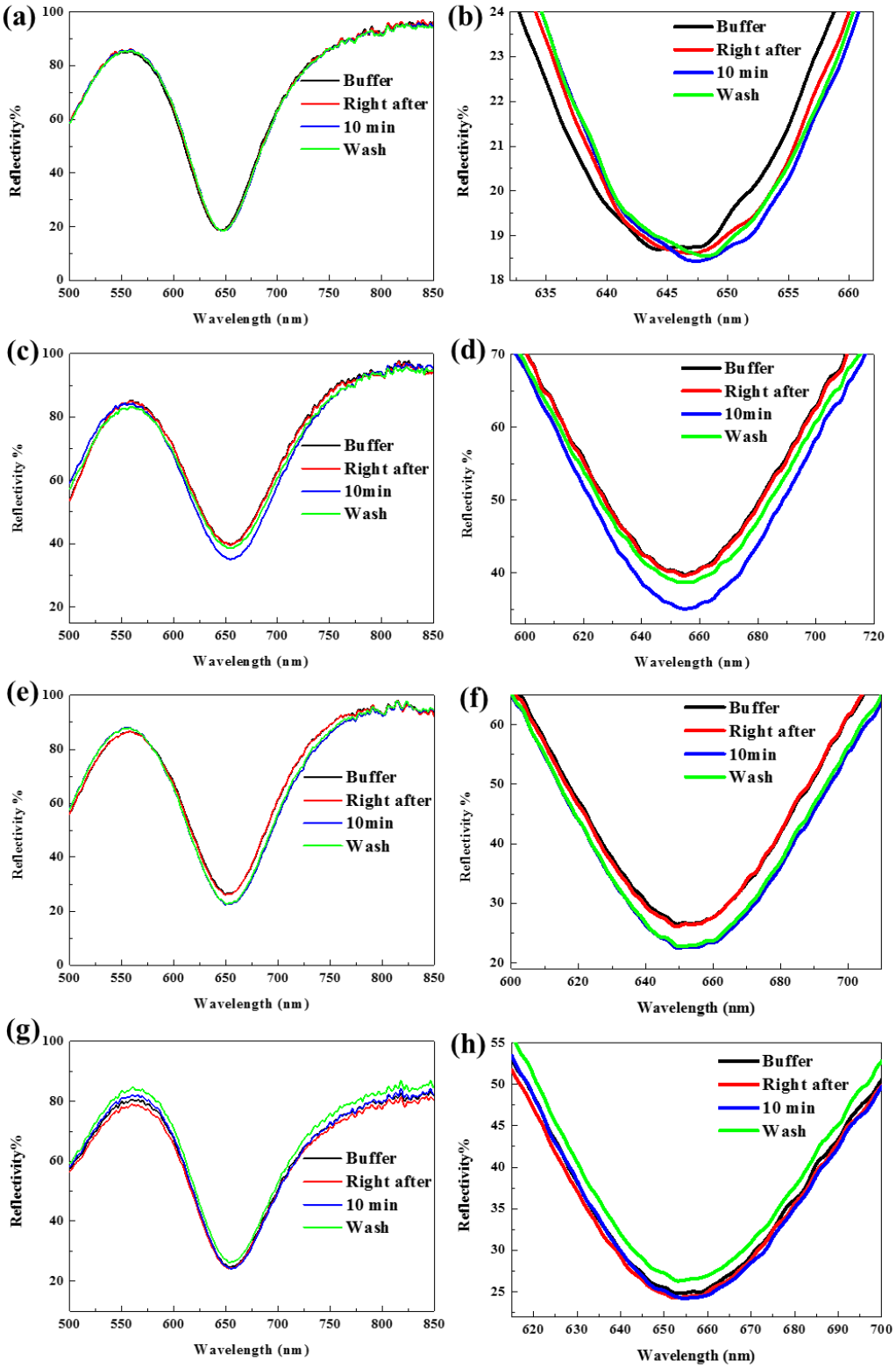

Fig. 3.13 SPR reflectivity graphs of (a) (b) the rabbit antigen solution, (c) (d) non-modified gold shell colloidosomes, (e) (f) modified gold shell colloidosomes attached with rabbit antigen, and (g) (h) modified gold shell colloidosomes attached with mouse antigen.

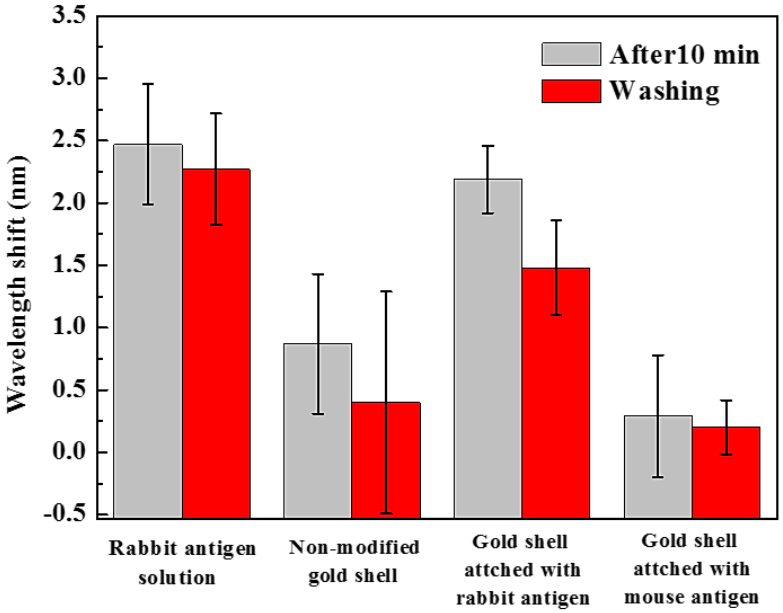

Fig. 3.14 Bar chart of the SPR wavelength shift after 10 min settling and after washing.

Fig. 3.13 shows SPR reflectivity graphs for the rabbit antigen solution, non-modified gold shell colloidosomes, modified gold shell colloidosomes attached with rabbit antigen and modified gold shell colloidosomes attached with mouse antigen. Fig. 3.14 shows a bar chart of the SPR wavelength shift after 10 min settling and after washing. The experiment is the same as reported for silver shells. The results also show the attachment of gold shell capsules to the modified surface.

The relatively large error bars in Fig. 3.14, across several repeat measurements are probably due to the low number of capsules captured by the gold film. As the capsules attach unevenly on the film, the interrogation zone under the light spot covers a different number of capsules resulting in a noticeable statistical variance. Nonetheless, the semi-quantitative SPR experiment shows that the gold shell capsules with antigens attached at the surface can combine with the surface of the gold film due to antibody-antigen interaction.

Similar to silver shells, after the immunoassay experiments for the modified gold shell colloidosomes, the gold film was removed and washed a further three times. There were still many modified gold shell capsules on the gold film as shown in Fig. 3.15. For the gold substrate, which was reacted to unmodified and mouse antigen modified gold shell colloidosomes, there were only a few impurities and dust on the surface, with no gold shells. This result suggests that the gold coated colloidosomes can be combined with proteins after

modification.

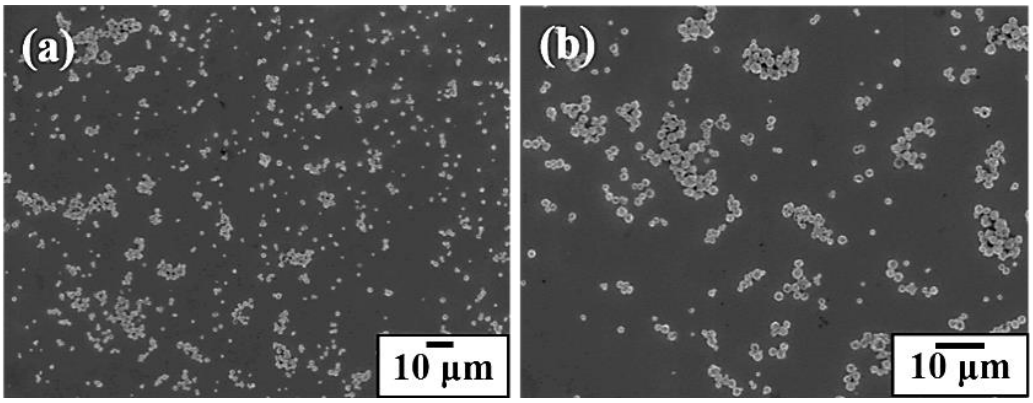

Fig. 3.15 SEM images of the rabbit antigen modified gold shell colloidosomes which were combined with SPR gold film after washing.

For both the silver and gold shell SPR experiments, we only achieved a low number of capsules captured on the gold film. Additionally, the capsules were attached unevenly on the film, and because the interrogation zone under the light spot covers a different number of capsules, there are relatively large error bars in the SPR wavelength shift bar chart and only a few nanometres red shift. In the literature, Lertvachirapaiboon et al. [159] reported a SPR peak shift for the antibody analyte of about 2-3 nm; then they tried to use the antibody-nanogold binding analyte leading to an enhancement to about 7 nm SPR peak shift. In order to produce an improvement in sensitivity for small molecule detection based on SPR bio-sensing, Hong et al. [-166] used gold nanoparticles on SPR surface to change the SPR resonance condition and cause the enhancement, resulting in a 7 nm wavelength shift from the classic gold SPR thin film. Consequently, more optimization should be explored for future research in order to achieve a more obvious SPR wavelength shift, and also, a higher loading efficiency of the metal capsules attached on the gold film of SPR.

3.3.3 Channel experiment

3.3.3.1 Using silver coated colloidosomes

A custom-made flow cell channel was used to perform targeted carriers experiments. A gold film, which was immobilized with anti-rabbit IgG, was set up at the bottom of the channel. After the experiment, the gold film coating with some dye-containing silver shell colloidosomes was subjected to ultrasound to break the shell and release the dye.

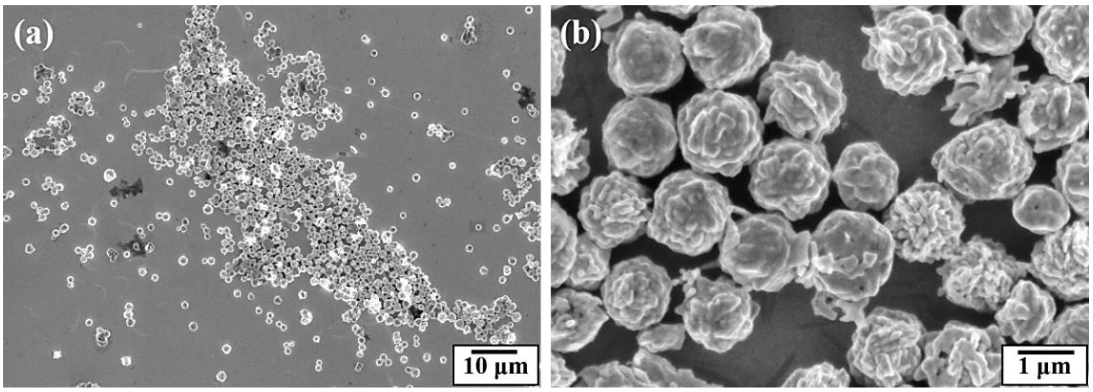

Fig. 3.16 SEM images of the channel gold film after combining with the dye-containing silver shell colloidosomes.

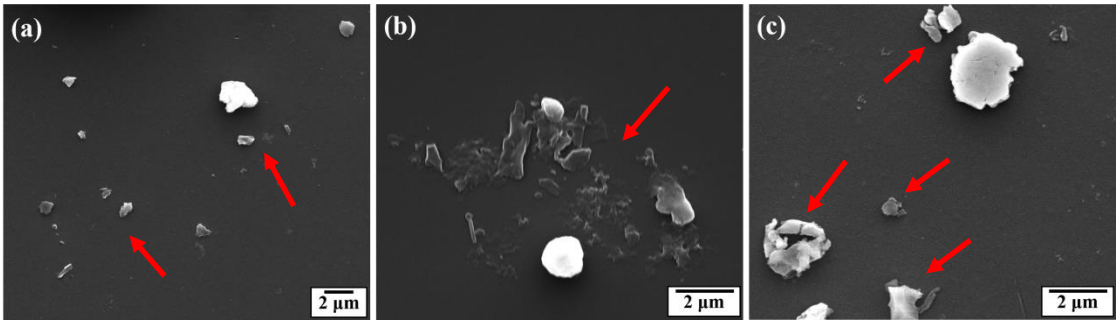

Fig. 3.17 SEM images of the channel gold film combining with dye-containing silver shell colloidosomes after ultrasound treatment. An ultrasonic probe, operating at a frequency of 20 kHz and power output of 50 W was used for 240 s.

Fig. 3.16 shows SEM images of the channel gold film after combining with dye-containing silver shell colloidosomes. One can observe a large number of dye-containing silver coated colloidosomes attached on the gold film after the immunoassay reaction. This attachment illustrates the possibility for silver coated colloidosomes to be used as targeted carriers. Fig. 3.17 shows SEM images of the channel gold film combining with dye-containing silver shell colloidosomes after ultrasound treatment, operating at a frequency of 20 kHz and power output of 50 W. It can be seen that after 240 s of ultrasound the capsules attached on the gold film were destroyed into fragments with only very few capsules remaining intact. This

indicates that the silver shell colloidosomes are promising to be used as targeted carriers for small molecules which can be released by ultrasound.

3.3.3.2 Using gold coated colloidosomes

Fig. 3.18 shows SEM images of the gold film after combining with dye-containing gold shell colloidosomes. A large number of the dye-containing gold coated colloidosomes attached on the gold film can be seen. After 240 s of ultrasound the capsules were destroyed into fragments with only a few capsules remaining intact as shown in Fig. 3.19. Similar to silver shell colloidosomes, the gold shell colloidosomes perform well as targeted carriers which can be released by ultrasound.

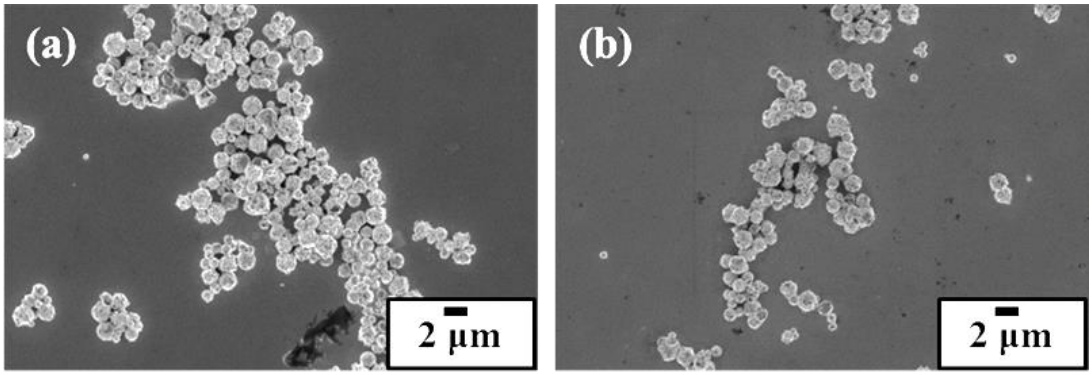

Fig. 3.18 SEM images of the channel gold film after combining with dye-containing gold shell colloidosomes.

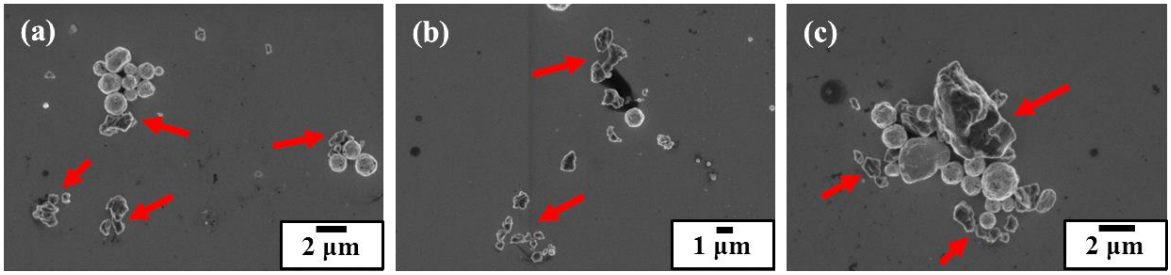

Fig. 3.19 SEM images of the channel gold film combining with dye-containing gold shell colloidosomes after ultrasound treatment. An ultrasonic probe, operating at a frequency of 20 kHz and power output of 50 W was used 240 s.

In this chapter, we used a label-free SPR biosensor and a custom-made channel to test the specific targeting of the functional capsules with rabbit antigen, in order to prove the antigen binding to colloidosomes. For future research, more characterization, can be explored to prove the protein binding to the metal coated colloidosome surface. For example, immunoelectron microscopy with antibodies is possible to test the binding proteins, in order to confirm the presence of the target antigens on the colloidosomes surface. [193] In addition,

it is also possible to use neutron and X-ray reflectivity techniques to test the binding proteins. [194] It is possible to observe the different adsorbed protein layer by screening out the other layers through contrast matching by measuring the partial proton densities of the different components. Therefore, it is possible to study the antigen recognition at the surface of the colloidosomes using neutron reflectivity. [194]

3.4 Conclusions

In this chapter, we present silver and gold coated colloidosomes which are capable of immunoassay targeting and small molecule encapsulation. Both types of colloidosomes can be ruptured using ultrasound treatment, operating at a frequency of 20 kHz and power output of 50 W. The metal coated colloidosomes were modified using 4,4'-dithiodibutyric acid and then combined with rabbit antigen. The Surface Plasmon Resonance biosensor, which was used for an immunoassay sensitivity measurement, proved that the two types of functional colloidosomes combined with the rabbit antigen can be captured by the rabbit antibody, which was immobilized on a gold film surface of SPR. For the SPR experiment, in order to achieve a higher loading efficiency of the metal capsules attached on the gold film of SPR, more optimization should be explored for future research. In summary, the functional silver and gold coated colloidosomes are promising for many future medical applications, including targeted carriers for small bioactive molecules with controlled drug delivery and externally triggered release.

Chapter 4.

Anticancer drug encapsulation - Doxorubicin

The results from this chapter have been published in ACS Applied Materials & Interfaces and Soft Matter:

Qian Sun, Hui Gao, Gleb B. Sukhorukov, Alexander F. Routh. *Silver Coated Colloidosomes as Carriers for an Anticancer Drug*. ACS Applied Materials & Interfaces, 2017, 9(38), 32599-32606.

Qian Sun, Yao Du, Elizabeth A. H. Hall, Dong Luo, Gleb B. Sukhorukov, Alexander F. Routh, *A Fabrication Method of Gold Coated Colloidosomes and Their Application as Targeted Drug Carriers*. Soft Matter, 2018, 14(14): 2594-2603.

4.1 Introduction

Small drug molecules play an important role in medical applications and are widely used in the pharmaceutical industry. Microcapsules have been developed and used to deliver such drugs to targeted areas. [93-98] The encapsulation of small molecules within particulate polymer shells still presents a significant challenge, since most particulate polymer shells tend to leak small molecules, due to their intrinsic high permeability. This greatly limits their practical application. To solve this problem, we describe a method for encapsulating an anticancer drug, doxorubicin, using both silver and gold coated colloidosomes. Doxorubicin hydrochloride (DOX) is a well-known anticancer drug which has been proven effective against various human malignancies, including various types of cancers. [195] In this chapter, we used doxorubicin hydrochloride as an example for drug encapsulation. Both the silver and gold coated colloidosomes can be triggered using a 50 W ultrasound and high intensity focused ultrasound (HIFU) with different durations. Then, a standard MTT assay on B50

cancer cells was used to test cell viability. We tested a few control samples, including water core silver or gold shell colloidosomes with and without ultrasound, and doxorubicin-containing silver or gold shell colloidosomes with and without ultrasound to test the toxicity of the capsules.

4.2 Experimental section

4.2.1 Materials

The base particulate polymer shell, silver shell and gold shell colloidosomes were made in exactly the same process as reported in sections 2.2.1, 2.2.2 and 2.2.3. The other chemicals used in the experiments were sodium dodecyl sulfate (SDS, Fisher Scientific), Allura Red AC dye (Sigma-Aldrich), buffer solution pH 10.0 (Sigma-Aldrich), 4,4'-dithiodibutyric acid (DDA, 95%, Sigma-Aldrich), and doxorubicin hydrochloride anticancer drug (98.0%, Sigma-Aldrich). They were all used as received without purification. The reason we used doxorubicin hydrochloride as a drug model is that this drug is commonly used for cancer research studies and does not affect the colloidosome synthesis process. It is small enough to diffuse from the porous particulate polymer shells. Fig. 4.1 shows the chemical structure of doxorubicin hydrochloride (DOX).

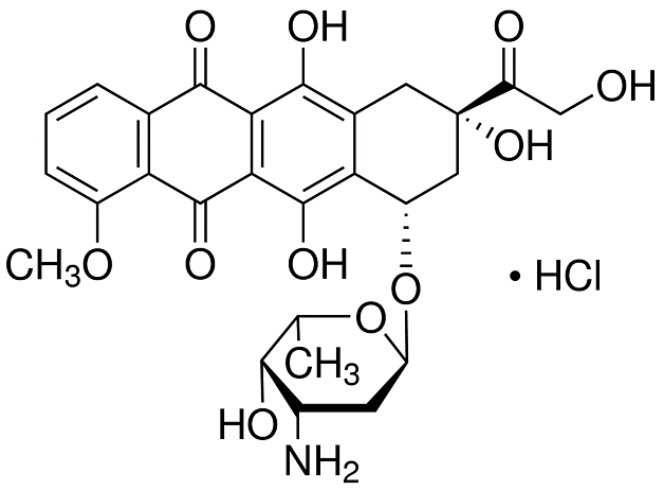

Fig. 4.1 Chemical structure of doxorubicin hydrochloride (DOX).

For cell culture and viability studies, the materials used were Dulbecco's modified eagles media (DMEM), fetal bovine serum (FBS), penicillin, streptomycin, trypsin, thiazolyl blue tetrazolium bromide (MTT), and dimethyl sulfoxide (DMSO). These were all supplied by

Sigma-Aldrich. Ultrapure deionised water, of resistivity 18.2 MΩ•cm, was produced by a Pure Lab Ultra apparatus. For mixing, a TopMix FB15024 vortex mixer (Fisher Scientific) was used.

4.2.2 Doxorubicin encapsulation

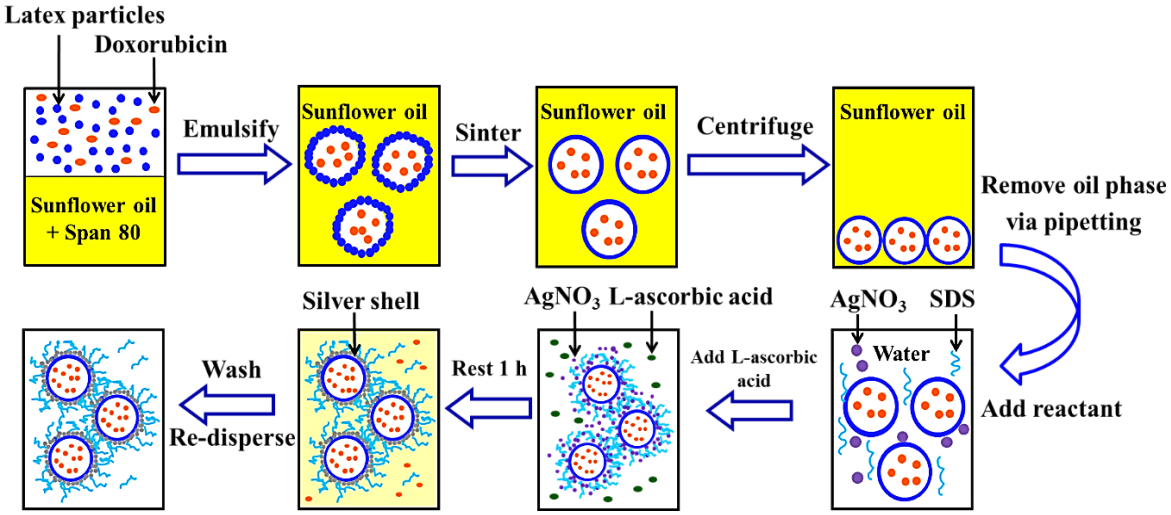

Fig. 4.2 Fabrication of doxorubicin-containing silver coated colloidosomes.

In this chapter, we used both silver and gold coated colloidosomes to encapsulate the anticancer drug doxorubicin. Fig. 4.2 shows schematically how doxorubicin-containing silver coated colloidosomes were formed. A Silverson high shear mixer (model SL2) was used to mix 200 mL sunflower oil and 4 mL of Span 80 in a 400 mL beaker. A separate aqueous phase containing 5.6 wt% latex particles and 2 mg/mL doxorubicin hydrochloride in a pH 10 buffer solution was made, and 2 mL of this aqueous phase was added into the sunflower oil, whilst applying shear. Five cycles of mixing and rest were applied, where shear was applied for 60 s, followed by 30 s rest. As mentioned in section 2.2.3, this cyclic process enabled the emulsion droplets which were more uniform and smaller to form.

To form the particulate polymer shells the emulsion mixture was heated in a water bath. To ensure rapid heat transfer, the emulsion mixture was split into five different tubes and when the temperature reached 50 ±0.5 ℃, the emulsions were heated for 1 h. To clean the capsules, 20 mL of the solution was centrifuged at 20 ℃ and 2500 rpm for 10 min. After removing the waste oil phase together with the small amount of drug solution which had leaked from the colloidosomes, 24 mL of a 0.1 wt % aqueous solution

of $AgNO_3$ and 2 mL of a 1 wt% aqueous solution of SDS were added and the mixture was agitated using the vortex mixer. Addition of 2 mL of a 15 wt% L-ascorbic acid aqueous solution started the silver formation which was allowed to proceed for 1 h. In this reaction, L-ascorbic acid is a reducing agent, which reduces silver ions into silver particles. To obtain the final aqueous dispersion of doxorubicin-containing silver coated microcapsules, the mixture was centrifuged, at 20 ℃ and 1500 rpm for 2 min followed by redispersal in a 0.1 wt% SDS solution, used to avoid colloidosome aggregation.

The steps followed to encapsulate the drug using gold coated colloidosomes were similar with the silver ones as above; the only difference is using 20 mL of 1 wt% aqueous solution of $HAuCl_4$ and 2 mL of 15 wt% aqueous solution of L-ascorbic acid to form a gold shell.

To disperse the capsules in pure water, a surface modification with 4,4'-dithiodibutyric acid (DDA) was carried out as described in section 3.2.2. A 20 mL solution of 0.5 wt% 4,4'-dithiodibutyric acid (DDA) in ethanol was mixed using the vortex and a known mass of silver or gold coated colloidosomes was added. Mixing by a magnetic stirrer for 48 h at room temperature allowed the reaction to proceed, after which the modified capsules were cleaned by three cycles of centrifuging at 1500 rpm for 2 min followed by re-dispersal in ultrapure water.

4.2.3 Release by ultrasonic treatment

An ultrasonic processor GEX 750 from Sonics & Materials Inc., USA was used to break the metal shell capsules. The method details and the ultrasound device are the same as reported in section 2.2.4. An ultrasonic probe, operating at a frequency of 20 kHz and power output of 50 W was used. The temperature change was kept below 5 ℃ by using an ice bath.

In addition, we also tried high intensity focused ultrasound (HIFU) to break the metal shell capsules. Fig. 4.3 shows a schematic of a home-made high intensity focused ultrasound device, which is provided by Prof Gleb Sukhorukov at Queen Mary, University of London. This set-up produces ultrasound with a frequency of 2.65MHz and a power of 6 W, similar to some medical devices [139]. To break metal shell

capsules, glass slides (1cm×1cm) were incubated in the PEI solution (2mg/mL, 0.5 M NaCl) for 30 min to coat them with PEI, and then washed three times with pure water. The metal shell microcapsules were dropped onto the glass slide and dried in air for further HIFU treatment. The slide was held with a tweezer and was located it the central area of HIFU and kept for a certain time. Finally, the slide was attached onto the SEM sample holder to measure the SEM images.

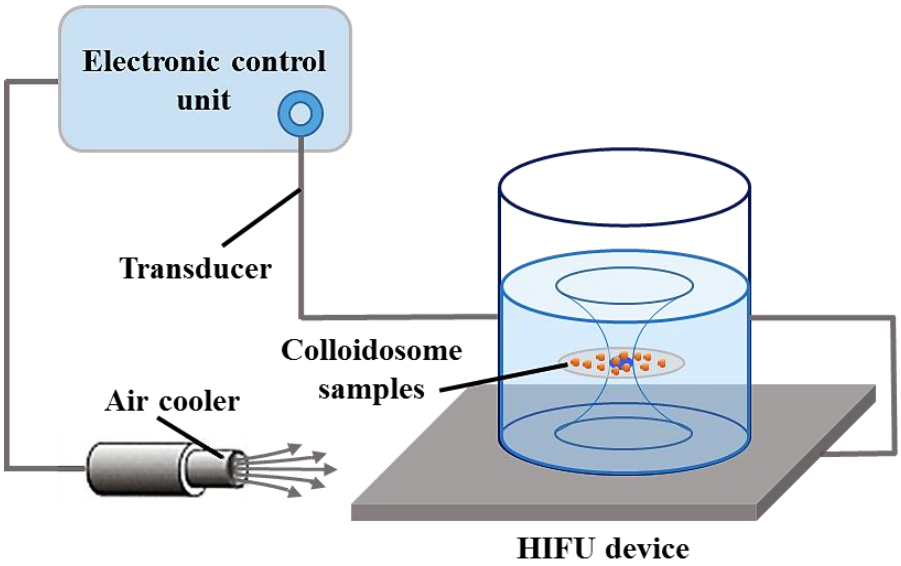

Fig. 4.3 Schematic of home-made high intensity focused ultrasound device, which is provided by Prof Gleb Sukhorukov Group at Queen Mary, University of London.

4.2.4 Cell culture and cell viability test

The cell viability tests were carried out by Hui Gao, Dong Luo and Prof Gleb Sukhorukov at Queen Mary, University of London. Cell viability was assessed via a standard MTT assay and examined by a BMG Fluostar Galaxy plate reader. Rat neuroblastoma B50 cells were cultured in DMEM supplemented with 10% FBS and penicillin-streptomycin (1%) containing 5% CO_2/95% air at 37 ℃. For cell viability studies, B50 cells were plated at 20 000 cells per well on 96 well plates. The next day microcapsules with different compositions and with or without ultrasonication, were added at ratios of 10, 20, or 50 capsules per cell to triplicate wells. The experiment was terminated when the total incubation times reached either 24, 48, or 72 h. Then a 100 μL thiazolyl blue tetrazolium bromide (MTT) solution (5 mg/mL in cell culture medium) was added to each well, and the plates were briefly shaken and then incubated for 3 h before dimethyl sulfoxide (DMSO) was added. Finally, cell viability

after coculturing with capsules for 24-72 h was assessed and read by a Multiskan Ascent plate reader. It is worth mentioning that a hemocytometer (a counting chamber) was used for determining the number of cells or microcapsules per unit volume of a suspension. The original cell and microcapsule suspensions were diluted low enough for counting on a hemocytometer under optical microscopy, and the concentrations of these original suspensions were calculated based on the dilution factor and the obtained number of cells or capsules per unit volume.

4.2.5 Sample characterization

The colloidosomes were characterised using SEM and CLSM. The method details and equipment were the same as described in section 2.2.6.

To test the drug encapsulation efficiency, a UV-Vis spectrophotometer equipped with a tungsten lamp (Thermo Scientific, model Heλios Gamma) was used for spectrometry measurements. The fluorescent doxorubicin was characterized by spectrophotometry in 10 mm path length polystyrene cuvettes. The absorbance value at 490 nm was recorded.

4.3 Results and discussion

4.3.1 Doxorubicin encapsulation

4.3.1.1 Using silver coated colloidosomes

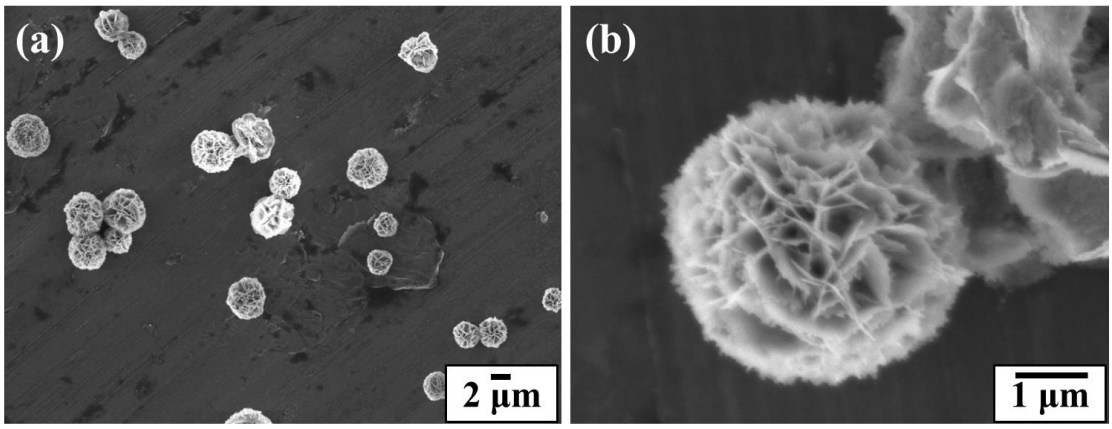

Fig. 4.4 SEM images of doxorubicin-containing silver coated colloidosomes: (a) low magnification, and (b) high magnification.

Fig. 4.4 shows SEM images of doxorubicin-containing silver coated colloidosomes. It can be seen that the particulate polymer shells are fully covered by sheet-like silver particles. The morphology of the silver shells doesn't change noticeably with doxorubicin encapsulation, compared with the water-core silver colloidosomes in Fig. 2.13. These capsules were then modified using DDA to disperse the drug-containing silver shell capsules in pure water, ready for cell viability tests.

The amount of fluorescent doxorubicin can be measured by a UV-Vis spectrophotometer. The calculation of the silver shell capsules drug loss data and encapsulation efficiency is shown in Table 4.1. During manufacture, 27.75 % of the total drug was lost in the waste oil phase, which may contain the lost drug in sunflower oil, and also, a small amount of drug which had leaked from the polymer shells after centrifugation. 49.75 % was lost in the washing solution. So, the remaining drug in the silver coated colloidosomes was about 22.50 %, which was the drug encapsulation efficiency.

Table 4.1 Calculation of the drug loss data and encapsulation efficiency of silver shells. All the drug data was measured three times to get an average result, and the standard error of the measurements were typically ±~3%, which are not shown for clarity. All the drug absorbance data was measure in the sensitive zone of the UV-Vis spectrophotometer.

Drug data	Mass	Total / lost drug	Encapsulation efficiency
Amount of drug added in the experiment	4.0 mg	100 %	----
Amount measured in the waste oil phase	1.11 mg	27.75 %	----
Amount measured in the washing solution	1.99 mg	49.75 %	----
Amount remaining drug in the silver shells	0.90 mg	----	22.50 %

4.3.1.2 Using gold coated colloidosomes

Fig. 4.5 shows SEM images of doxorubicin-containing gold coated colloidosomes. It can be seen that the particulate polymer shells are fully covered by gold particles. The morphology of the gold shells doesn't change noticeably and are still spherical with doxorubicin encapsulation, compared with the water-core gold coated colloidosomes in Fig. 2.17. These capsules were also modified using DDA for dispersing in pure water, ready for cell viability tests.

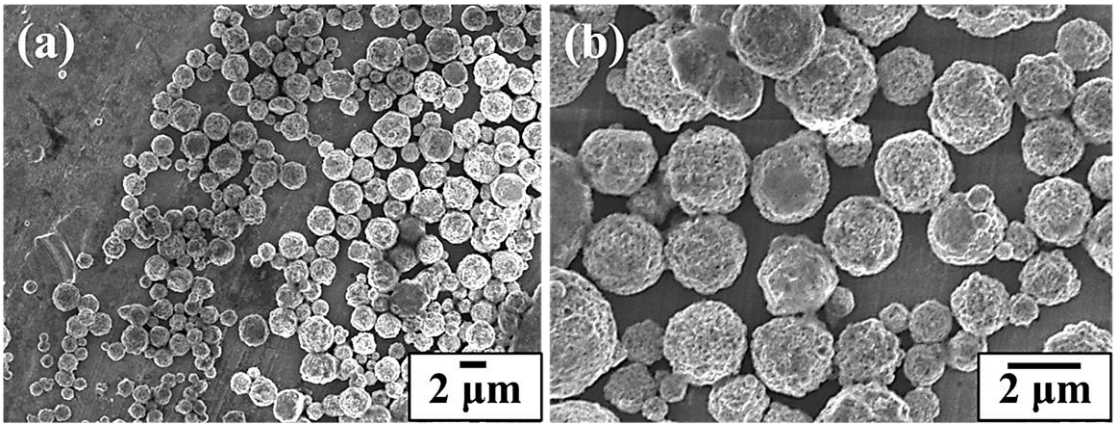

Fig. 4.5 SEM images of doxorubicin-containing gold coated colloidosomes: (a) low magnification, and (b) high magnification.

The calculation of the gold shell capsules drug loss data and encapsulation efficiency is shown in Table 4.2. During manufacture, 27.75 % of the total drug was lost in the waste oil phase. 56.25 % was lost in the washing solution. So the remaining drug in

the gold coated colloidosomes was about 16.0 %. This result suggests the gold coated colloidosomes have a lower drug loading efficiency compared with 22.50 % of silver coated colloidosomes.

Table 4.2 Calculation of the drug loss data and encapsulation efficiency of gold shells. All the drug data was measured three times to get an average result, and the standard error of the measurements were typically ±~3%, which are not shown for clarity. All the drug absorbance data was measure in the sensitive zone of the UV-Vis spectrophotometer.

Drug data	**Mass**	**Total / lost drug**	**Encapsulation efficiency**
Amount of drug added in the experiment	4.0 mg	100 %	----
Amount measured in the waste oil phase	1.11 mg	27.75 %	----
Amount measured in the washing solution	2.25 mg	56.25 %	----
Amount remaining in the gold shells	0.64 mg	----	16.0 %

4.3.2 Release by ultrasonic treatment

4.3.2.1 Silver coated colloidosomes

Using ultrasound probe. Fig 4.6 shows SEM images of doxorubicin-containing colloidosomes with a silver shell before and after 120 s of ultrasound treatment. Fig. 4.7 shows CLSM images of the same silver coated capsules before and after ultrasound treatment. An ultrasonic probe, operating at a frequency of 20 kHz and power output of 50 W was used for 120 s.

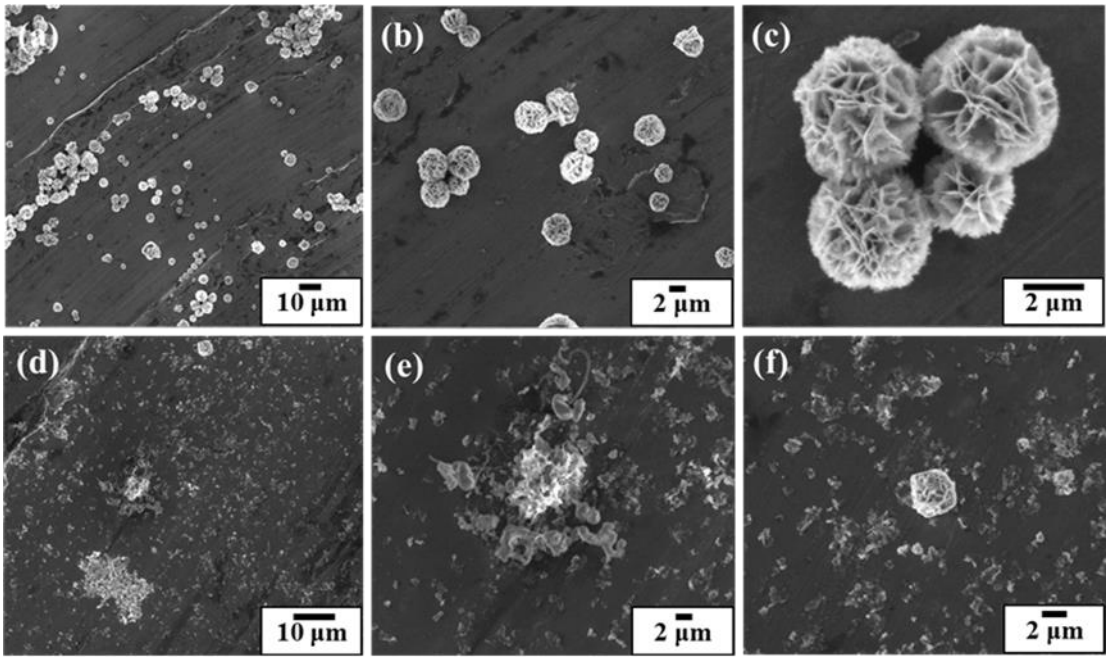

Fig. 4.6 SEM images of doxorubicin-containing silver coated colloidosomes before and after ultrasound treatment: (a) (b (c) without ultrasound treatment, and (d) (e) (f) after 120 s of ultrasound treatment. An ultrasonic probe, operating at a frequency of 20 kHz and power output of 50 W was used for 120 s.

After 120 s of ultrasound treatment, the silver shell capsules were seen to be broken into fragments and most of the capsules were destroyed. There were a large number of small dots appearing in the CLSM images in Fig. 4.7, which are likely to be the small pieces of broken shell, and some doxorubicin which was attched to the small broken shells. To see if there was any released doxorubicin, a futher cell viability experiment was performed.

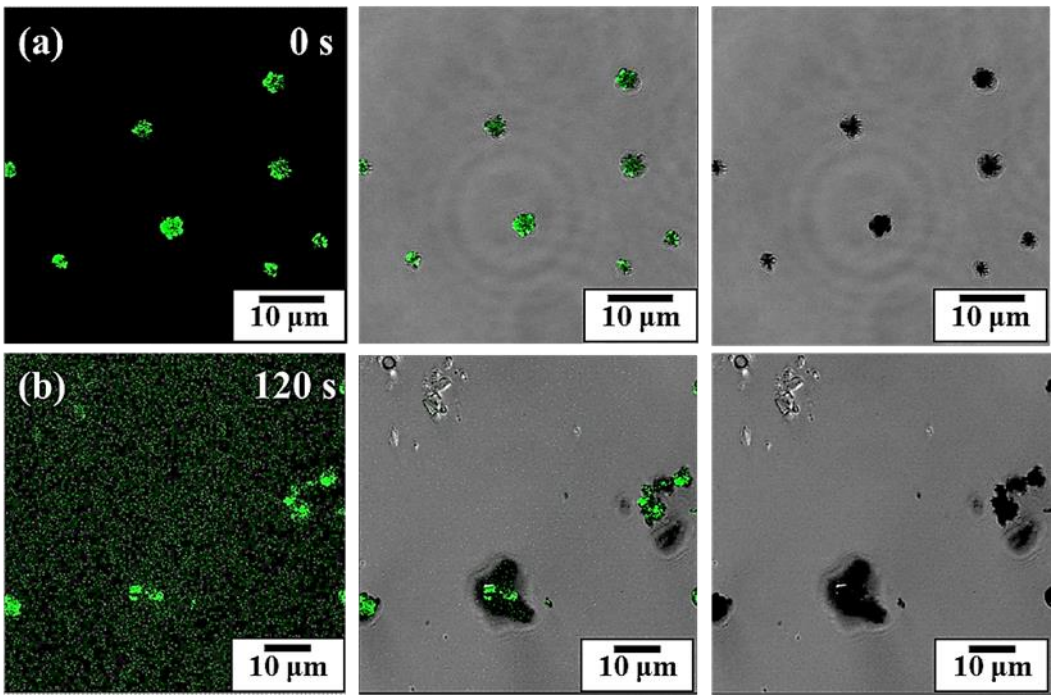

Fig. 4.7 CLSM images of doxorubicin-containing silver coated colloidosomes before and after 120 s of ultrasound treatment, with λex =480 nm, fluorescent drug (left), bright field (right), and merged (middle) images. The ultrasound was operated at a frequency of 20 kHz and power output of 50 W for 120 s: (a) without ultrasound treatment, and (b) after 120 s of ultrasound treatment.

Fig. 4.8 shows CLSM images of the surface of some doxorubicin-containing silver coated capsules. When focusing onto the surface of these capsules, there was also some fluorescent doxorubicin appearing, which cannot be easily washed off. This indicates that the drug was not only sealed in the silver shells, but some was also attached on the surface of the capsules. The possible reason is that during the formation of silver shells, the doxorubicin which is sealed inside the polymer shell may diffuse from the polymer shells and may attach onto the surface of the silver shells.

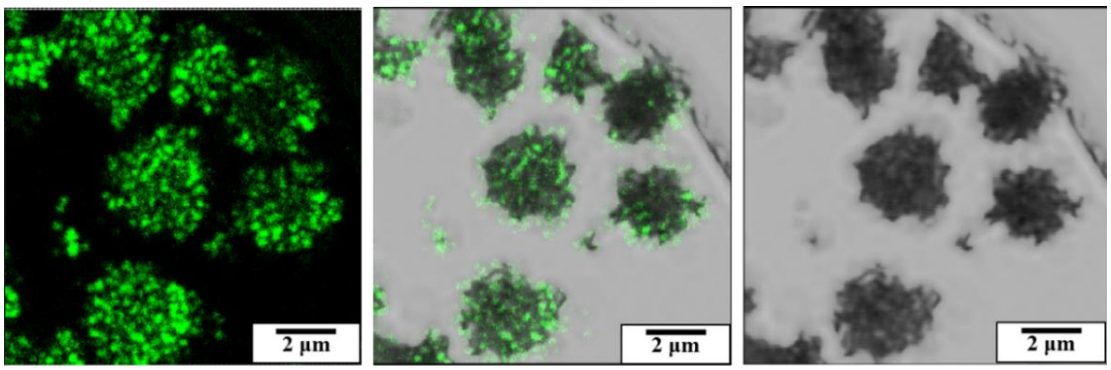

Fig. 4.8 CLSM images of the surface of some doxorubicin-containing silver coated colloidosomes with λex =480 nm, fluorescent drug (left), bright field (right), and merged (middle) images.

Using HIFU. For the ultrasound treatment with a high power of 50 W, a few minutes is enough to break most of the silver coated colloidosomes and release the drug solution. However, considering the application, we also tried high intensity focused ultrasound (HIFU) with a frequency of 2.65 MHz and a power of 6 W, which can be used for some cancer treatments. Fig. 4.9 shows SEM images of the doxorubicin-containing silver shell colloidosomes before and after 120 s of HIFU treatment. It is clearly seen that part of the silver shells were deformed and broken after exposure to HIFU, however, there were still a large number of intact colloidosomes. This may be caused by the lower power of the ultrasound, where a relatively long duration time is needed to damage the silver coated colloidosomes.

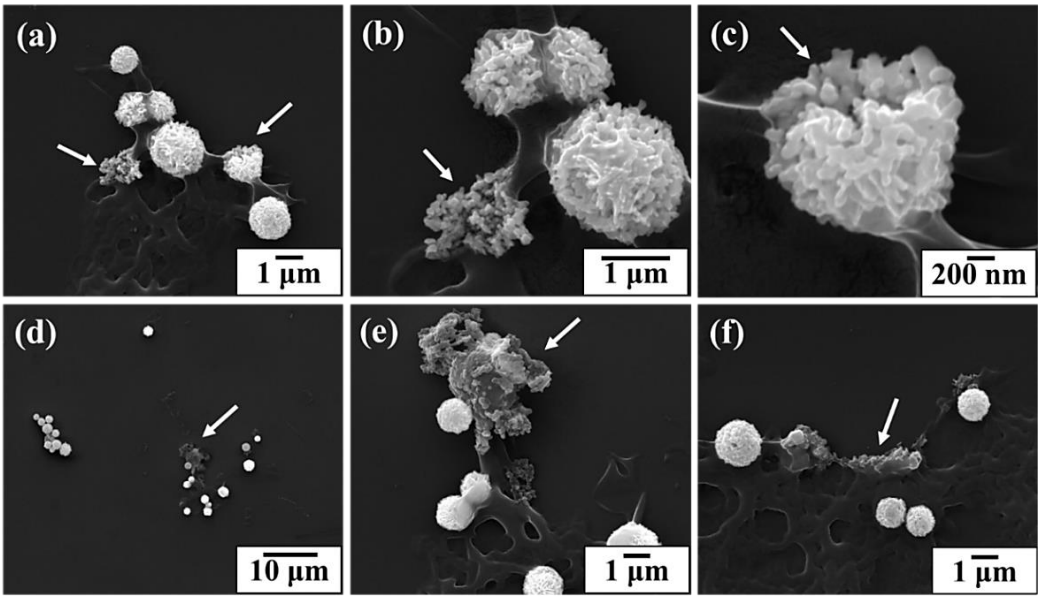

Fig. 4.9 SEM images of doxorubicin-containing silver coated colloidosomes before and after 120 s of HIFU ultrasound treatment, with a frequency of 2.65MHz and a power of 6 W. (a)-(f) showing different magnifications.

4.3.2.2 Gold coated colloidosomes

Using ultrasound probe. Fig. 4.10 shows SEM images of doxorubicin-containing gold coated colloidosomes and the same capsule samples after 240 s of ultrasound treatment, operating at a frequency of 20 kHz and power output of 50 W. As we can see, after 240 s of ultrasound treatment, most of the doxorubicin-containing gold coated colloidosomes were broken into small fragments. We also tried to use CLSM to take some fluorescent images to test the doxorubicin attached in or on gold shell capsules. However, since the gold shells quench fluorescent signal, no fluorescent

images were obtained.

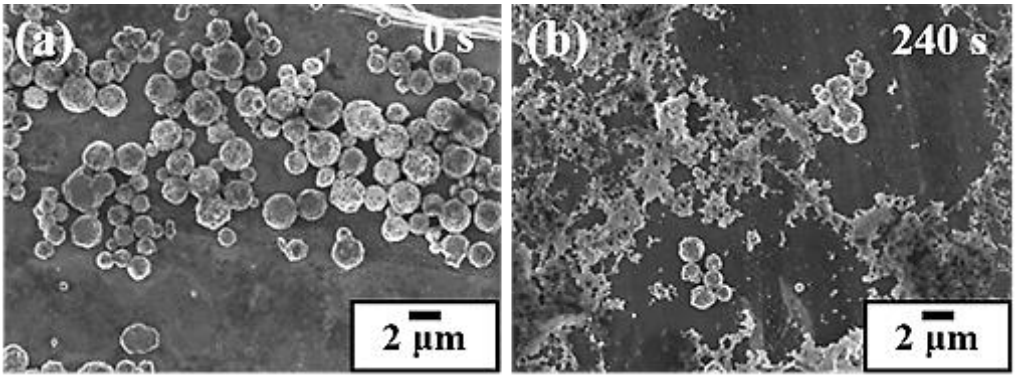

Fig. 4.10 SEM images of doxorubicin-containing gold coated colloidosomes before and after ultrasound treatment: (a) without ultrasound treatment, and (b) after 240 s of ultrasound treatment. An ultrasonic probe, operating at a frequency of 20 kHz and power output of 50 W was used for 240 s.

Using HIFU. For the ultrasound treatment with a high power of 50 W, a few minutes is enough to break most of the gold coated colloidosomes and release the drug solution. Here, we also tried high intensity focused ultrasound (HIFU) with a frequency of 2.65 MHz and a power of 6 W to break the gold coated colloidosomes. Fig. 4.11 shows the SEM images of doxorubicin-containing gold shell colloidosomes after 120 s of HIFU treatment. It is clearly seen that part of the gold shells were deformed and broken. But there were still a large number of intact colloidosomes.

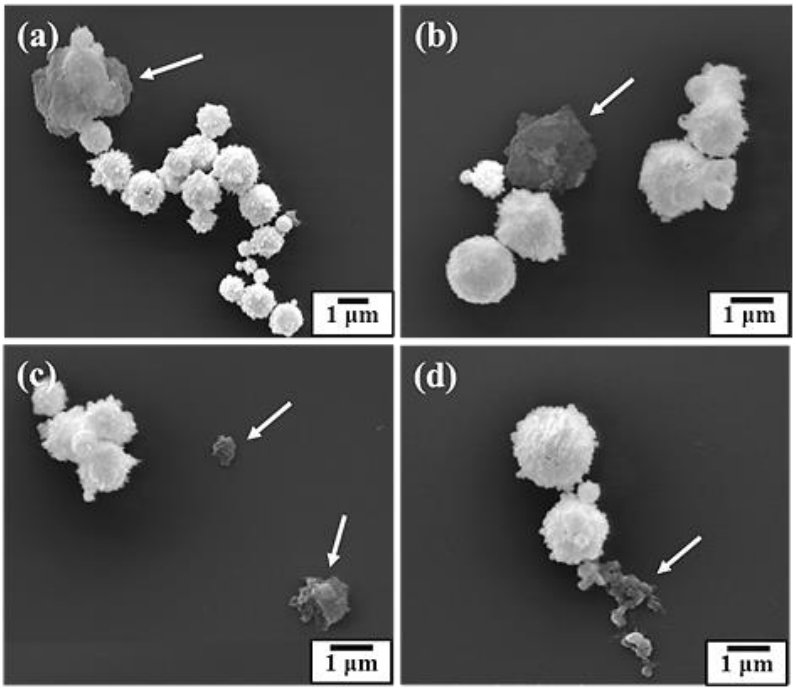

Fig. 4.11 SEM images of doxorubicin-containing gold coated colloidosomes before and after 120 s of HIFU ultrasound treatment, with a frequency of 2.65MHz and a power of 6 W. (a)-(d) showing different magnifications.

In this part, we used two types of ultrasound treatment to break both the doxorubicin-containing silver and gold coated colloidosomes. For the high power (50 W) ultrasound probe, it is possible to break most of the metal coated colloidosomes and release the drugs. When using a HIFU treatment for a few minutes, part of the metal shells was deformed and broken, and there was still a large percentage of metal shell colloidosomes intact. In order to use HIFU treatment to break capsules, further research needs to be done to improve the release efficiency using HIFU for the metal capsules.

4.3.3 Cell viability test

4.3.3.1 Using silver coated colloidosomes

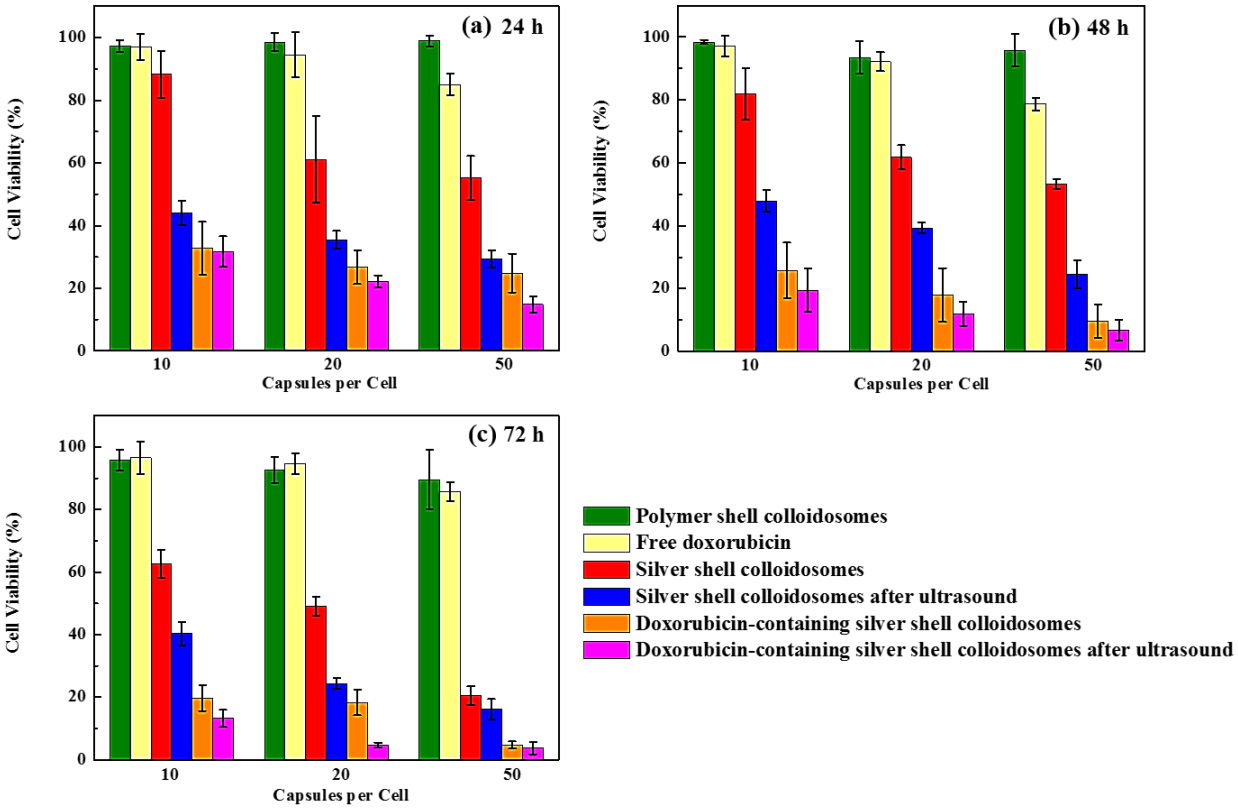

Fig. 4.12 Viability of B50 cells mixed with different amounts of particulate polymer shell colloidosomes, free doxorubicin, silver shell colloidosomes, silver shell colloidosomes after 120 s ultrasound, doxorubicin-containing silver shell colloidosomes and doxorubicin-containing silver shell colloidosomes after 120 s ultrasound. (a) 24 h, (b) 48 h, and (c) 72 h at 37 °C. The error bars show the standard deviations. The ultrasound treatment was operated at a frequency of 20 kHz and power output of 50 W in an ice bath, before adding into the B50 cells.

A cytotoxicity study was carried out in vitro at different capsules/cell concentrations for B50 cancer cells for up to 72 h. Fig. 4.12 shows the viability of the B50 cells when mixed with different amounts of particulate polymer shell colloidosomes, free doxorubicin, silver shell colloidosomes, silver shell colloidosomes after 120 s ultrasound, doxorubicin-containing silver shell colloidosomes and doxorubicin-containing silver shell colloidosomes after 120 s ultrasound. The experiments were carried out for (a) 24 h, (b) 48 h, and (c) 72 h at 37 ℃, and measured by an MTT assay relative to the control. To break the silver shells, ultrasound was used for 120 s at a frequency of 20 kHz and power output of 50 W, before adding into the B50 cells.

Cells are very sensitive to the external particles, hence, the concentration of the introduced particles is a key factor that determines their cell toxicity. Usually, higher the concentration of the drug carriers, the lower the cell viability is. In this study, we set up the capsule/cell ratio at 10, 20 and 50 to investigate the cell viability. 50 capsules/cell showed relative high cell toxicity, therefore ratios higher than 50 were not carried out. On the contrary, the data demonstrated a very low cytotoxicity at 10 capsules/cell, so we did not try a lower concentration. When prolonging the incubation time, more cells might be affected by the introduction of external capsules. For controlled instant release of drugs, capsules can be up taken by cells within 6 hours, and then triggered by external stimuli, i.e., ultrasound, hence a good biocompatibility within 48 hours is enough to secure the delivery of encapsulated cargoes by colloidosomes to the targeted area. In addition, a higher concentration of capsules means a higher amount of drugs that can be delivered.

As seen in Fig. 4.12, for 10 capsules/cell, both the particulate polymer shells and free doxorubicin show low toxicity to the cancer cells with a cell viability more than 95% from 24 h to 72 h. The results of silver shells indicate low cytotoxicity, in Fig. 4.12a, showing the cell viability at more than 90% during the first 24 h and in Fig. 4.12b more than 80% after 48 h. After 72 h, in Fig. 4.12c, the cell viability of silver shells dropped to around 60%, indicating an increased toxicity to cells when prolonging the incubation time. After ultrasound treatment, the broken silver shells display a relatively high cytotoxicity with a cell viability of around 50% during the first 48 h and around 40% after 72 h. The possible reason is that after ultrasound the pieces of broken shell are smaller compared with intact capsules, which become more toxic to living cells [196-199]. The doxorubicin-containing silver shell colloidosomes also lead to a low cell viability, showing around 20% after 72 h in Fig. 4.12c. A possible reason for this is that when making the silver shell colloidosomes, the drug may diffuse through the particulate polymer shell and may attach on the surface of the silver shells. Even after three washing processes, the attached drug seems to not be easily washed off. The doxorubicin on the surface may then be toxic to the cancer cells, leading to the decreased cell viability. The doxorubicin-containing silver shells after 120 s of ultrasound treatment illustrate a higher cytotoxicity, displaying a viability of about 15% after 72 h. This is because of the released drug, the broken silver shells and the drug attached on the surface of the capsules all killing the cancer cells. At 10

capsules/cell, the free doxorubicin at this concentration is not high enough to kill too many cells; when increasing the concentration, the effect was more obvious.

The cell viability tests of 20 capsules/cell display a similar trend. Both the particulate polymer shells and free doxorubicin show low toxicity to cancer cells. However, the silver shell results indicate a higher cytotoxicity compared with particulate polymer shells, in Fig. 4.12b, showing the cell viability at about 60% during the first 48 h. After 72 h, in Fig 4.12c, the cell viability of silver shells dropped to around 50%. After ultrasound treatment, the broken silver shells display a relatively high cytotoxicity, showing a cell viability of around 40% during the first 48 h and lower than 30% after 72 h. The doxorubicin-containing silver shell colloidosomes also lead to a low cell viability, showing around 20% after 72 h in Fig. 4.12c. After 120 s of ultrasound treatment, it illustrates a higher cytotoxicity, displaying a viability of about 5% after 72 h.

The cell toxicity of silver shell capsules was significantly higher than the particulate polymer shell capsules, when the concentration reached 50 capsules/cell. The free doxorubicin at this concentration is more toxic than 10 and 20 capsules/cell, showing a cell viability of 85% after 24 h, 78% after 48 h and 86% after 72 h. An increase in the amount of silver and doxorubicin means the cytotoxicity is increased. The silver shell capsules display a viability value of about 20% after 72 h in Fig. 4.12c. After ultrasound treatment, the broken silver shells display a cell viability of around 15% after 72 h in Fig. 4.12c. Both the doxorubicin-containing silver shell colloidosomes and the ones after ultrasound lead to a low cell viability, showing around 5% after 72 h.

The toxicity of silver particles to living cells was reported by some researchers as well. For example, Yen et al. [153] used murine macrophage cells to test the toxicity of different concentrations and sizes of silver nanoparticles. For the concentration of 1 ppm, there was no significant effect on cell viability. When using a concentration of 10 ppm, the cell proliferation or viability decreased dramatically. In addition, the cytotoxic effect of small size silver nanoparticles (2-5 nm) to macrophages was more obvious than that of large size silver nanoparticles (20-40 nm). These conclusions are similar to our experimental results. For water-core silver colloidosomes, the high concentration of the colloidosomes has a higher toxicity than the low concentration.

In addition, after breaking by ultrasound, the silver shells were broken into small pieces resulting in a higher toxicity.

According to the cell viability results, all the capsule concentration, size and composition can determine the final proliferation and death rate of cells. After triggering the silver shells using ultrasound, the combined effects of the released doxorubicin, the broken silver shell capsule fragments and the possible drug attached on the surface of the capsules all may kill cancer cells. It is also clear that the number of capsules is also a crucial design parameter.

4.3.3.2 Using gold coated colloidosomes

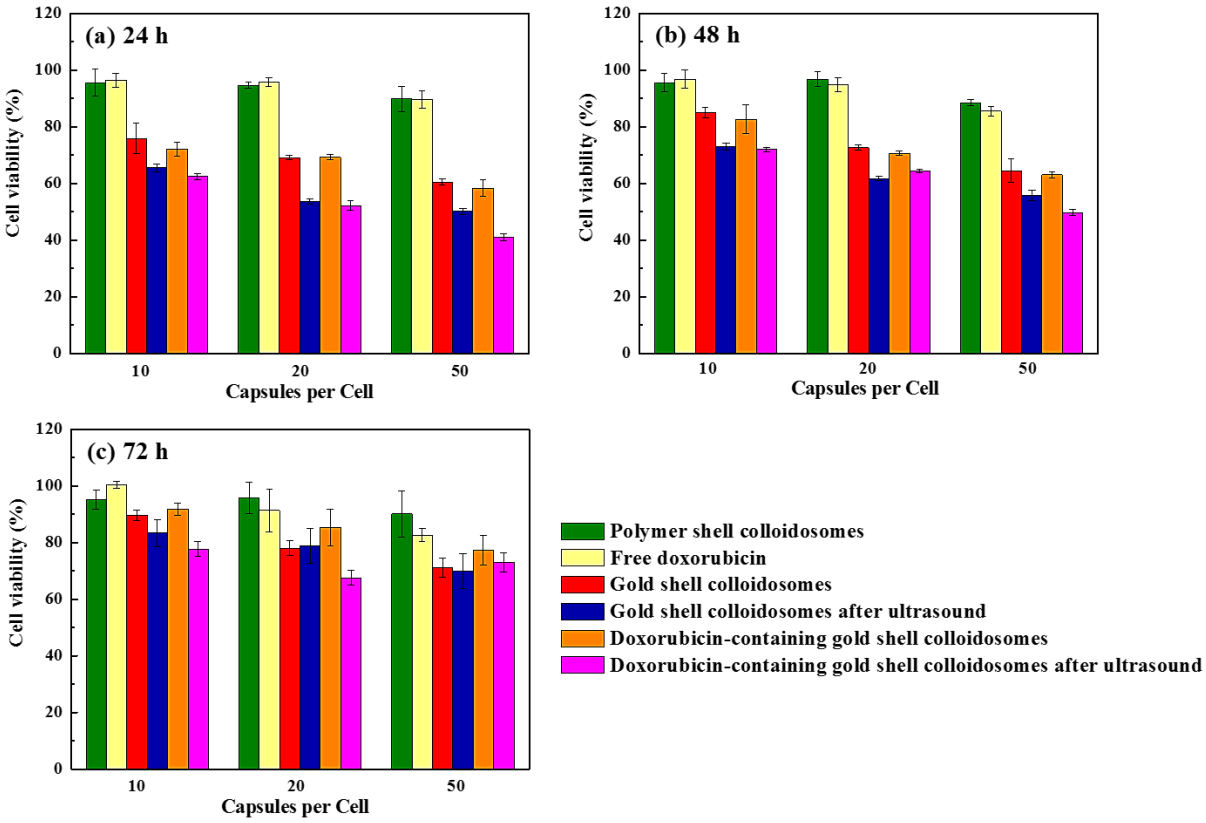

Fig. 4.13 Viability of B50 cells mixed with different amounts of particulate polymer shell colloidosomes, free doxorubicin, gold shell colloidosomes, gold shell colloidosomes after 240 s ultrasound, doxorubicin-containing gold shell colloidosomes and doxorubicin-containing gold shell colloidosomes loading doxorubicin after 240 s ultrasound. (a) 24 h, (b) 48 h, and (c) 72 h at 37 °C. The error bars show the standard deviations. The ultrasound treatment was operated at a frequency of 20 kHz and power output of 50 W in an ice bath, before adding into the B50 cells.

The cell viability experiment was repeated with the gold shell capsules. As seen in Fig. 4.13a, after 24 h, both the particulate polymer shells and free doxorubicin indicate no toxicity to cancer cells, showing a cell viability of more than 94% at the concentration of 10 and 20 capsules per cell, and more than 89% at 50 capsules per cell. The blank water-core gold coated colloidosomes results indicate a low cytotoxicity showing the cell viability at more than 70% for 10 and 20 capsules per cell, and more than 60% for 50 capsules per cell. After using ultrasound to break the gold shells, the cell viability of the broken water-core gold shells dropped by about 10% for all capsule concentrations. This suggests that the small broken shells are more toxic to the cancer cells compared with the intact gold coated capsules. The cell viability of gold coated colloidosomes loading doxorubicin display a very similar cytotoxicity to the blank gold shells, with a cell viability of more than 70% for 10 and 20

capsules per cell and more than 58% for 50 capsules per cell. After ultrasound, the doxorubicin-containing gold shell colloidosomes lead to a lower cell viability of 62% for 10 capsules, 52% for 20 capsules per cell and around 40% for 50 capsules per cell. This suggests that both the released doxorubicin and broken gold fragments can kill cancer cells. For free doxorubicin, only a higher concentration of capusles, 50 capsules per cell, result in an obvious effect on cells. This suggests that the released doxorucin is not enough to kill cells at the concentration of 10 and 20 capsules per cell.

As can be seen in Fig. 4.13a, b and c, at different time points, the gold shells have an effect on cell viability. At later times of 48 and 72 h, the cell viability increased compared with 24 h. This indicates that the gold shells have an inhibiting effect on cell viability, specifically at early times, and later this effect is diluted and cells recover and return to proliferation. There might be different reasons for the observation. Firstly, cells prefer to initially reject any external materials, and they need some time to get used to their environment. It is worth mentioning that, after 48 h, all gold samples still display the same trend as seen after 24 h, but with a higher cell viability. This suggests that the B50 cells are acclimatizing to the capsules with a gold coating and displaying good cell proliferation. Secondly, other factors, such as the concentration, size and composition of the gold particles, can influence the final proliferation and death rate of cells. Nevertheless, the data suggests that the gold coated colloidosomes have no major negative effect on cell viability. The silver coated colloidosomes display a higher toxicity. For example, after 72 h, the broken water core silver coated colloidosomes show a cell viability of around 40% at a concentration of 10 capsules per cell, however, the gold ones show a viability of 70% at the same concentration. Compared with silver shell colloidosomes, the gold shells show lower toxicity to cells, and lower drug encapsulation efficiency. To find out why gold coated colloidosomes have no major negative effect on cell viability, we may need further research.

4.4 Conclusions

In this chapter, our study has demonstrated a method for encapsulating an anticancer drug using both silver and gold coated colloidosomes. These two types of colloidosomes are impermeable for small molecules drugs and can be triggered using ultrasound. After 120 s of ultrasound treatment for silver shells and 240 s of ultrasound treatment for gold shells, most of the capsules were destroyed into small pieces and only a few survived. We propose the possibility to use the metal coated capsules for delivery of anticancer drugs, i.e., doxorubicin. For silver coated colloidosomes, at 10 capsules/cell, they have a low cytotoxicity, showing a cell viability of more than 90% during the first 24 h and more than 60% after 72 h. With prolonging the numbers of the capsules, the cytotoxicity of the silver shells increases heavily. After triggering the doxorubicin-containing silver shells using ultrasound, the combined effects of the released doxorubicin, the broken silver shell capulse fragments and the possible drug attached on the surface of the capsules all may kill cancer cells. Compared with silver ones, the gold shells seem to be less toxic to cells, and have a lower drug loading efficiency.

Chapter 5.

Antibiotic encapsulation - Kanamycin

The results from this chapter have been published in Frontiers in Chemistry:

Qian Sun, Ziyan Zhao, Elizabeth A. H. Hall, Alexander F. Routh. *Metal Coated Colloidosomes as Carriers for an Antibiotic*. Frontiers in Chemistry, 2018, 6: 196.

5.1 Introduction

In chapter 4, we demonstrated a method for encapsulating an anticancer drug using both silver and gold coated colloidosomes, and tested the cell viability of B50 cancer cells. To investigate the application of the metal coated colloidosomes in another biological system, *Escherichia Coli* (*E.coli*) bacteria were chosen and mixed with colloidosomes which contain the antibiotic kanamycin. *E.coli* have been studied extensively and are an ideal model organism. Kanamycin is an aminoglycoside antibiotic that induces its bactericidal effect by introducing errors in protein synthesis through tRNA mismatch upon binding to the bacterial ribosome [200].

This chapter describes a method for encapsulating an antibiotic kanamycin using silver or gold coated colloidosomes. The colloidosomes are impermeable and can be triggered using ultrasound. After triggering the metal shells by ultrasound, the released antibiotic, the broken fragments and the possible antibiotic attached on the suface of the capluses may all kill *E.coli*. For a constant concentration of capsules, silver shells display a very slightly higher toxicity than gold ones. The gold coated colloidosomes can load a higher concentration of kanamycin than silver shells. There are also some interesting morphological changes to the silver shell capsules upon encapsulation of the antibiotic and we report on these in this chapter.

5.2 Experimental section

5.2.1 Materials

The base latex particles and particulate polymer shell colloidosomes were made in exactly the same process as reported in section 2.2.1. The deionized water in all experiments had a resistivity of 18.2 MΩ•cm and was produced by a Pure Lab Ultra apparatus. Other chemicals, including sodium dodecyl sulfate (SDS, Fisher Scientific), buffer solution pH 10.0 (Sigma-Aldrich), 4,4'-dithiodibutyric acid (DDA, 95%, Sigma-Aldrich), and kanamycin monosulphate (Sigma-Aldrich) were all used as received without purification. The vortex mixer was a TopMix FB15024 (Fisher Scientific).

For cell viability studies, pET-24a (+) plasmid with a kanamycin resistant site (Novagen) was transferred into *Escherichia Coli* BL21 (DE3) competent cells (Novagen). The cells were grown in Luria Bertani (LB) Media, which contains 50 μg/mL kanamycin. The LB media was prepared with 10 g/L tryptone (mirobiologically tested, Sigma-Aldrich), 5 g/L yeast extract (for use in microbial growth medium, Sigma-Aldrich), 10 g/L NaCl (Sigma-Aldrich), and 1.5% (w/v) Agar powder (Thermo Fisher Scientific).

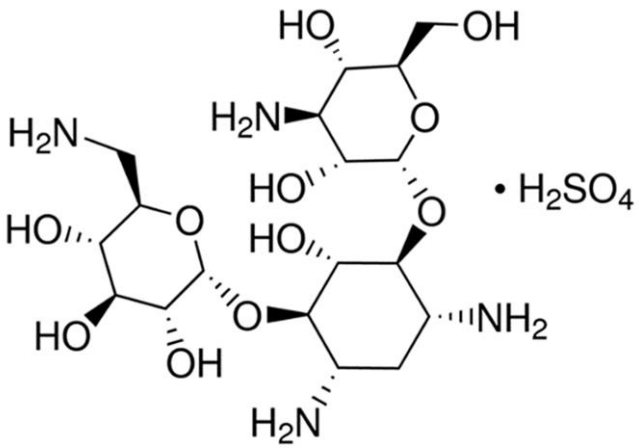

Fig. 5.1 Chemical structure of kanamycin monosulphate.

5.2.2 Antibiotic encapsulation

Fig. 5.2 shows the fabrication method of kanamycin-containing gold coated colloidosomes. A Silverson high shear mixer (model SL2) was used to mix 4 mL Span 80 with 200 mL sunflower oil in a 400 mL beaker. The latex particle suspension (11.2 wt% in pH 10 buffer solution) was mixed with 12.5 mg/mL kanamycin monosulphate, to get a mixture, which contained 5.6 wt% latex particles and 6.25 mg/mL kanamycin monosulphate in buffer solution. 2 mL of this mixture was then added into the sunflower oil. After emulsification, the mixture was heated in a water bath at 50 ±0.5 ℃. This allows the latex particles to merge into a smooth shell.

After sintering, 20 mL of the emulsion mixture was centrifuged at 2500 rpm for 10 min at 20 ℃. The oil was removed via pipetting and 20 mL of 1 wt % aqueous solution of $HAuCl_4$ and 2 mL of 1 wt% aqueous SDS solution were added, and the microcapsules were redispersed in the aqueous phase using a vortex mixer. Then 2 mL of L-ascorbic acid solution (15 wt% in water) was added to the tube and rested for 1 h to allow the gold forming reaction. After the gold forming reaction, the mixture was centrifuged at 1500 rpm for 2 min at 20 ℃ to recover the sediment and the supernatant was removed via pipetting. The resulting gold coated colloidosomes, loaded with kanamycin, were washed and redispersed, using a 0.1 wt% SDS solution, used to avoid colloidosome aggregation.

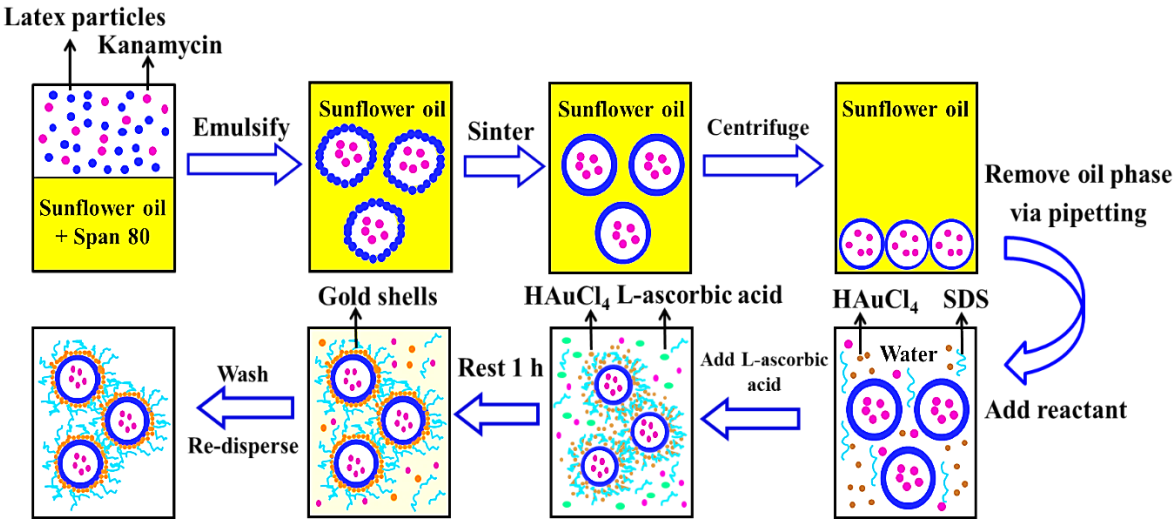

Fig. 5.2 Fabrication method of kanamycin-containing gold coated colloidosomes.

The SDS surfactant solution affects the cell viability. However, without the surfactant the capsules are heavily aggregated in water. Consequently, we used 4,4'-dithiodibutyric acid

(DDA) to modify the capsule surfaces, which allows the metal shell capsules to disperse in pure water. A known mass of silver or gold coated colloidosomes were dispersed in 0.5 wt% 4,4'-dithiodibutyric acid (DDA) in ethanol and then gently mixed by a magnetic stirrer for 48 hours at room temperature. After the reaction, the whole mixture was centrifuged at 1500 rpm for 2 min. The supernatant was removed using a pipette. The modified capsules were washed and redispersed three times using ultra-pure water.

To make kanamycin-containing silver coated colloidosomes, the method is similar to that for the gold shell capsules. For silver shells, 24 mL of $AgNO_3$ solution (0.1 wt% in water) and 2 mL of SDS (1 wt% in water) were added in each tube. Then 2 mL of L-ascorbic acid solution (15 wt% in water) was added and rested for 1 h allowing the silver forming reaction.

5.2.3 Release by ultrasonic treatment

Remote activation of microcapsules was conducted using an ultrasonic probe operating at a frequency of 23 kHz and 50W. To break the metal shell capsules, the suspension of microcapsules was subjected to ultrasound sonication, performed using an ultrasonic processor (Sanyo soniprep 150). The probe was placed into a 5 mL capsule suspension in a 50 mL plastic tube. An ice bath was applied to ensure that the temperature change of the capsule suspension was less than 5 ℃.

5.2.4 Cell viability test

The kanamycin resistant *E.coli* BL21 (DE3) cells were grown for 16 hours in 10 mL LB medium supplemented with 50 μg/mL kanamycin. 100 μL of the overnight culture were then transferred to 50 mL falcon tubes containing the same LB medium for inoculation. The growth of cells was monitored by measuring the optical density at 600 nm (OD_{600}) of the cell culture using a UV-Visible spectrophotometer (Infinite M200 Tecan). The treatments were added to the cells, when the culture OD_{600} was approximately 0.7. For blank kanamycin measurements, 1 mL of kanamycin solution at various concentrations was added to the cells to obtain final concentrations between 50 and 5000 μg/mL. For metal shell capsules, blank silver/gold shells and silver/gold shells loading kanamycin with intact shells were added to the cell culture, achieving a final concentration in the range of 7.1×10^5 to 3.5×10^8 capsules/mL. A hemocytometer (a counting chamber) was used for determining the number of microcapsules per unit volume of a suspension. For drug release experiments, the same

concentrations of ultrasound-broken capsules were added to the cell culture. Treated cells were then grown for 24 hours. All cultures were shaken at 37 ℃, 225 rpm in a multitron shaker (Infors HT). The resulting cell cultures were then diluted in LB media and spread evenly on a 90 mm LB Agar plate supplemented with 50 μg/mL kanamycin, to result in 30-300 CFU per agar plate. The plates were then grown at 37 ℃ in an incubator (Heraeus Instruments) for 16 hours before the CFU for each plate was counted.

5.2.5 Sample characterization

The gold and silver coated colloidosomes were characterised using SEM and EDX. The equipment was the same as described in section 2.2.6. The growth of cells was monitored by measuring the optical density at 600 nm (OD600) of the cell culture using a UV-Visible spectrophotometer (Infinite M200 Tecan).

5.3 Results and discussion

5.3.1 Antibiotic encapsulation

5.3.1.1 Using gold coated colloidosomes

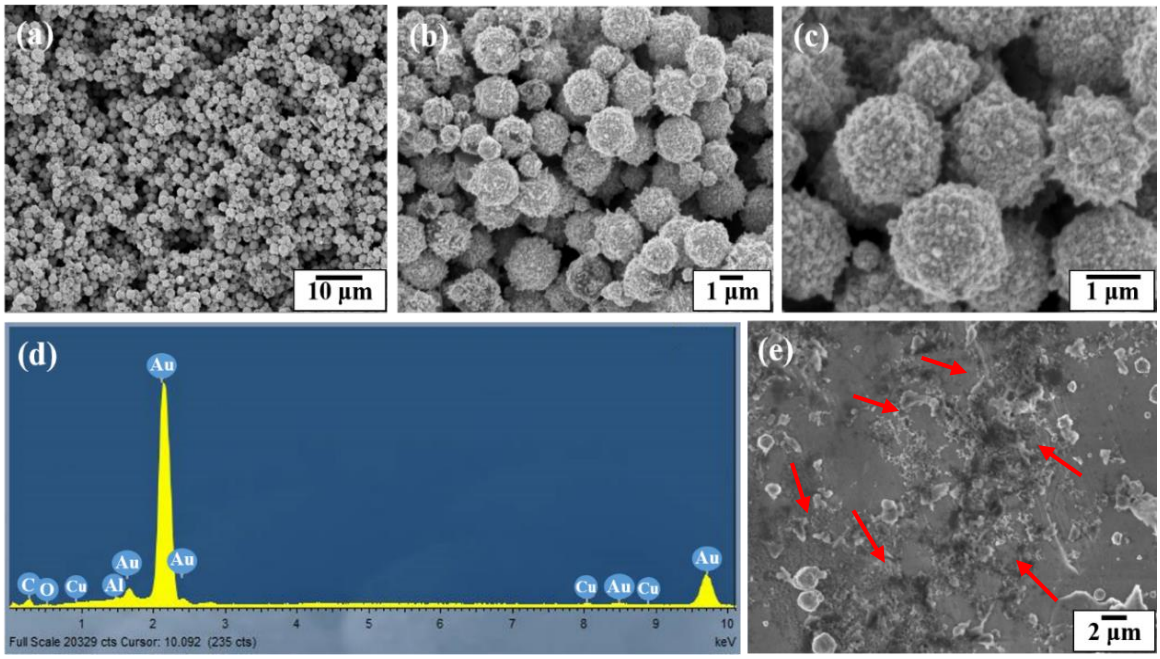

Fig. 5.3 (a) (b) (c) SEM and (d) EDX images of kanamycin-containing gold coated colloidosomes, and (e) the same kanamycin-containing gold coated colloidosomes after ultrasound treatment, operating at a frequency of 23 kHz and 50W.

Fig. 5.3a to 5.3c show SEM images of kanamycin-containing gold coated colloidosomes. It can be seen that the particulate polymer shells were fully covered by gold particles. After loading kanamycin, the morphology of the gold shells does not significantly change, compared with the water-core gold coated colloidosomes in Fig. 2.17, and the gold shell capsules remain spherical. Fig. 5.3d shows the corresponding EDX image which has high gold peaks, suggesting that the particles surrounding the surface of the colloidosomes are gold. There are also carbon and oxygen peaks, arising from the particulate polymer shell. The aluminium and copper peaks were caused by the SEM stub. To release the encapsulated drug, ultrasound was used to trigger the capsules. As shown in Fig. 5.3e, after 480 s sonication, only a few colloidosomes survived and there were a large number of small pieces of broken shell. For this experiment, we used a longer time in order to break most of the capsules, compared with the time previously reported for water-core gold shell colloidosomes in section 2.3.3.2.

5.3.1.2 Using silver coated colloidosomes

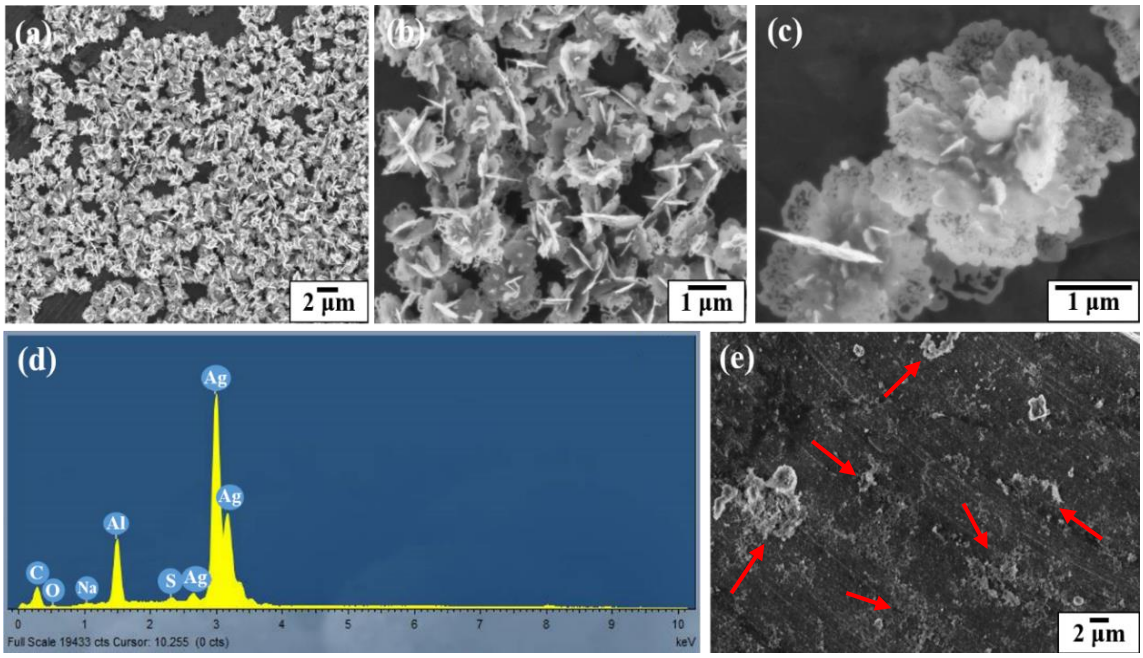

Fig. 5.4 (a) (b) (c) SEM and (d) EDX images of kanamycin-containing silver coated colloidosomes, and (e) the same kanamycin-containing silver coated colloidosomes after 240 s of ultrasound treatment, operating at a frequency of 23 kHz and 50W.

Fig. 5.4a to 5.4c show the SEM image of the silver coated colloidosomes which contained kanamycin. As can be seen, the particulate polymer shells were fully covered by sheet-like silver particles. After loading kanamycin, the morphology of the silver shells changes from the water-core silver shell capsules shown in Fig. 2.13. The sheet-like silver particles, surrounding the surface of the particulate polymer shells, were thinner and some silver sheets became hollow at the edge. In the silver forming process, the kanamycin may affect the silver ions converting into metallic silver. This is likely because kanamycin might associate with the silver precursor [201] and prevent it from forming shell shaped capsules.

Fig. 5.4d shows the corresponding EDX image which has high silver peaks. The sodium and sulfur peaks were caused by the SDS surfactant. As shown in Fig. 5.4e, after 240 s sonication, most of the silver coated colloidosomes are broken into fragments. For this experiment, we also used a longer time in order to break most of the capsules, compared with the time previously reported for water-core silver shell colloidosomes in section 2.3.3.1.

Fig. 5.5 shows SEM images of the silver coated colloidosomes encapsulating varying amounts of kanamycin. When the original kanamycin concentration was increased to 25.0 mg/mL, the silver particles became thinner. When the concentration increased to 50.0 mg/mL, there was no silver shell, just separate sheet-like silver particles aggregated. However, for gold shells, there was no obvious effect of kanamycin concentration as shown in Fig. 5.5d.

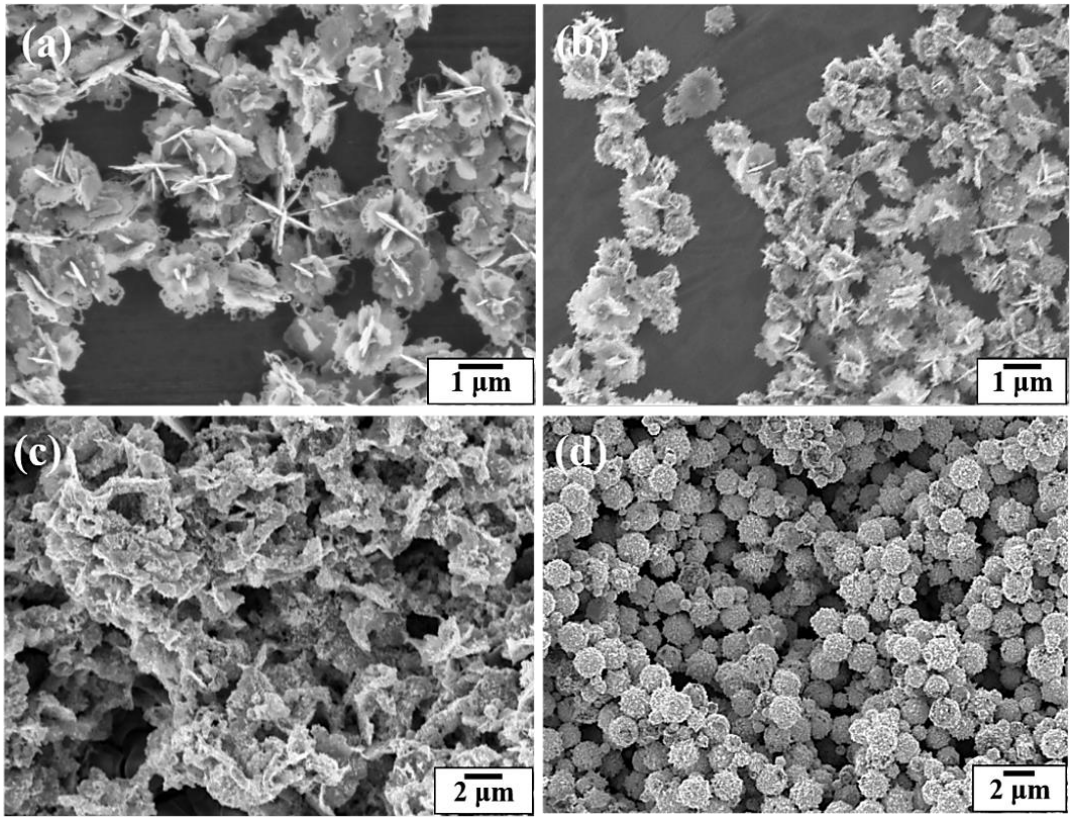

Fig. 5.5 SEM images of the silver coated colloidosomes using varying amounts of kanamycin to produce the metal shells: (a) 12.5 mg/mL, (b) 25.0 mg/mL, (c) 50.0 mg/mL, and (d) gold coated colloidosomes using 50.0 mg/mL kanamycin.

5.3.2 Cell viability test

The application of the metal coated colloidosomes as small molecule drug carriers was investigated in a bacteria system. The CFU/mL data in Fig. 5.6 to 5.8 are calculated by counting the average number of the diluted cell colonies. The standard error of the results is shown by the error bars.

5.3.2.1 Free kanamycin cell viability test

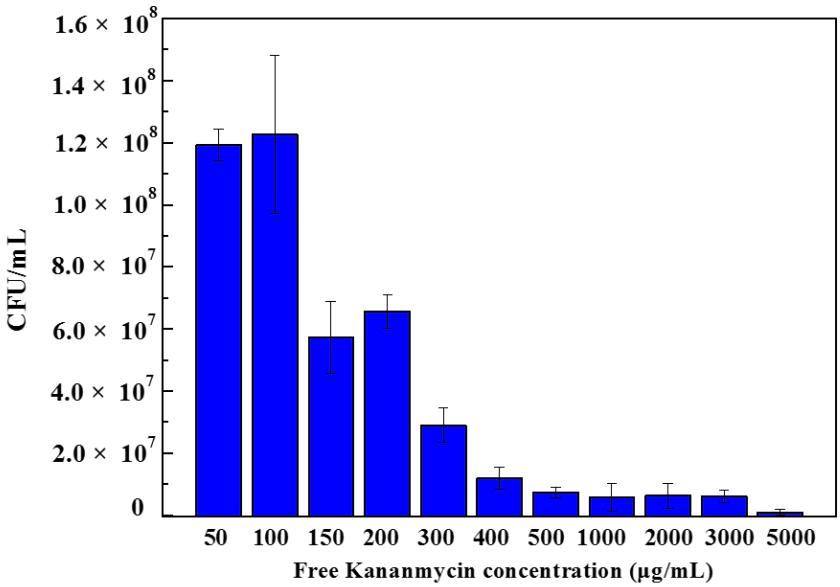

Fig. 5.6 Colony forming units results obtained after 24 h incubation of E.coli bacteria with different concentrations of free kanamycin.

Fig. 5.6 shows the colony forming units results obtained after 24 h incubation of *E.coli* bacteria with different concentrations of free kanamycin. As can be seen, at a concentration of 50 and 100 µg/mL kanamycin, the bacteria grew to 1.2 × 10^8 CFU/mL. When the concentration increased to 150 µg/mL, the numbers of CFU dropped to 5.7 ×10^7 CFU/mL. When the concentration increased to 200 µg/mL, the result was increased slightly to 6.6 × 10^7 CFU/mL, although within the error of the experiment. The *E.coli* strain being investigated contains a pET-24a(+) plasmid with a kanamycin resistant gene, which produces aminoglycoside modifying enzymes. Such strains survive the kanamycin treated media at low drug concentrations. Therefore, by adding a certain amount of kanamycin, we can ensure that the cells being grown are the kanamycin resistant cells and are not contaminated by any environmental bacteria. A low concentration of kanamycin shows a beneficial effect for cell growth. With an increasing amount of kanamycin, the inhibition of

cells increased. There is a complete inhibition for *E.coli* at 5000 μg/mL kanamycin, when nearly all of the cells were killed.

5.3.2.2 Gold coated colloidosomes cell viability test

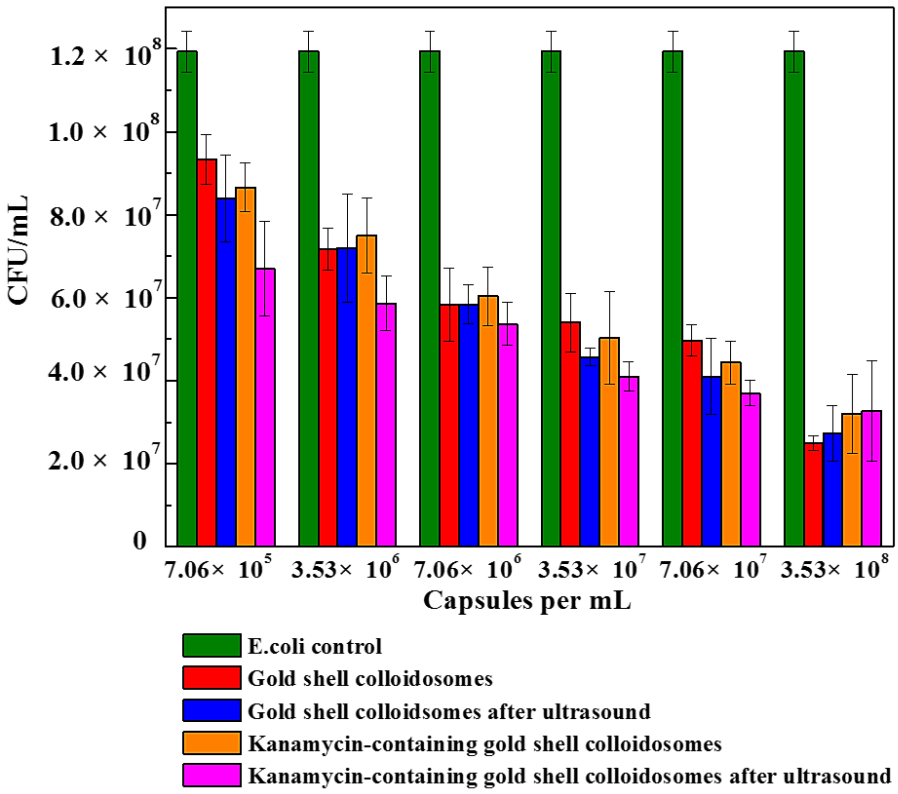

Fig. 5.7 Colony forming units results obtained after 24 h incubation of *E.coli* bacteria with different concentrations of water-core gold coated colloidosomes loading with and without kanamycin, water-core gold coated colloidosomes after ultrasound, kanamycin-containing gold coated colloidosomes, and kanamycin-containing gold coated colloidosomes after ultrasound. The error bars show the standard deviations. The ultrasound treatment was operated at a frequency of 23 kHz and power output of 50 W for 480 s in an ice bath, before adding into the *E.coli*.

Fig. 5.7 shows the cell viability results obtained after 24 h incubation of *E.coli* bacteria with different number concentrations of water-core gold coated colloidosomes, water-core gold coated colloidosomes after ultrasound, kanamycin-containing gold coated colloidosomes, and kanamycin-containing gold coated colloidosomes after ultrasound. In order to break the gold shells, ultrasound was applied for 480 s, before adding the resulting solution to the bacteria.

As seen in Fig. 5.7, there was a CFU decrease in all of the gold shell treated samples compared to the blank *E.coli* culture with 50 μg/mL kanamycin. This indicates the gold

coated colloidosomes are toxic to the *E.coli* culture. The toxicity increases with increasing concentration of gold coated colloidosomes. With a concentration of 7.06×10^5 capsules/mL the toxic effect from the colloidosomes after ultrasound results in a cell viability of approximately 6.7×10^7 CFU/mL, a 25 % drop from the case without ultrasound. Increasing the concentration of capsules, the toxicity becomes more obvious. When the number of the capsules reaches to 3.53×10^8 capsules/mL, the encapsulation of kanamycin had minimal extra benefit, with the capsules themselves hindering the cell viability.

5.3.2.3 Silver coated colloidosomes cell viability test

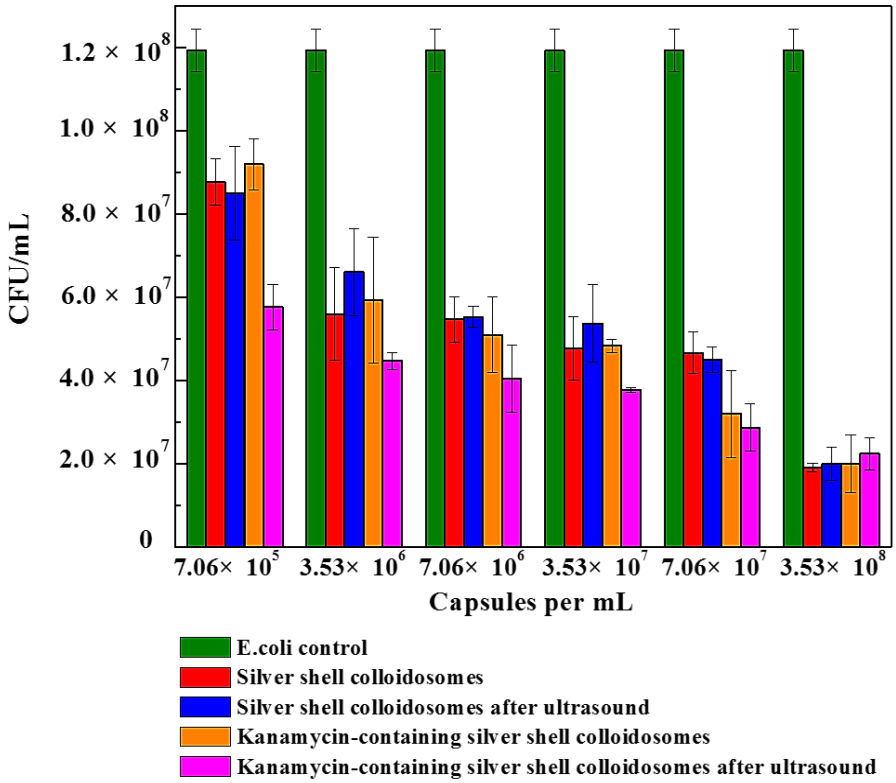

Fig. 5.8 Colony forming units results obtained after 24 h incubation of *E.coli* bacteria with different concentrations of water-core silver coated colloidosomes, water-core silver coated colloidosomes after ultrasound, kanamycin-containing silver coated colloidosomes, and kanamycin-containing silver coated colloidosomes after ultrasound. The error bars show the standard deviations. The ultrasound treatment was operated at a frequency of 23 kHz and power output of 50 W for 240 s in an ice bath, before adding into the *E.coli*.

Fig. 5.8 shows the cell viability results obtained after 24 h incubation of *E.coli* with different amounts of water-core silver coated colloidosomes, water-core silver coated colloidosomes after ultrasound, kanamycin-containing silver coated colloidosomes, and kanamycin-containing silver coated colloidosomes after ultrasound. Before rupture, there is minimal

toxicity difference between the empty and kanamycin containing capsules. After ultrasound, the kanamycin has a significant effect on cell viability. In order to break silver shells, the ultrasound was applied for 240 s before adding the resulting solution into the bacteria.

The effect of the silver coated colloidosomes on cell viability shows a similar trend to the gold capsules, with the cell viability decreasing, compared with the *E.coli* control. The effect on cell viability of silver coated colloidosomes loading kanamycin after ultrasound was most dramatic because of the released antibiotic and the possible antibiotic attached on the suface of the broken shells. For the lowest concentration of silver shells, the cell viability after kanamycin released dropped by 34% compared with other capsules. Increasing the concentration of capsules, the toxic effect becomes enhanced.

Both the silver and gold shells colloidosomes are toxic to this bacterial system. With a low concentration of 7.06×10^5 capsules/mL, the difference of toxicity between gold and silver colloidosomes is not significant. Increasing the concentration of capsules, the cell viability is slightly different. For example, at a concentration of 3.53×10^8 capsules/mL, for gold shells after ultrasound, there are around 3×10^7 CFU remaining, and for silver shell capsules after ultrasound around 2×10^7 CFU remain. This slight difference is likely to be because the silver shells, especially silver shell fragments in nano-size as well as any silver ions are toxic to biological systems and are leading to the death of bacteria. [196, 197]

For this *E.coli* bacterial system, the effect of nano-size silver shell fragments on cells is not very obvious, compared with the B50 cancer cell system in chapter 4. In addition, the cell viabilities between different concentration samples are not obvious enough and also with a relatively large error bar. So, this chapter is only showing the qualitative results of the antibiotic-containing metal shell capsules on cells.

5.4 Conclusions

In this chapter, we demonstrate a method for encapsulating an antibiotic kanamycin using gold or silver coated colloidosomes, and then triggered the capsules using ultrasound. To investigate the application of the capsules in a bacterial system, *E.coli* bacteria were chosen as a model organism. After triggering the metal shells by ultrasound, the released antibiotic, the broken fragments, and some antibiotic which may be attaching onto the capsule surface, all may kill *E.coli*. Both the silver and gold shells colloidosomes are toxic to this bacteria system. Compared with silver coated colloidosomes, gold ones can load a higher concentration of kanamycin.

Chapter 6.

Conclusions and future work

6.1 Conclusions

In this thesis, particulate polymer shell colloidosomes coated with a silver or gold shell were prepared and investigated to load drugs and use them as drug carriers. After optimizing the reaction conditions, the silver coated colloidosomes were prepared by making the particulate polymer shell first, then reacting L-ascorbic acid with silver nitrate in the wash solution. The particulate polymer shells are fully covered by sheet-like silver particles to form a silver shell, which may form a film to improve the strength and permeability of the colloidosomes. Similar to the silver shells, the gold coated colloidosomes were prepared by making the particulate polymer shell first, then reacting L-Ascorbic acid with $HAuCl_4$ in the wash solution. The gold shells are spherical and cover the particulate polymer shells, which may also improve the strength and permeability of the colloidosomes. Both these two types of colloidosomes were successfully demonstrated to encapsulate Allura Red AC dye solution and the shell of these structures was ruptured using ultrasound treatment, operating at a frequency of 20 kHz and power output of 50 W. The encapsulation efficiency of silver coated colloidosomes is 22.7%, and 15.7% for gold coated colloidosomes.

To investigate the metal shell capsules for biological targeting applications, the colloidosomes were modified using 4,4'-dithiodibutyric acid and combined with rabbit antigen. The Surface Plasmon Resonance biosensor, which was used for an immunoassay sensitivity measurement, proved that the two types of modified colloidosomes combined with the rabbit IgG can be captured by the anti-rabbit IgG, which was immobilized on the gold film of SPR surface. After attaching on the gold film, both types of colloidosomes can be ruptured using ultrasound treatment, operating at a frequency of 20 kHz and power output of 50 W. For the SPR experiment, in order to achieve a higher loading efficiency of the metal capsules attached on the gold film of SPR, more optimization should be explored for future

research. The functional modified silver or gold coated colloidosomes are promising for many future medical applications including targeted carriers for small bioactive molecules with controlled drug delivery and externally triggered release.

To use the capsules as drugs carriers, our study demonstrates a method for encapsulating an anticancer drug, doxorubicin. The doxorubicin-containing metal coated colloidosomes are impermeable to small molecule drugs and can be triggered using ultrasound, operating at a frequency of 20 kHz and power output of 50 W. After 120 s of ultrasound treatment for silver coated colloidosomes and 240 s for gold coated colloidosomes, most of the capsules were destroyed into small pieces and only a few survived. In addition, we also tried high intensity focused ultrasound with a frequency of 2.65 MHz and a power of 6 W to break the metal coated colloidosomes. Some of the metal shells were deformed and broken, but there were still a large percentage of intact metal shell colloidosomes, when using a HIFU treatment for a few minutes. Further research needs to be done to improve the release efficiency using HIFU for the metal capsules. We then tested the cell viability of B50 cancer cells and propose the possibility to use the metal shell capsules for delivery of anticancer drugs, i.e., doxorubicin. For silver coated colloidosomes, at 10 capsules/cell, a cell viability of more than 90% during the first 24 h and more than 60% after 72 h are seen. Increasing the number of capsules, the cytotoxicity of the silver shells increases heavily. It is also clear that all the capsule concentration, size and composition can determine the final proliferation and death rate of cells. After triggering the silver shells using ultrasound, the combined effects of the released doxorubicin, the broken silver coated capsule fragments and the possible drug attached on the surface of the capsules all may kill cancer cells. Compared with silver ones, the gold shells show less toxicity to cells and have no major negative effect on cancer cells, but a lower drug loading efficiency.

In addtion, we demonstrate a method for encapsulating an antibiotic, kanamycin, using gold or silver coated colloidosomes. After triggering the metal shells by ultrasound, the released antibiotic, the broken fragments and the possible antibiotic attached on the suface of the capluses may all kill *E.coli*. For the same concentration of capsules, silver shells display a slight higher toxicity compared with gold shell capsules. However, the gold coated colloidosomes can load a higher concentration of kanamycin.

Overall, both the aqueous core silver and gold coated colloidosomes are successful for long time encapsulation of small molecule drug materials. The capsule surface can be attached

with proteins to achieve biological targeting. Both silver and gold shell colloidosomes are impermeable and can seal the drugs. Silver shells result in a lower cell viability compared with gold shells. For triggering the capsules, we have demonstrated the use of ultrasound treatment.

6.2 Limitation and future work

Traditional particulate polymer shell colloidosomes leak low molecular weight encapsulated materials due to their intrinsic shell permeability. To solve this problem, we have demonstrated growing a second inorganic shell, leading to the successful long term encapsulation of small molecule materials. The encapsulation efficiency of silver coated colloidosomes is 22.7%, and 15.7% for gold coated colloidosomes. Although the silver shell can change the permeability of the particulate polymer shells, we also decreased the encapsulation efficiency to a certain extent, which is lower than some drug delivery materials, for example, a loading efficiency between 22.4% and 45.6% for mesoporous PLGA-SiO_2 [181]. So, it is clear that the further optimisation possibilities exist.

In addition, in the SPR experiments, the interrogation zone under the light spot covers a relatively low and different numbers of capsules, so there were relatively large error bars in the SPR wavelength shift bar chart and only a few nanometres red shift for SPR wavelength. In order to produce an improvement in sensitivity for capsule detection, we can try to modify the SPR surface, such as using gold nanoparticles or silica nanoparticles, to enhance the signals. [166]

More importantly, in order to use the impermeable capsules as drug carriers, there is a need to reduce the overall size when used for in vitro and in vivo delivery [202]. Therefore, as well as encapsulation of small molecule materials, we also wish to make nano-size colloidosomes. Currently, we use latex particles with a diameter of 153 nm for capsules with a diameter of 1-2 μm. To achieve the smaller size, it will require making smaller emulsion droplets stabilized with latex particles. The first step is to review and select latex particles, such as monodisperse polystyrene lattices [203]. For the organic phase, we will start with sunflower and vegetable oils. The next step is to emulsify the latex suspensions in the oil phase. To achieve small emulsion sizes, the easiest way is to change the shear rate applied using the

mixer. Preliminary investigations indicate that this does not result in the order of magnitude reduction in droplet size.

We will investigate using a rotating packed bed (RPB) to increase intensification of micromixing and to make small emulsion droplets. Fig. 6.1 shows a schematic diagram of the device. A RPB can generate a high gravity environment to strongly intensify micromixing and mass transfer by the high shearing force. This will produce high-quality emulsions via the formation of ultrafine and uniform oil droplets. [204, 205] In a typical RPB, there is a motor with a rotating shaft which is combined with the packing part. When the shaft starts rotating, it leads to a rotation of the packing part as well. There are some small holes on the inlet metal tubes. Normally, the reactant is input by a peristaltic pump, and then goes through the small holes on the inlet, reaching the packing part. The packing, with a high rotating speed, can strongly intensify the mixing and the shear force can separate the reactant droplets creating more reaction surface areas. Finally, the products will be collected from a liquid outlet.

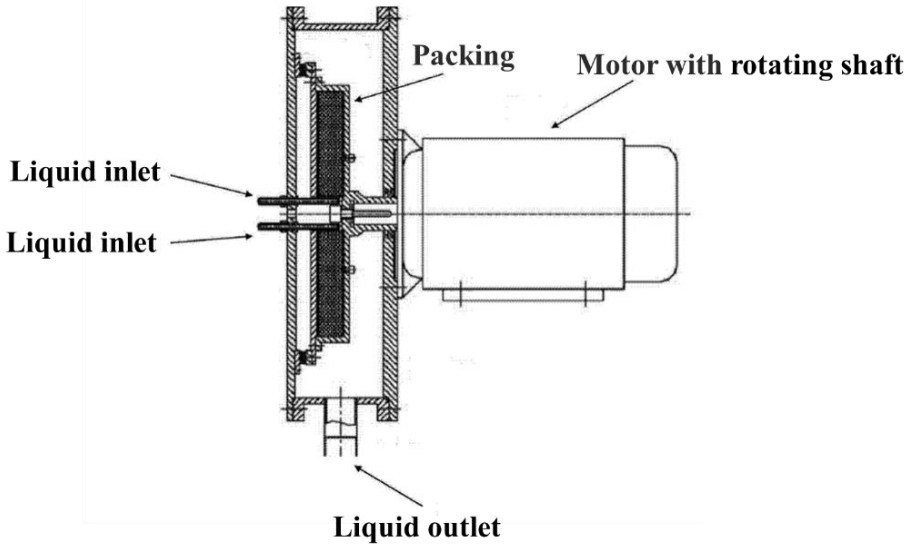

Fig. 6.1 Schematic diagram of a rotating packed bed.

We will also try more conventional emulsification methods, such as a high-shear mixer, ultrasound and a microfluidic reactor. After collecting the colloidosomes, the droplet size will be measured by dynamic light scattering (DLS), scanning electron microscopy (SEM) and transmission electron microscopy (TEM).

References

[1] Gong Y, Zhu A M, Zhang Q G, Ye M L, Wang H T, Liu Q L. *Preparation of cell-embedded colloidosomes in an oil-in-water emulsion*. ACS Applied Materials & Interfaces, 2013, 5(21): 10682-10689.

[2] Esser-Kahn A P, Odom S A, Sottos N R, White S R, Moore J S. *Triggered release from polymer capsules*. Macromolecules, 2011, 44(14): 5539-5553.

[3] Desai K G H, Jin Park H. *Recent developments in microencapsulation of food ingredients*. Drying Technology, 2005, 23(7): 1361-1394.

[4] Langer R. *Drug delivery and targeting*. Nature, 1998, 392: 5-10.

[5] Meier W. *Polymer nanocapsules*. Chemical Society Reviews, 2000, 29(5): 295-303.

[6] Velev O D, Furusawa K, Nagayama K. *Assembly of latex particles by using emulsion droplets as templates. 1. Microstructured hollow spheres*. Langmuir, 1996, 12(10): 2374-2384.

[7] Lensen D, Vriezema D M, van Hest J. *Polymeric microcapsules for synthetic applications*. Macromolecular Bioscience, 2008, 8(11): 991-1005.

[8] McClements D J. *Encapsulation, protection, and release of hydrophilic active components: Potential and limitations of colloidal delivery systems*. Advances in Colloid and Interface Science, 2015, 219: 27-53.

[9] Keen P H R, Slater N K H, Routh A F. *Encapsulation of yeast cells in colloidosomes*. Langmuir, 2011, 28(2): 1169-1174.

[10] Keen P H R, Slater N K H, Routh A F. *Encapsulation of amylase in colloidosomes*. Langmuir, 2014, 30(8): 1939-1948.

[11] Keen P H R, Slater N K H, Routh A F. *Encapsulation of lactic acid bacteria in colloidosomes*. Langmuir, 2012, 28(46): 16007-16014.

[12] De Vos P, Faas M M, Spasojevic M, Sikkema J. *Encapsulation for preservation of functionality and targeted delivery of bioactive food components*. International Dairy

Journal, 2010, 20(4): 292-302.

[13] Van Soest J J G. *Encapsulation of fragrances and flavours: a way to control odour and aroma in consumer products, flavours and fragrances*. Springer Berlin Heidelberg, 2007: 439-455.

[14] Gibbs B F, Selim K, Alli I, Mulligan C N. *Encapsulation in the food industry: a review*. International Journal of Food Sciences and Nutrition, 1999, 50(3): 213-224.

[15] Bean K, Black C F, Govan N, Reynolds P, Sambrook M R. *Preparation of aqueous core/silica shell microcapsules*. Journal of Colloid and Interface Science, 2012, 366(1): 16-22.

[16] O'Sullivan M, Zhang Z, Vincent B. *Silica-shell/oil-core microcapsules with controlled shell thickness and their breakage stress*. Langmuir, 2009, 25(14): 7962-7966.

[17] Yow H N, Routh A F. *Release profiles of encapsulated actives from colloidosomes sintered for various durations*. Langmuir, 2008, 25(1): 159-166.

[18] Atkin R, Davies P, Hardy J, Vincent B. *Preparation of aqueous core/polymer shell microcapsules by internal phase separation*. Macromolecules, 2004, 37(21): 7979-7985.

[19] Yow H N, Routh A F. *Formation of liquid core-polymer shell microcapsules*. Soft Matter, 2006, 2(11): 940-949.

[20] Velev O D, Furusawa K, Nagayama K. *Assembly of latex particles by using emulsion droplets as templates. 2. Ball-like and composite aggregates*. Langmuir, 1996, 12(10): 2385-2391.

[21] Velev O D, Nagayama K. *Assembly of latex particles by using emulsion droplets. 3. Reverse (water in oil) system*. Langmuir, 1997, 13(6): 1856-1859.

[22] Dinsmore A D, Hsu M F, Nikolaides M G, Marquez M, Bausch A R, Weitz D A. *Colloidosomes: selectively permeable capsules composed of colloidal particles*. Science, 2002, 298(5595): 1006-1009.

[23] Hsu M F, Nikolaides M G, Dinsmore A D, Bausch A R, Vernita D. Gordon V D, Chen X, Hutchinson J W, Weitz D A. *Self-assembled shells composed of colloidal particles:*

fabrication and characterization. Langmuir, 2005, 21(7): 2963-2970.

[24] Yi G R, Manoharan V N, Klein S, Brzezinska K R, Pine D J, Lange F F, Yang S M. *Monodisperse micrometer-scale spherical assemblies of polymer particles*. Advanced Materials, 2002, 14(16): 1137-1140.

[25] Ashby N P, Binks B P, Paunov V N. *Formation of giant colloidosomes by transfer of pendant water drops coated with latex particles through an oil-water interface*. Physical Chemistry Chemical Physics, 2004, 6(17): 4223-4225.

[26] Donath E, Sukhorukov G B, Caruso F, Davis S A, Möhwald H. *Novel hollow polymer shells by colloid-templated assembly of polyelectrolytes*. Angewandte Chemie International Edition, 1998, 37(16): 2201-2205.

[27] Sukhorukov G B, Donath E, Lichtenfeld H, Knippel E, Knippel M, Budde A, Möhwald H. *Layer-by-layer self-assembly of polyelectrolytes on colloidal particles*. Colloids and Surfaces A: Physicochemical and Engineering Aspects, 1998, 137(1-3): 253-266.

[28] Kotov N A, Dekany I, Fendler J H. *Layer-by-layer self-assembly of polyelectrolyte-semiconductor nanoparticle composite films*. The Journal of Physical Chemistry, 1995, 99(35): 13065-13069.

[29] Shenoy D B, Antipov A A, Sukhorukov G B, Möhwald H. *Layer-by-layer engineering of biocompatible, decomposable core-shell structures*. Biomacromolecules, 2003, 4(2): 265-272.

[30] Antipov A A, Sukhorukov G B. *Polyelectrolyte multilayer capsules as vehicles with tunable permeability*. Advances in Colloid and Interface Science, 2004, 111(1): 49-61.

[31] Schuetz P, Caruso F. *Semiconductor and metal nanoparticle formation on polymer spheres coated with weak polyelectrolyte multilayers*. Chemistry of Materials, 2004, 16(16): 3066-3073.

[32] Blomberg E, Poptoshev E, Claesson P M, Caruso F. *Surface interactions during polyelectrolyte multilayer buildup. 1. Interactions and layer structure in dilute electrolyte solutions*. Langmuir, 2004, 20(13): 5432-5438.

[33] Tiarks F, Landfester K, Antonietti M. *Preparation of polymeric nanocapsules by*

miniemulsion polymerization. Langmuir, 2001, 17(3): 908-918.

[34] Berg J, Sundberg D, Kronberg B. *Microencapsulation of emulsified oil droplets by in-situ vinyl polymerization*. Journal of Microencapsulation, 1989, 6(3): 327-337.

[35] Shulkin A, Stöver H D H. *Photostimulated phase separation encapsulation*. Macromolecules, 2003, 36(26): 9836-9839.

[36] Dowding P J, Atkin R, Vincent B, Bouillot P. *Oil core/polymer shell microcapsules by internal phase separation from emulsion droplets. II: controlling the release profile of active molecules*. Langmuir, 2005, 21(12): 5278-5284.

[37] Dowding P J, Atkin R, Vincent B, Bouillot P. *Oil core-polymer shell microcapsules prepared by internal phase separation from emulsion droplets. I. Characterization and release rates for microcapsules with polystyrene shells*. Langmuir, 2004, 20(26): 11374-11379.

[38] Zydowicz N, Nzimba-Ganyanad E. *PMMA microcapsules containing water-soluble dyes obtained by double emulsion/solvent evaporation technique*. Polymer Bulletin, 2002, 47(5): 457-463.

[39] Lorenceau E, Utada A S, Link D R, Cristobal G, Joanicot M, Weitz D A. *Generation of polymerosomes from double-emulsions*. Langmuir, 2005, 21(20): 9183-9186.

[40] Bouchemal K, Briançon S, Perrier E, Fessi H, Bonnet I, Zydowicz N. *Synthesis and characterization of polyurethane and poly (ether urethane) nanocapsules using a new technique of interfacial polycondensation combined to spontaneous emulsification*. International Journal of Pharmaceutics, 2004, 269(1): 89-100.

[41] Rosenthal A M, Chang T M S. *The incorporation of lipid and Na+-K+-ATPase into the membranes of semipermeable microcapsules*. Journal of Membrane Science, 1980, 6: 329-338

[42] Okahata Y, Lim H, Hachiya S, Nakamura G. I. *Bilayer-coated capsule membranes. IV.: Control of NaCl permeability by phase transition of synthetic bilayer coatings, depending on their hydrophilic head groups*. Journal of Membrane Science, 1984, 19(3): 237-247.

[43] Janssen L, Te Nijenhuis K. *Encapsulation by interfacial polycondensation. I. The capsule production and a model for wall growth*. Journal of Membrane Science, 1992, 65(1-2): 59-68.

[44] Frere Y, Danicher L, Gramain P. *Preparation of polyurethane microcapsules by interfacial polycondensation*. European Polymer Journal, 1998, 34: 193-199.

[45] Scott C, Wu D, Ho C C, Co C C. *Liquid-core capsules via interfacial polymerization: a free-radical analogy of the nylon rope trick*. Journal of the American Chemical Society, 2005, 127(12): 4160-4161.

[46] Hayward R C, Utada A S, Dan N, Weitz D A. *Dewetting instability during the formation of polymersomes from block-copolymer-stabilized double emulsions*. Langmuir, 2006, 22(10): 4457-4461.

[47] Utada A S, Lorenceau E L, Link D R, Kaplan P D, Stone H A, Weitz D A. *Monodisperse double emulsions generated from a microcapillary device*. Science, 2005, 308(5721): 537-541.

[48] Brinkhuis R P, Rutjes F P J T, van Hest J C M. *Polymeric vesicles in biomedical applications*. Polymer Chemistry, 2011, 2(7): 1449-1462.

[49] Discher B M, Hammer D A, Bates F S, Discher D E. *Polymer vesicles in various media*. Current Opinion in Colloid & Interface Science, 2000, 5(1): 125-131.

[50] Lee J C M, Bermudez H, Discher B M, Sheehan M A, Won Y Y, Bates F S, Discher D E. *Preparation, stability, and in vitro performance of vesicles made with diblock copolymers*. Biotechnology and Bioengineering, 2001, 73(2): 135-145.

[51] Meng F, Hiemstra C, Engbers G H M, Feijen J. *Biodegradable polymersomes*. Macromolecules, 2003, 36(9): 3004-3006.

[52] Gordon V D, Chen X, Hutchinson J W, Bausch A R, Marquez M, Weitz D A. *Self-assembled polymer membrane capsules inflated by osmotic pressure*. Journal of the American Chemical Society, 2004, 126(43): 14117-14122.

[53] Sun Q, Gao H, Sukhorukov G B, Routh A F. *Silver-coated colloidosomes as carriers for an anticancer drug*. ACS Applied Materials & Interfaces, 2017, 9(38): 32599-32606.

[54] Sun Q, Du Y, Zhao Z, Gao H, Sukhorukov G B, Routh A F. *Functional silver-coated colloidosomes as targeted carriers for small molecules*. Langmuir, 2017, 33(15): 3755-3764.

[55] Gao H, Goriacheva O A, Tarakina N V, Sukhorukov G B. *Intracellularly biodegradable polyelectrolyte/silica composite microcapsules as carriers for small molecules*. ACS Applied Materials & Interfaces, 2016, 8(15): 9651-9661.

[56] Gao H, Wen D, Sukhorukov G B. *Composite silica nanoparticle/polyelectrolyte microcapsules with reduced permeability and enhanced ultrasound sensitivity*. Journal of Materials Chemistry B, 2015, 3(9): 1888-1897.

[57] Skirtach A G, Antipov A A, Shchukin D G, Sukhorukov G B. *Remote activation of capsules containing Ag nanoparticles and IR dye by laser light*. Langmuir, 2004, 20(17): 6988-6992.

[58] Sun Q, Routh A F. *Aqueous core colloidosomes with a metal shell*. European Polymer Journal, 2016, 77: 155-163.

[59] Chiwele I, Jones B E, Podczeck F. *The shell dissolution of various empty hard capsules*. Chemical and Pharmaceutical Bulletin, 2000, 48(7): 951-956.

[60] Gun W J, Routh A F. *Formation and characterization of pH-responsive liquid core microcapsules*. Langmuir, 2013, 29(40): 12541-12548.

[61] Kim B S, Vinogradova O I. *pH-Controlled swelling of polyelectrolyte multilayer microcapsules*. The Journal of Physical Chemistry B, 2004, 108(24): 8161-8165.

[62] De Geest B G, Vandenbroucke R E, Guenther A M, Sukhorukov G B, Hennink W E, Sanders N N, Demeester J, De Smedt S C. *Intracellularly degradable polyelectrolyte microcapsules*. Advanced Materials, 2006, 18(8): 1005-1009.

[63] Ochs C J, Such G K, Caruso F. *Modular assembly of layer-by-layer capsules with tailored degradation profiles*. Langmuir, 2010, 27(4): 1275-1280.

[64] Itoh Y, Matsusaki M, Kida T, Akashi M. *Enzyme-responsive release of encapsulated proteins from biodegradable hollow capsules*. Biomacromolecules, 2006, 7(10): 2715-2718.

[65] Hitchcock J P, Tasker A L, Baxter E A, Biggs S R, Cayre O J. *Long-term retention of small, volatile molecular species within metallic microcapsules*. ACS Applied Materials & Interfaces, 2015, 7(27): 14808-14815.

[66] Hitchcock J P, Baxter E A M, Biggs S R, Cayre O J, Holland L A M, Tasker L A. *Coated microcapsules*. U.S. Patent 9,951,293. 2018-4-24.

[67] Mendelsohn J D, Barrett C J, Chan V V, Pal A J, Mayes A M, Rubner M F. *Fabrication of microporous thin films from polyelectrolyte multilayers*. Langmuir, 2000, 16(11): 5017-5023.

[68] Ameloot R, Vermoortele F, Vanhove W, Roeffaers M B J, Sels B F, De Vos D E. *Interfacial synthesis of hollow metal-organic framework capsules demonstrating selective permeability*. Nature Chemistry, 2011, 3(5): 382.

[69] Ochs M, Carregal-Romero S, Rejman J, Braeckmans K, De Smedt S C, Parak W J. *Light-addressable capsules as caged compound matrix for controlled triggering of cytosolic reactions*. Angewandte Chemie International Edition, 2013, 52(2): 695-699.

[70] Antipov A A, Sukhorukov G B, Leporatti S, Radtchenko I L, Donath E, Mohwald H. *Polyelectrolyte multilayer capsule permeability control*. Colloids and Surfaces A: Physicochemical and Engineering Aspects, 2002, 198: 535-541.

[71] Kidane A, Bhatt P P. *Recent advances in small molecule drug delivery*. Current Opinion in Chemical Biology, 2005, 9(4): 347-351.

[72] Chen Z. *Small-molecule delivery by nanoparticles for anticancer therapy*. Trends in molecular medicine, 2010, 16(12): 594-602.

[73] Chertok B, Moffat B A, David A E, Yu F, Bergemann C, Ross B D., Yang V C. *Iron oxide nanoparticles as a drug delivery vehicle for MRI monitored magnetic targeting of brain tumors*. Biomaterials, 2008, 29(4): 487-496.

[74] Ho K, Lapitsky Y, Shi M, Shoichet M S. *Tunable immunonanoparticle binding to cancer cells: thermodynamic analysis of targeted drug delivery vehicles*. Soft Matter, 2009, 5(5): 1074-1080.

[75] Verma R K, Garg S. *Drug delivery technologies and future directions*. Pharmaceutical

Technology, 2001, 25(2): 1-14.

[76] Research and Markets. *Global markets and technologies for advanced drug delivery systems*, 2016, Report ID: 3641381.

[77] Saranya S, Radha K V. *Review of nanobiopolymers for controlled drug delivery*. Polymer-Plastics Technology and Engineering, 2014, 53(15): 1636-1646.

[78] Gillies E R, Frechet J M J. *Dendrimers and dendritic polymers in drug delivery*. Drug Discovery Today, 2005, 10(1): 35-43.

[79] Morachis J M, Mahmoud E A, Almutairi A. *Physical and chemical strategies for therapeutic delivery by using polymeric nanoparticles*. Pharmacological Reviews, 2012, 64(3): 505-519.

[80] Riley T, Stolnik S, Heald C R, Xiong C D, Garnett M C, Illum L, Davis S S, Purkiss S C, Barlow R J, Gellert P R. *Physicochemical evaluation of nanoparticles assembled from Poly (lactic acid)-Poly (ethylene glycol)(PLA-PEG) block copolymers as drug delivery vehicles*. Langmuir, 2001, 17(11): 3168-3174.

[81] Lassalle V, Ferreira M L. *PLA nano-and microparticles for drug delivery: an overview of the methods of preparation*. Macromolecular Bioscience, 2007, 7(6): 767-783.

[82] Kataoka K, Harada A, Nagasaki Y. *Block copolymer micelles for drug delivery: design, characterization and biological significance*. Advanced Drug Delivery Reviews, 2001, 47(1): 113-131.

[83] Rösler A, Vandermeulen G W M, Klok H A. *Advanced drug delivery devices via self-assembly of amphiphilic block copolymers*. Advanced Drug Delivery Reviews, 2012, 64: 270-279.

[84] Brannon-Peppas L. *Recent advances on the use of biodegradable microparticles and nanoparticles in controlled drug delivery*. International Journal of Pharmaceutics, 1995, 116(1): 1-9.

[85] Pillai O, Panchagnula R. *Polymers in drug delivery*. Current Opinion in Chemical Biology, 2001, 5(4): 447-451.

[86] Sato T, Kanke M, Schroeder H G, DeLuca P P. *Porous biodegradable microspheres for controlled drug delivery. I. Assessment of processing conditions and solvent removal techniques*. Pharmaceutical Research, 1988, 5(1): 21-30.

[87] Park J H, Allen M G, Prausnitz M R. *Biodegradable polymer microneedles: fabrication, mechanics and transdermal drug delivery*. Journal of Controlled Release, 2005, 104(1): 51-66.

[88] Cheng J, Teply B A, Sherifi I, Sung J, Luther G, Gu F X, Levy-Nissenbaum E, Radovic-Moreno A F, Langer R, Farokhzad O C. *Formulation of functionalized PLGA-PEG nanoparticles for in vivo targeted drug delivery*. Biomaterials, 2007, 28(5): 869-876.

[89] Chan J M, Zhang L, Yuet K P, Liao G, Rhee J W, Langer R, Farokhzad O C. *PLGA-lecithin-PEG core-shell nanoparticles for controlled drug delivery*. Biomaterials, 2009, 30(8): 1627-1634.

[90] Kim D H, Martin D C. *Sustained release of dexamethasone from hydrophilic matrices using PLGA nanoparticles for neural drug delivery*. Biomaterials, 2006, 27(15): 3031-3037.

[91] Semete B, Booysen L, Lemmer Y, Kalombo L, Katata L, Verschoor J, Swai H S. *In vivo evaluation of the biodistribution and safety of PLGA nanoparticles as drug delivery systems*. Nanomedicine: Nanotechnology, Biology and Medicine, 2010, 6(5): 662-671.

[92] Hans M L, Lowman A M. *Biodegradable nanoparticles for drug delivery and targeting*. Current Opinion in Solid State and Materials Science, 2002, 6(4): 319-327.

[93] Eloy J O, de Souza M C, Petrilli R, Barcellos J P A, Lee R J, Marchetti J M. *Liposomes as carriers of hydrophilic small molecule drugs: strategies to enhance encapsulation and delivery*. Colloids and Surfaces B: Biointerfaces, 2014, 123: 345-363.

[94] Decher G. *Fuzzy nanoassemblies: toward layered polymeric multicomposites*. Science, 1997, 277(5330): 1232-1237.

[95] Solans C, Izquierdo P, Nolla J, Azemar N, Garcia-Celma M J. *Nano-emulsions*. Current Opinion in Colloid & Interface Science, 2005, 10(3): 102-110.

[96] Zha L, Banik B, Alexis F. *Stimulus responsive nanogels for drug delivery*. Soft Matter,

2011, 7(13): 5908-5916.

[97] Hu S H, Tsai C H, Liao C F, Liu D M, Chen S. Y. *Controlled rupture of magnetic polyelectrolyte microcapsules for drug delivery*. Langmuir, 2008, 24(20): 11811-11818.

[98] Park J W, Hong K, Kirpotin D B, Papahadjopoulos D, Benz C C. *Immunoliposomes for cancer treatment*. Advances in Pharmacology, 1997, 40: 399-435.

[99] Pattni B S, Chupin V V, Torchilin V P. *New developments in liposomal drug delivery*. Chemical Reviews, 2015, 115(19): 10938-10966.

[100] Gregoriadis G. *Engineering liposomes for drug delivery: progress and problems*. Trends in Biotechnology, 1995, 13(12): 527-537.

[101] Torchilin V P. *Immunoliposomes and PEGylated immunoliposomes: possible use for targeted delivery of imaging agents*. Immunomethods, 1994, 4(3): 244-258.

[102] Torchilin V P. *Recent advances with liposomes as pharmaceutical carriers*. Nature Reviews Drug Discovery, 2005, 4(2): 145-160.

[103] Kitagawa S. *Metal-organic frameworks (MOFs)*. Chemical Society Reviews, 2014, 43(16): 5415-5418.

[104] Férey G, Serre C. *Large breathing effects in three-dimensional porous hybrid matter: facts, analyses, rules and consequences*. Chemical Society Reviews, 2009, 38(5): 1380-1399.

[105] Serre C, Mellot-Draznieks C, Surblé S, Audebrand N, Filinchuk Y, Férey G. *Role of solvent-host interactions that lead to very large swelling of hybrid frameworks*. Science, 2007, 315(5820): 1828-1831.

[106] Horcajada P, Chalati T, Serre C, Gillet B, Sebrie C, Baati T, Eubank J F, Heurtaux D, Clayette P, Kreuz C, Chang J S, Hwang Y K, Marsaud V, Bories P N, Cynober L, Gil S, Férey G, Couvreur P, Gref R. *Porous metal-organic-framework nanoscale carriers as a potential platform for drug delivery and imaging*. Nature Materials, 2010, 9(2): 172-178.

[107] Horcajada P, Serre C, Vallet-Regí M, Sebban M, Taulelle F, Férey G. *Metal-organic*

frameworks as efficient materials for drug delivery. Angewandte Chemie International Edition, 2006, 118(36): 6120-6124.

[108] Horcajada P, Serre C, Maurin G, Ramsahye N A, Balas F, Vallet-Regi M, Sebban M, Taulelle F, Férey G. *Flexible porous metal-organic frameworks for a controlled drug delivery*. Journal of the American Chemical Society, 2008, 130(21): 6774-6780.

[109] Della Rocca J, Liu D, Lin W. *Nanoscale metal-organic frameworks for biomedical imaging and drug delivery*. Accounts of Chemical Research, 2011, 44(10): 957-968.

[110] Graf N, Lippard S J. *Redox activation of metal-based prodrugs as a strategy for drug delivery*. Advanced Drug Delivery Reviews, 2012, 64(11): 993-1004.

[111] Barbe C, Bartlett J, Kong L, Finnie K, Lin H Q, Larkin M, Bush A, Calleja G. *Silica particles: a novel drug-delivery system*. Advanced Materials, 2004, 16(21): 1959-1966.

[112] Ciriminna R, Sciortino M, Alonzo G, Schrijver A D, Pagliaro M. *From molecules to systems: Sol-gel microencapsulation in silica-based materials*. Chemical Reviews, 2010, 111(2): 765-789.

[113] Rao K S, El-Hami K, Kodaki T, Matsushige K, Makino K. *A novel method for synthesis of silica nanoparticles*. Journal of Colloid and Interface Science, 2005, 289(1): 125-131.

[114] Chen M, Wu L, Zhou S, You B. *A method for the fabrication of monodisperse hollow silica spheres*. Advanced Materials, 2006, 18(6): 801-806.

[115] Zou H, Schlaad H. *Sodium silicate route to coat polymer particles with silica*. Colloid and Polymer Science, 2014, 292(7): 1693-1700.

[116] Slowing I I, Vivero-Escoto J L, Wu C W, Lin V S Y. *Mesoporous silica nanoparticles as controlled release drug delivery and gene transfection carriers*. Advanced Drug Delivery Reviews, 2008, 60(11): 1278-1288.

[117] Tang F, Li L, Chen D. *Mesoporous silica nanoparticles: synthesis, biocompatibility and drug delivery*. Advanced Materials, 2012, 24(12): 1504-1534.

[118] Zheng M M, Ruan G D, Feng Y Q. *Hybrid organic-inorganic silica monolith with*

hydrophobic/strong cation-exchange functional groups as a sorbent for micro-solid phase extraction. Journal of Chromatography A, 2009, 1216(45): 7739-7746.

[119] Jal P K, Patel S, Mishra B K. *Chemical modification of silica surface by immobilization of functional groups for extractive concentration of metal ions*. Talanta, 2004, 62(5): 1005-1028.

[120] Singh R, Lillard Jr J W. *Nanoparticle-based targeted drug delivery*. Experimental and Molecular Pathology, 2009, 86(3): 215-223.

[121] Herrero-Vanrell R, Rincon A C, Alonso M, Reboto V, Molina-Martinez I T, Rodríguez-Cabello J C. *Self-assembled particles of an elastin-like polymer as vehicles for controlled drug release*. Journal of Controlled Release, 2005, 102(1): 113-122.

[122] Kreuter J. *Nanoparticles*. Colloidal Drug Delivery Systems, 1994: 219-342.

[123] Panyam J, Williams D, Dash A, Leslie-Pelecky D, Labhasetwar V. *Solid-state solubility influences encapsulation and release of hydrophobic drugs from PLGA/PLA nanoparticles*. Journal of Pharmaceutical Sciences, 2004, 93(7): 1804-1814.

[124] Sun C, Lee J S H, Zhang M. *Magnetic nanoparticles in MR imaging and drug delivery*. Advanced Drug Delivery Reviews, 2008, 60(11): 1252-1265.

[125] Liu Z, Robinson J T, Tabakman S M, Yang K, Dai H J. *Carbon materials for drug delivery & cancer therapy*. Materials Today, 2011, 14(7-8): 316-323.

[126] Paciotti G F, Myer L, Weinreich D, Goia D, Pavel N, McLaughlin R E, Tamarkin L. *Colloidal gold: a novel nanoparticle vector for tumor directed drug delivery*. Drug Delivery, 2004, 11(3): 169-183.

[127] Slomkowski S, Alemán J V, Gilbert R G, Hess M, Horie K, Jones R G, Kubisa P, Meisel I, Mormann W, Penczek S, Stepto R F. *Terminology of polymers and polymerization processes in dispersed systems (IUPAC Recommendations 2011)*. Pure and Applied Chemistry, 2011, 83(12): 2229-2259.

[128] Rösler A, Vandermeulen G W M, Klok H A. *Advanced drug delivery devices via self-assembly of amphiphilic block copolymers*. Advanced Drug Delivery Reviews, 2012, 64: 270-279.

[129] Yang L, Alexandridis P. *Physicochemical aspects of drug delivery and release from polymer-based colloids*. Current Opinion in Colloid & Interface Science, 2000, 5(1-2): 132-143.

[130] Allen C, Maysinger D, Eisenberg A. *Nano-engineering block copolymer aggregates for drug delivery*. Colloids and Surfaces B: Biointerfaces, 1999, 16(1-4): 3-27.

[131] Hoare T R, Kohane D S. *Hydrogels in drug delivery: Progress and challenges*. Polymer, 2008, 49(8): 1993-2007.

[132] Qiu Y, Park K. *Environment-sensitive hydrogels for drug delivery*. Advanced Drug Delivery Reviews, 2001, 53(3): 321-339.

[133] Mills J K, Needham D. *Targeted drug delivery*. Expert Opinion on Therapeutic Patents, 1999, 9(11): 1499-1513.

[134] Torchilin V. *Tumor delivery of macromolecular drugs based on the EPR effect*. Advanced Drug Delivery Reviews, 2011, 63(3): 131-135.

[135] Sahoo S K, Sawa T, Fang J, Tanaka S, Miyamoto Y, Akaike T, Maeda H. *Pegylated zinc protoporphyrin: a water-soluble heme oxygenase inhibitor with tumor-targeting capacity*. Bioconjugate Chemistry, 2002, 13(5): 1031-1038.

[136] Moghimi S M, Hunter A C, Murray J C. *Long-circulating and target-specific nanoparticles: theory to practice*. Pharmacological Reviews, 2001, 53(2): 283-318.

[137] Galvin P, Thompson D, Ryan K B, McCarthy A, Moore A C, Burke C S, Dyson M, MacCraith B D, Gun'ko Y K, Byrne M T, Volkov Y, Keely C, Keehan E, Howe M, Duffy C, MacLoughlin R. *Nanoparticle-based drug delivery: case studies for cancer and cardiovascular applications*. Cellular and Molecular Life Sciences, 2012, 69(3): 389-404.

[138] Reichelt R. *Scanning electron microscopy*. Science of Microscopy. Springer, New York, NY, 2007: 133-272.

[139] Smith K C A, Oatley C W. *The scanning electron microscope and its fields of application*. British Journal of Applied Physics, 1955, 6(11): 391.

[140] Kapp O H, Sun Y, Kim K J, Crewe A V. *Modification of a scanning electron microscope to produce Smith-Purcell radiation*. Review of Scientific Instruments, 2004, 75(11): 4732-4741.

[141] Bibi S, Kaur R, Henriksen-Lacey M, McNeil, S E, Wilkhu J, Lattmann E, Christensen D, Mohammed A R, Perrie Y. *Microscopy imaging of liposomes: from coverslips to environmental SEM*. International Journal of Pharmaceutics, 2011, 417(1): 138-150.

[142] Manero J M, Gil F J, Padros E, Planell J A. *Applications of environmental scanning electron microscopy (ESEM) in biomaterials field*. Microscopy Research and Technique, 2003, 61(5): 469-480.

[143] Shindo D, Oikawa T. *Energy dispersive X-ray spectroscopy, analytical electron microscopy for materials science*. Springer Japan, 2002: 81-102.

[144] d'Alfonso A J, Freitag B, Klenov D, Allen L J. *Atomic-resolution chemical mapping using energy-dispersive X-ray spectroscopy*. Physical Review B, 2010, 81(10): 100101.

[145] Kanda K. *Energy dispersive X-ray spectrometer*: U.S. Patent 5,065,020. 1991-11-12.

[146] Williams D B, Carter C B. *The transmission electron microscope*. Transmission Electron Microscopy. Springer, Boston, MA, 1996: 3-17.

[147] Wang Z L. *Transmission electron microscopy of shape-controlled nanocrystals and their assemblies*. The Journal of Physical Chemistry B, 2000, 104: 1153-1175.

[148] Kuntsche J, Horst J C, Bunjes H. *Cryogenic transmission electron microscopy (cryo-TEM) for studying the morphology of colloidal drug delivery systems*. International Journal of Pharmaceutics, 2011, 417(1): 120-137.

[149] Dey V R N. *The basics of confocal microscopy*. Laser Scanning, Theory and Applications, 978-953.

[150] Gao P, Nienhaus G U. *Confocal laser scanning microscopy with spatiotemporal structured illumination*. Optics Letters, 2016, 41(6): 1193-1196.

[151] Houpt P M, Draaijer A. *Confocal laser scanning microscope*: U.S. Patent 4,863,226.

1989-9-5.

[152] Knebel W, Ulrich H. *Confocal laser scanning microscope*: U.S. Patent 6,388,807. 2002-5-14.

[153] Hell S W, Wichmann J. *Breaking the diffraction resolution limit by stimulated emission: stimulated-emission-depletion fluorescence microscopy*. Optics Letters, 1994, 19(11): 780-782.

[154] Santi P A. *Light sheet fluorescence microscopy: a review*. Journal of Histochemistry & Cytochemistry, 2011, 59(2): 129-138.

[155] Leung B O, Chou K C. *Review of super-resolution fluorescence microscopy for biology*. Applied Spectroscopy, 2011, 65(9): 967-980.

[156] Zhao J, Cao S, Liao C, Wang Y, Wang G J, Xu X Z, Fu C L, Xu G W, Lian J R, Wang Y P. *Surface plasmon resonance refractive sensor based on silver-coated side-polished fiber*. Sensors and Actuators B: Chemical, 2016, 230: 206-211.

[157] Sharma A K, Jha R, Gupta B D. *Fiber-optic sensors based on surface plasmon resonance: a comprehensive review*. IEEE Sensors Journal, 2007, 7(8): 1118-1129.

[158] Homola J, Yee S S, Gauglitz G. *Surface plasmon resonance sensors*. Sensors and Actuators B: Chemical, 1999, 54(1): 3-15.

[159] Lertvachirapaiboon C, Baba A, Ekgasit S, Shinbo K, Kato K, Kaneko F. *Transmission surface plasmon resonance techniques and their potential biosensor applications*. Biosensors and Bioelectronics, 2018, 99: 399-415.

[160] Huang Y H, Ho H P, Kong S K, Kabashi A V. *Phase-sensitive surface plasmon resonance biosensors: methodology, instrumentation and applications*. Annalen Der Physik, 2012, 524(11): 637-662.

[161] Abayzeed S A, Smith R J, Webb K F, Somekh M G, See C W. *Responsivity of the differential-intensity surface plasmon resonance instrument*. Sensors and Actuators B: Chemical, 2016, 235: 627-635.

[162] Then W L, Aguilar M I, Garnier G. *Quantitative blood group typing using surface*

plasmon resonance. Biosensors and Bioelectronics, 2015, 73: 79-84.

[163] Krupin O, Wang C, Berini P. *Selective capture of human red blood cells based on blood group using long-range surface plasmon waveguides*. Biosensors and Bioelectronics, 2014, 53: 117-122.

[164] Jiang G, Baba A, Ikarashi H, Xu R, Locklin J, Kashif K R, Shinbo K, Kato K, Kaneko F, Advincula R. *Signal enhancement and tuning of surface plasmon resonance in Au nanoparticle/polyelectrolyte ultrathin films*. The Journal of Physical Chemistry C, 2007, 111(50): 18687-18694.

[165] Szabo A, Stolz L, Granzow R. *Surface plasmon resonance and its use in biomolecular interaction analysis (BIA)*. Current Opinion in Structural Biology, 1995, 5(5): 699-705.

[166] Hong X, Hall E A H. *Contribution of gold nanoparticles to the signal amplification in surface plasmon resonance*. Analyst, 2012, 137(20): 4712-4719.

[167] Plum M A, Menges B, Fytas G, Butt H J, Steffen W. *Resonance enhanced dynamic light scattering*. Review of Scientific Instruments, 2011, 82(1): 015102.

[168] Sartor M. *Dynamic light scattering*. University of California, San Diego, 2003: 2-21.

[169] Goldburg W I. *Dynamic light scattering*. American Journal of Physics, 1999, 67(12): 1152-1160.

[170] Hindley J, Gedroyc W M, Regan L, Stewart E, Tempany C, Hynnen K, Macdanold N, Inbar Y, Itzchak Y, Rabinovici J, Kim K, Geschwind J F, Hesley G, Gostout B, Ehrenstein T, Hengst S, Sklair-Levy M, Shushan A, Jolesz F. *MRI guidance of focused ultrasound therapy of uterine fibroids: early results*. American Journal of Roentgenology, 2004, 183(6): 1713-1719.

[171] Mottin C C, Moretto M, Padoin A V, Swarowsky A M, Toneto M G, Glock L, Repetto G. *The role of ultrasound in the diagnosis of hepatic steatosis in morbidly obese patients*. Obesity Surgery, 2004, 14(5): 635-637.

[172] Kennedy J E. *High-intensity focused ultrasound in the treatment of solid tumours*. Nature Reviews Cancer, 2005, 5(4): 321.

[173] Hill C R, Ter Haar G R. *High intensity focused ultrasound-potential for cancer treatment*. The British Journal of Radiology, 1995, 68(816): 1296-1303.

[174] Gai M, Frueh J, Tao T, Petrov A V, Petrov V V, Shesterikov E V, Tverdokhlebov S I, Sukhorukov G B. *Polylactic acid nano-and microchamber arrays for encapsulation of small hydrophilic molecules featuring drug release via high intensity focused ultrasound*. Nanoscale, 2017, 9(21): 7063-7070.

[175] Skoog D A, Holler F J, Crouch S R. *Principles of instrumental analysis*. Cengage Learning, 2017, 169-173.

[176] Łobiński R, Marczenko Z. *Recent advances in ultraviolet-visible spectrophotometry*. Critical Reviews in Analytical Chemistry, 1992, 23(1-2): 55-111.

[177] Perkampus H H, Grinter H C. *UV-Vis spectroscopy and its applications*. Berlin: Springer-Verlag, 1992, 26-80.

[178] Lamsal R, Harroun S G, Brosseau C L, Gagnon G A. *Use of surface enhanced Raman spectroscopy for studying fouling on nanofiltration membrane*. Separation and Purification Technology, 2012, 96: 7-11.

[179] Khulbe K C, Matsuura T. *Characterization of synthetic membranes by Raman spectroscopy, electron spin resonance, and atomic force microscopy; a review*. Polymer, 2000, 41(5): 1917-1935.

[180] Smith G D, Clark R J H. *Raman microscopy in archaeological science*. Journal of Archaeological Science, 2004, 31(8): 1137-1160.

[181] Vallet-Regí M, Balas F, Arcos D. *Mesoporous materials for drug delivery.* Angewandte Chemie International Edition, 2007, 46(40): 7548-7558.

[182] Dulkeith E, Ringler M, Klar T A, Feldmann J. *Gold nanoparticles quench fluorescence by phase induced radiative rate suppression*. Nano Letters, 2005, 5(4): 585-589.

[183] Matveeva E G, Shtoyko T, Gryczynski I, Irina A, Zygmunt G. *Fluorescence quenching/enhancement surface assays: Signal manipulation using silver-coated gold nanoparticles*. Chemical Physics Letters, 2008, 454(1-3): 85-90.

[184] Homola J. *Present and future of surface plasmon resonance biosensors*. Analytical and Bioanalytical Chemistry, 2003, 377(3): 528-539.

[185] Nakanishi K, Sakiyama T, Imamura K. *On the adsorption of proteins on solid surfaces, a common but very complicated phenomenon*. Journal of Bioscience and Bioengineering, 2001, 91(3): 233-244.

[186] Prime K L, Whitesides G M. *Adsorption of proteins onto surfaces containing end-attached oligo (ethylene oxide): a model system using self-assembled monolayers*. Journal of the American Chemical Society, 1993, 115(23): 10714-10721.

[187] Saikin S K, Olivares-Amaya R, Rappoport D, Stopa M, Aspuru-Guzik A. *On the chemical bonding effects in the Raman response: Benzenethiol adsorbed on silver clusters*. Physical Chemistry Chemical Physics, 2009, 11(41): 9401-9411.

[188] Wang H, Levin C S, Halas N J. *Nanosphere arrays with controlled sub-10-nm gaps as surface-enhanced Raman spectroscopy substrates*. Journal of the American Chemical Society, 2005, 127(43): 14992-14993.

[189] Girardi E, Holdom M D, Davies A M, Sutton B J, Beavil A J. *The crystal structure of rabbit IgG-Fc*. Biochemical Journal, 2009, 417(1): 77-83.

[190] Endo T, Yamamura S, Nagatani N, Morita Y, Takamura Y, Tamiya E. *Localized surface plasmon resonance based optical biosensor using surface modified nanoparticle layer for label-free monitoring of antigen-antibody reaction.* Science and Technology of Advanced Materials, 2005, 6(5): 491.

[191] Butler J E, Ni L, Nessler R, Joshi K S, Suter M, Rosenberg B, Chang J, Brown W R, Cantarero L A. *The physical and functional behavior of capture antibodies adsorbed on polystyrene*. Journal of Immunological Methods, 1992, 150(1-2): 77-90.

[192] Henriksen-Lacey M, Christensen D, Bramwell V W, Lindenstrøm T, Agger E M, Andersen P, Perrie Y. *Liposomal cationic charge and antigen adsorption are important properties for the efficient deposition of antigen at the injection site and ability of the vaccine to induce a CMI response*. Journal of Controlled Release, 2010, 145(2): 102-108.

[193] Schmidt A M, Vianna M, Gerlach M, Brett J, Ryan J, Kao J, Esposito C, Hegarty H, Hurley W, Clauss M. *Isolation and characterization of two binding proteins for advanced glycosylation end products from bovine lung which are present on the endothelial cell surface*. Journal of Biological Chemistry, 1992, 267(21): 14987-14997.

[194] Sackmann E, Tanaka M. *Supported membranes on soft polymer cushions: fabrication, characterization and applications*. Trends in Biotechnology, 2000, 18(2): 58-64.

[195] Gnapareddy B, Dugasani S R, Ha T, Paulson B, Hwang T, Kim T, Kim J H, Oh K, Park S H. *Chemical and physical characteristics of doxorubicin hydrochloride drug-doped salmon DNA thin films*. Scientific Reports, 2015, 5: 12722.

[196] Zhou H, Mu Q, Gao N, Liu A, Xing Y, Gao S, Zhang Q, Qu G B, Chen Y Y, Liu G, Zhang B, Yan B. *A nano-combinatorial library strategy for the discovery of nanotubes with reduced protein-binding, cytotoxicity, and immune response*. Nano Letters, 2008, 8(3): 859-865.

[197] Mu Q, Jiang G, Chen L, Zhou H, Fourches D, Tropsha A, Yan B. *Chemical basis of interactions between engineered nanoparticles and biological systems*. Chemical Reviews, 2014, 114(15): 7740-7781.

[198] AshaRani P V, Low Kah Mun G, Hande M P, Valiyaveettil S. *Cytotoxicity and genotoxicity of silver nanoparticles in human cells*. ACS Nano, 2008, 3(2): 279-290.

[199] Yen H J, Hsu S, Tsai C L. *Cytotoxicity and immunological response of gold and silver nanoparticles of different sizes*. Small, 2009, 5(13): 1553-1561.

[200] Feldman M B, Terry D S, Altman R B, Blanchard S C. *Aminoglycoside activity observed on single pre-translocation bibosome complexes*. Nature Chemical Biology, 2010, 6, 54-62.

[201] Xu Y, Han T, Li X, Sun L, Zhang Y, Zhang Y. *Colorimetric detection of kanamycin based on analyte-protected silver nanoparticles and aptamer-selective sensing mechanism*. Analytica Chimica Acta, 2015, 891: 298-303.

[202] Carpita N, Sabularse D, Montezinos D, Delmer D P. *Determination of the pore size of cell walls of living plant cells*. Science, 1979, 205(4411): 1144-1147.

[203] Goodwin J W, Hearn J, Ho C C, Ottewill R H. *Studies on the preparation and characterisation of monodisperse polystyrene laticee*. Colloid and Polymer Science, 1974, 252(6): 464-471.

[204] Zhao H, Shao L, Chen J F. *High-gravity process intensification technology and application*. Chemical Engineering Journal, 2010, 156(3): 588-593.

[205] Sun Q, Chen B, Wang M, Zhang C, Zeng X F, Wang J X, Chen J F. *Preparation of transparent suspension of lamellar magnesium hydroxide nanocrystals using a high-gravity reactive precipitation combined with surface modification*. Industrial & Engineering Chemistry Research, 2015, 54(2): 666-671.